Universitätsklinikum Tübingen

Neurologische Universitätsklinik

Hertie-Institut für Klinische Hirnforschung, Neurologie mit Schwerpunkt neurodegenerative Erkrankungen

# Mitochondrial DNA in Extracellular Vesicles: A Diagnostic Biomarker for Parkinson's Disease?

Inaugural-Dissertation

zur Erlangung des Doktorgrades

der Medizin

der Medizinischen Fakultät

der Eberhard-Karls-Universität

zu Tübingen

vorgelegt von

**Hans Justus Siegrist**

2024

Dekan: Professor Dr. Bernd Pichler

1. Berichterstatter: Professor Dr. Thomas Gasser

2. Berichterstatter: Professor Dr. Olaf Rieß

Tag der Disputation: 03.04.2024

# List of Contents

# List of Abbreviations

| | |
|---|---|
| **αSyn** | α-Synuclein |
| **ACTB** | human β-actin gene |
| **AD** | Alzheimer's disease |
| **AFM** | atomic force microscopy |
| **APC** | antigen-presenting cell |
| **BBB** | blood-brain barrier |
| **BCA** | bicinchoninic acid |
| **bp** | base pairs |
| **BSA** | bovine serum albumin |
| **CBD** | cortico-basal degeneration |
| **cfDNA** | cell-free circulating DNA |
| **CD** | cluster of differentiation |
| **cGAS** | GMP–AMP synthase |
| **CNS** | central nervous system |
| **CSF** | cerebrospinal fluid |
| **$C_t$ value** | cycle threshold value |
| **DC** | dendritic cell |
| **DLB** | dementia with Lewy bodies |
| **DLS** | dynamic light scattering |
| **DNA** | deoxyribonucleic acid |
| **dPCR** | digital PCR |
| **dsDNA** | double-stranded DNA |
| **ESCRT** | endosomal sorting complex required for transport |
| **EVs** | extracellular vesicles |
| **GPe/i** | external/internal pallidal segments |
| **HDL** | high-density lipoprotein |
| **HEPES** | 4-(2-hydroxyethyl)-1-piperazineethanesulfonic acid |
| **HSP** | heat shock protein |
| **ILV** | intraluminal vesicle |
| **IP** | immunoprecipitation |
| **IPD** | idiopathic Parkinson's disease |
| **ISEV** | International Society for Extracellular Vesicles |

| | |
|---|---|
| **L1CAM** | L1 cell adhesion molecule |
| **LAMP** | lysosomal-associated membrane protein |
| **LB** | Lewy body |
| **LRRK2** | leucine-rich repeat kinase 2 |
| **MSA** | multi-system atrophy |
| **miRNA** | micro-RNA |
| **mtDNA** | mitochondrial DNA |
| **MW** | molecular weight |
| **MVB** | multivesicular body |
| **n** | number of replicats |
| **ND1** | NADH-dehydrogenase, subunit 1 (complex I) |
| **ND4** | NADH-dehydrogenase, subunit 4 (complex I) |
| **NMS** | non-motor symptoms |
| **NTA** | nanoparticle tracking analysis |
| **PBS** | phosphate-buffered saline |
| **PCR** | polymerase chain reaction |
| **PD** | Parkinson's disease |
| **PEG** | polyethylene glycol |
| **PIC** | protease inhibitor cocktail |
| **PINK1** | PTEN-induced kinase 1 |
| **POLG** | DNA polymerase γ |
| **PSP** | progressive nuclear palsy |
| **qPCR** | quantitative PCR |
| **Rab** | Ras-related in brain |
| **RNA** | ribonucleic acid |
| **ROS** | reactive oxygen species |
| **rpm** | rounds per minute |
| **RPS** | resistive pulse sensing |
| **rRNA** | ribosomal RNA |
| **rtPCR** | quantitative real-time PCR |
| **SD** | standard deviation |
| **SEC** | size-exclusion chromatography |
| **SDS** | sodium dodecyl sulfate |
| **SN (c/r)** | substantia nigra (pars compacta/pars reticulata) |

| | |
|---|---|
| **SNARE** | soluble N-ethylmaleimide-sensitive factor attachment proteins receptor |
| **STING** | stimulator of interferon genes |
| **STN** | subthalamic nucleus |
| **TBE** | tris/borate/EDTA |
| **TBS** | tris buffered saline |
| **TCA** | tri-chloroacetic acid |
| **TEM** | transmission electron microscopy |
| **TFAM** | mitochondrial transcription factor A |
| **tRNA** | transfer-RNA |
| **TSG101** | tumor susceptibility gene 101 |
| **UC** | ultracentrifugation |
| **VLDL** | very-low-density lipoprotein |
| **Vps4** | vacuolar protein sorting-associated protein 4 |
| **WB** | Western Blot |
| **x g** | times gravitational acceleration |

# List of Figures

# List of Tables

# 1. Introduction

## 1.1. Extracellular Vesicles (EVs)

### 1.1.1. History of EVs

EVs were first discovered in 1983 by Harding and Stahl and their findings were later confirmed by Pan and Johnstone, 1985. These independent research groups showed that reticulocytes release transferrin receptors associated with small vesicles into the extracellular space when they mature into erythrocytes (Harding and Stahl 1983). This process was considered for the cell to get rid of the transferrin receptor as a mechanism to remove obsolete proteins. Reticulocytes were incubated with a gold-labelled anti-transferrin receptor antibody, which was internalized into the cells after a few minutes and observed on the surface of 100-200 nm vesicles inside the cell. After a longer incubation time, 50 nm bodies with the transferrin receptor on their external surface were found inside larger multivesicular bodies (MVBs) (1-1,5 µm), but no transferrin receptors were found on the membrane of the MVBs. The limiting membrane of the MVBs then fused with the plasma membrane, releasing the transferrin receptor-bearing vesicles into the extracellular space, revealed by electron microscopy (EM) (Pan et al. 1985). Even two years earlier in 1981, it was reported, that cultured cells release the plasma-membrane-bound enzymes ATPase and 5'-nucleotidase into the serum-free media (Trams et al. 1981). These enzymes were associated with vesicles originating from a specific domain of the plasma membrane. A few years later, Rose Johnstone introduced the term "exosome" for these extracellular vesicles (Johnstone et al. 1987). Another breakthrough in EV research was the discovery of the role of EVs in the immune response, proved by the finding that B lymphocytes secrete vesicles carrying molecules modulating the immune response in the recipient cell (Raposo et al. 1996). Two years later it was shown, that dendritic cells release antigen-presenting exosomes carrying immune agents with an anti-tumour effect in mice (Zitvogel et al. 1998). Since then, the field of EV research grew and still grows, including two scientific societies (International Society for Extracellular Vesicles and The American Society for Exosomes and Microvesicles) with their own

journal (Journal of Extracellular Vesicles). After studying the physiological and pathological function of EVs, the use of EVs for diagnostics and clinical treatment has attracted attention to the scientific community. Even the Nobel Prize in Physiology or Medicine 2013 was awarded to three researchers working in the field of vesicles (James E. Rothman, Randy W. Schekman, and Thomas C. Südhof) "for their discoveries of machinery regulating vesicle traffic, a major transport system in our cells (Zierath and Lendahl 2013)."

According to the “International Society for Extracellular Vesicles” stated in their positional paper “Minimal information for studies of extracellular vesicles 2018 (MISEV2018): a position statement of the International Society for Extracellular Vesicles and update of the MISEV2014 guidelines”, the generic term “extracellular vesicles (EVs)” should be used for all particles which are released from cells, consisting of a lipid bilayer and unable to replicate (Théry et al. 2018). Due to the lack of specific markers for EV subtypes such as exosomes, microvesicles, or apoptotic bodies, a distinction in various subpopulations would not be expedient. Describing the physical properties of EVs like size, density, or biochemical composition instead is recommended. Below, the term “exosome” is only used when it is used in the cited article.

### 1.1.2. The biological composition of EVs

EVs are biological nanostructures secreted by all studied cell types so far and can be found in most human biological fluids (blood, urine, breastmilk, CSF, *etc.*), but also in cell culture supernatant and tissue. They consist of a phospholipid bilayer originating from the plasma membrane of the secreting cell (Thery, Zitvogel, and Amigorena 2002). There is still no consensus about how to divide the whole EV population into subpopulations, but the most common classification distinguishes between ectosomes and exosomes (Cocucci and Meldolesi 2015): Ectosomes are assembled at the plasma membrane and are released into the extracellular space by direct outward budding of the membrane. Ectosomes consist of three main subgroups: microvesicles, microparticles, and large vesicles (including apoptotic bodies) (reviewed by (Kalluri and LeBleu 2020)). Exosomes with a diameter between 40 and 160 nm (on average 100 nm) on the other

hand originate from endosomes and are released from the cell when the endosome fuses with the plasma membrane. An overview of the three main EV classes exosomes, microvesicles, and apoptotic bodies is provided in table 1. Most isolation techniques fail to separate these subpopulations and unique markers for these subtypes are still lacking (Jeppesen et al. 2019). Similar to the heterogeneity in size, the cargo of EVs and their protein composition can differ widely depending on the original cell type and the isolation method (Willms et al. 2018). Exosomal cargo includes various proteins, nucleic acids (DNA, different RNA species (mRNA, miRNA, tRNA, *etc.*)), amino acids, lipids, and metabolites (Keerthikumar et al. 2016). The protein compound of EVs can be split up into ubiquitous proteins, that are often part of the biogenesis of EVs (e.g., cytosolic proteins, proteins involved in membrane fusion and signal transduction) and cell-specific proteins, depending on the donor cell type. Tetraspanins, proteins with four transmembrane domains such as CD9, CD63, and CD81, are highly enriched on EVs (especially exosomes) making them a suitable EV marker (Thery, Zitvogel, and Amigorena 2002). Other molecular markers include TSG101, HSC70, HSP90, Alix, Calnexin, and Flotillin-1 (Thery et al. 2006; Borges, Reis, and Schor 2013).

***Table 1:*** *Overview of EV subtypes (based on (Gyorgy et al. 2011; Borges, Reis, and Schor 2013; Kalluri and LeBleu 2020; Gurung et al. 2021))*

| | **exosomes** | **microvesicles / microparticles** | **apoptotic bodies** |
|---|---|---|---|
| **diameter** | 40 – 160 nm (100 nm on average) | 100 – 1,000 nm | 1 – 5 µm |
| **structure** | phospholipid bilayer | phospholipid bilayer | phospholipid bilayer |
| **biogenesis** | exocytosis via fusion of MVBs with the plasma membrane | budding/blebbing of the plasma membrane (releasing signal: apoptosis/activation of membrane receptors --> increase of intracellular $Ca^{2+}$) | blebbing of apoptotic cells (vesicles can contain organelles) |
| **source** | (almost) every living cell type (eukaryotes and prokaryotes) | especially red blood cells, platelets, and endothelial cells | apoptotic cells |
| **markers** | CD63, CD9, Alix, TSG101, HSP70 | Annexin V, Flotillin-2, selectin, integrin | Annexin V, DNA, histones |

| | | | |
|---|---|---|---|
| **function** | cell-cell-communication | cell-cell-communication | clearance of apoptotic cells |
| **note** | | inconsistent terminology | |

### 1.1.3. Biogenesis of EVs

The difference in the biogenesis between ectosomes (like microvesicles or apoptotic bodies) and exosomes is already described above. This section will focus on the biogenesis of exosomes. The first step in the generation of exosomes is the de-novo formation of an early endosome through inward budding of the plasma membrane (figure 1). The Golgi network and endoplasmic reticulum are also involved in this process (Hessvik and Llorente 2018). When early endosomes mature into late endosomes, they accumulate intraluminal vesicles (ILVs) which are formed by inward budding of the limiting endosomal membrane (Stoorvogel et al. 1991). These ILVs in the lumen of an MVB are the future exosomes. Although most of the MVBs are degraded by the fusion with lysosomes or autophagosomes, some of the MVBs fuse with the plasma membrane releasing the former ILVs (now called exosomes) into the extracellular space (Colombo, Raposo, and Thery 2014). CD63, LAMP1/2, and other molecules associated with late endosomes could be identified as signals that allow the MVB to fuse with the plasma membrane (Jaiswal, Andrews, and Simon 2002). It is important to note that the exosomal membrane is primarily of endosomal origin and due to the “reverse budding” of the ILVs from the MVB membrane, cytosolic proteins can be found inside the exosomes and the extracellular domain of transmembrane receptors is orientated towards the lumen of the MVB (Thery, Zitvogel, and Amigorena 2002). The ESCRT machinery (endosomal sorting complex required for transport) plays an important role in the formation of MVBs (Williams and Urbe 2007). This machinery consists of about 30 proteins that assemble into 5 complexes (ESCRT-0, -I, -II, -III, and Vsp4) with associated proteins (Schmidt and Teis 2012). ESCRT-0 recognizes and sorts ubiquitinylated cargo, ESCRT-I and -II promote inward budding of the endosomal membrane, ESCRT-III binds to ESCRT-II necessary to “cut off” the forming vesicle from the membrane, releasing an ILV into the MVB and finally Vps4 plays an important role in the disassembly of the ESCRT machinery and recycling (Gurung et al. 2021). Other proteins associated with the ESCRT machinery like

Alix and TSG101 can also be found in exosome preparations (Théry et al. 2001). However, ESCRT-depleted mammalian cells are also able to produce MVBs indicating that there is also an ESCRT-independent mechanism of exosome biogenesis (Stuffers et al. 2009). One mechanism includes complex lipids such as ceramide, which can form lipid rafts into membranes facilitating inward budding of the ILVs (Trajkovic et al. 2008). In the same manner, cholesterol is also able to increase the release of exosomes (Strauss et al. 2010). Tetraspanins contribute to the biogenesis of exosomes as well: The common exosomal marker CD63 (a tetraspanin) seems to be involved in the formation of small ILVs and the regulation of the size of these ILVs (Edgar, Eden, and Futter 2014). Intracellular vesicle transport (for example to the plasma membrane) is achieved through the interaction between the cytoskeleton and Rab GTPases (Stenmark 2009). RAB11 for example, which was first reported, modulates the exosome pathway and contributes to exosome secretion (Savina, Vidal, and Colombo 2002). The final step, the fusion of the MVB with the plasma membrane, is carried out by SNARE proteins and the synaptotagmin family (Jahn and Scheller 2006). Most cells seem to need a stimulus inducing the release of exosomes: It was shown that the rise of the intracellular calcium concentration triggers the secretion of exosomes (Savina et al. 2003). However, some tumor cells are able to release spontaneously plasma membrane derived EVs called “oncosomes” (Di Vizio et al. 2012).

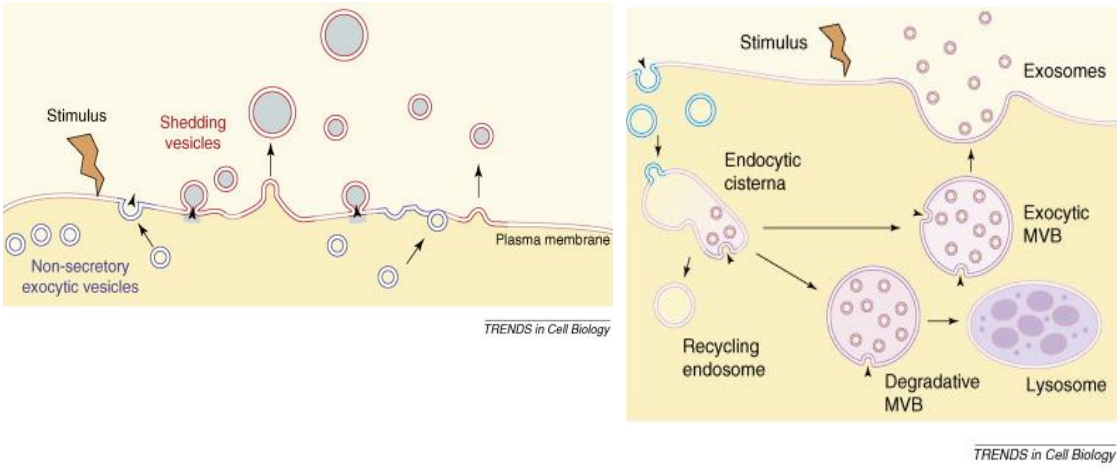


***Figure 1: Molecular mechanisms of the generation of microvesicles (left) and exosomes (right).*** *Microvesicles are released by direct budding of specialised parts of the plasma membrane (lipid rafts in red). Exosomes originate from ILVs inside of MVBs and are released into the extracellular space when the MVB fuses with the plasma membrane.*

### 1.1.4. Function of EVs

#### 1.1.4.1. Physiological functions of EVs

The first discovered function of EVs was a “garbage disposal system” of cells to get rid of unnecessary proteins (e.g., when reticulocytes mature into erythrocytes they release transferrin receptors in small vesicles (Harding and Stahl 1983)). But that is just the tip of the iceberg and 40 years of EV research revealed plenty of other functions of EVs. It is now unquestioned, that EVs play a crucial role in cell-to-cell communication. Two mechanisms allow EVs to trigger signalling when reaching the target cell: Either via direct interaction, binding with their transmembrane proteins to surface receptors of a cell and activating a downstream signalling cascade, or via membrane fusion with the plasma membrane of the target cell respectively internalization followed by the release of their cargo into the cytosol of the cell (Gurung et al. 2021). Both mechanisms allow the EVs to modify protein expression in target cells. The role of EVs in the adaptive and innate immune system was firstly reported in 1996 when it could be shown that B lymphocytes secrete antigen-presenting vesicles (Raposo et al. 1996). Exosomes secreted by antigen-presenting cells (APCs) carry MHC-II (major histocompatibility complex II) on their surface, allowing them to present peptide-antigens to specific T lymphocytes and activate them (Vincent-Schneider et al. 2002). Also large EVs released from dendritic cells (DCs) can efficiently induce the activation of $CD4^+$ T cells and promote a T helper 1 response *in vitro* (Tkach et al. 2017). Exosomes released from macrophages infected with *Mycobacterium tuberculosis* carry mycobacterial antigens that could induce an antibacterial immune response in mice, underlining their role in the immune system (Cheng and Schorey 2013). On the other hand, exosomes can promote viral infections by carrying and disseminating viral components or by using the vesicle biogenesis for their own survival (Crenshaw et al. 2018). Another function of EVs involves human reproduction and pregnancy. It was postulated that seminal exosomes promote sperm maturation when they pass the male reproductive tract (Sullivan et al. 2005). A growing number of studies also deal with breast milk EVs and their influence on the regulation of immune response and inflammation in infants. miRNA in breast milk exosomes for example seems to have an immune-related function, increasing the number of

regulatory T cells in the blood and contributing to immune tolerance (Zhou et al. 2012). Other functions of EVs include stem cell development and differentiation, tissue repair and regeneration, as well as anti-inflammatory and neuronal functions (reviewed by (Rashed et al. 2017). Needless to say, that EVs not only contribute to the normal physiology but also participate in the pathophysiology of multiple diseases, especially the cancer life cycle.

#### 1.1.4.2. EVs in the central nervous system (CNS)

In contrast to other cell types, neurons secrete a relatively low number of EVs into the cerebrospinal fluid (CSF) (Lizarraga-Valderrama and Sheridan 2021). Nevertheless, they contribute to a normal neuronal function. *In vitro* experiments with cultured cells showed that EVs are released from neurons, glial cells (oligodendrocytes and astrocytes), and microglia (Fauré et al. 2006; Krämer-Albers et al. 2007; Potolicchio et al. 2005). Neuron-derived EVs contribute to the transfer of information across synapses. Exosomes internalized at the presynaptic terminal of neurons can induce local changes in synaptic plasticity by modifying mRNA trafficking and translation within the target cell (Chivet et al. 2013). Exosomes are also part of the signalling between neurons and glial cells, for example regulating protein expression in astrocytes (Lizarraga-Valderrama and Sheridan 2021). Astrocyte-derived EVs with Synapsin I as cargo were shown to stimulate neurite outgrowth and promote the survival of hippocampal neurons in mice (Wang et al. 2011). An inhibitory effect on the differentiation of oligodendrocytes and myelin formation could be observed in small exosome-like vesicles derived from oligodendrocytes (Bakhti, Winter, and Simons 2011). In a study from 2019, purified exosomes harvested from rodent cultures were injected into the lateral ventricles of P4 mouse brains, resulting in increased hippocampal neurogenesis (Sharma et al. 2019).

EVs from CNS cells are not just found in the CSF, they can also cross the blood-brain barrier (BBB) in both directions. Studies have shown that on the one hand peripheral exosomes can transport short interfering RNA (siRNA) to the brain in mice (Alvarez-Erviti, Seow, Yin, et al. 2011) implicating a therapeutic use to deliver drugs across the BBB into the CNS and on the other hand, exosomes containing glioblastoma-specific RNA

as well as astrocyte-derived EVs could be isolated from human blood serum (Noerholm et al. 2012; Goetzl et al. 2016). Since neuronal-derived EVs in human blood only account for a small subpopulation within the total blood EV population (the number of neuronal-derived L1CAM$^+$ EVs in plasma was reported to be 90-95% lower than the number of total EVs in plasma (Mustapic et al. 2017)), neuronal-specific markers on the surface of EVs are needed to isolate EVs from neuronal origin. The transmembrane protein L1CAM for example could be identified to be enriched on neuronal-derived EVs allowing it to serve as a potential target to enrich for neuronal-derived EVs (Mustapic et al. 2017). In the same study, the authors could show that neuron-specific proteins like p-tau, neuron-specific enolase, MAP2, NCAM, or NFL were enriched in L1CAM$^+$ EVs compared to total plasma EVs. These findings suggest the conclusion that neuronal-derived EVs can be isolated from the peripheral circulation and that they can serve as "a potential window into brain pathologic processes" (Mustapic et al. 2017). For the controversy about L1CAM as a suitable marker for neuronal-derived EVs, please refer to the discussion section.

#### 1.1.4.3. The role of EVs in Parkinson's Disease

There is a growing understanding of the role EVs play in the pathophysiology of neurodegenerative diseases like PD suggesting their use as a diagnostic and therapeutic tool. Based on the demonstration, that exosomes from prion-infected neuronal cells can initiate prion propagation in healthy recipient cells and are even able to cause prion disease in mice (Vella et al. 2007), the "Trojan horse" hypothesis was formulated, postulating that neurons ship pathogenic agents via exosomes from cell to cell throughout brain areas, "infecting" other cells, leading to protein oligomerization and finally cell death (Ghidoni, Benussi, and Binetti 2008). This hypothesis is supported by the observation, that CSF exosomes filled with α-Synuclein (αSyn) from PD and DLB patients can induce oligomerization of αSyn in a reporter cell line suggesting that it is a pathogenic species of αSyn (Stuendl et al. 2016). It is also long known that intracellular αSyn oligomers cause the death of neurons (Sung et al. 2001). However, extracellular αSyn oligomers were shown to exist in two fractions: either free or associated with exosomes. Interestingly, exosomal αSyn oligomers were more likely to be taken up by recipient cells and were

more toxic than the free αSyn oligomers (Danzer et al. 2012). Furthermore, it was discovered that αSyn overexpressing SH-SY5Y cells release αSyn carrying exosomes, which transferred αSyn to normal SH-SY5Y cells (Alvarez-Erviti, Seow, Schapira, et al. 2011). In the same study, the role of the autophagy-lysosomal pathway was underlined by the observation, that lysosomal inhibition in the donor cell increased the exosomal αSyn release and its transmission between cells (Alvarez-Erviti, Seow, Schapira, et al. 2011). Extracellular and exosomal αSyn aggregates are normally degraded by microglia, the primary phagocytes in the brain (Brück et al. 2016), but when treated with human αSyn fibrils, they also release αSyn containing exosomes capable of inducing αSyn oligomerization in recipient neurons (Guo et al. 2020). To summarize, exosomal αSyn seems to contribute in the prion-like spread of αSyn throughout the brain, inducing oligomerization of αSyn in "infected" cells and propagating the neurodegenerative process. But the picture is a little bit more complex since exosomes in PD can also have neuroprotective effects (Tomlinson et al. 2015).

Another protein that links EVs and PD is the enzyme ATPase 13A2, encoded by the ATP13A2 gene (also known as PARK9), an autosomal recessive form of early-onset parkinsonism (Ramirez et al. 2006). ATP13A2 is localized at MVBs and therefore involved in the biogenesis of EVs (Tsunemi, Hamada, and Krainc 2014). *In vivo* and *in vitro* experiments demonstrated, that reduced function of ATP13A2 (due to mutation or knockdown) leads to lysosomal dysfunction and enhances αSyn misfolding and accumulation in the cells (Kong et al. 2014). On the other hand, overexpression of ATP13A2 was associated with reduced αSyn toxicity, decreased intracellular αSyn levels, and increased αSyn externalization via exosomes (Tsunemi, Hamada, and Krainc 2014; Kong et al. 2014). Due to its neuroprotective effect, overexpression of ATP13A2 could be detected in surviving neurons of the substantia nigra from PD brains (Ramonet et al. 2012).

### 1.1.5. Isolation and Characterization of EVs

Several techniques allow the enrichment of a sample for EVs that target different biophysical properties of EVs (size, density, solubility, surface proteins). The oldest and most commonly used method is probably differential ultracentrifugation (UC). Table 2

summarizes the most applied isolation techniques as well as their advantages and disadvantages.

***Table 2:*** *Overview of different EV isolation techniques with their advantages and disadvantages (based on (Furi, Momen-Heravi, and Szabo 2017), (Kang, Kim, and Park 2017) and (Li et al. 2017)).*

| **method** | | **functioning** | **advantages** | **disadvantages** |
|---|---|---|---|---|
| **UC** | | series of different centrifugation steps, pelleting the EVs at 100,000 x g | - relative cheap<br>- no special material required<br>- suitable for large sample volumes | - low yield of EVs<br>- relative high protein and lipoprotein contamination<br>- contamination with non-vesicular macromolecules<br>- the integrity of EVs could be damaged<br>- time-consuming<br>- ultracentrifuge is required<br>- no “standard protocol” available<br>- inconsistencies in reproducibility<br>- aggregation of EVs |
| **solution sedimentation** | | combination of centrifugation and precipitation of EVs in a sucrose gradient | - relative cheap<br>- no special material required<br>- purer solution than UC only | - low yield of EVs<br>- time-consuming |
| **Size exclusion** | **ultra-filtration** | series of membrane filters with increasingly narrower pore sizes separating particles depending on their molecular weight or size | - time-saving<br>- moderate purity<br>- functional integrity of the EVs is preserved | - clogging and vesicle trapping on the membrane can lower the isolation efficiency |
| | **SEC** | particles pass through a porous stationary phase, depending on their hydrodynamic radii particles result in different elution fractions | - high purity<br>- functional integrity of the EVs is preserved | - special equipment needed<br>- not suitable for large sample volumes<br>- long run time |

| | | | |
|---|---|---|---|
| **Immunoaffinity capture-based techniques (IP)** | EVs are captured by taking advantage of immunoaffinitive interactions between (membrane-bound) proteins on EVs and their antibodies (e.g. antibody-coated magnetic beads) | - high purity<br>- high capture efficiency (small volumes sufficient)<br>- isolation of subpopulations of EVs possible, e.g. from one origin (depending on the antibody) | - usually low yields of EVs (only a subpopulation of all EVs is isolated)<br>- not suitable for large sample volumes<br>- time-consuming<br>- EVs can be damaged in the elution process from the antibody-coated beads<br>- high reagent costs (beads, antibodies, …)<br>- sorting by size is not possible |
| **precipitation** | precipitation solution containing polyethylene glycol (PEG) that ties up water molecules forcing less soluble components out of solution, collection of the EVs by centrifugation or filtration | - high yield of EVs<br>- time-saving<br>- easy to perform | - samples have to be pre-cleaned (removing cells and cellular debris)<br>- high protein contamination through co-precipitation (especially when using blood serum)<br>- special kit required |
| **microchip-based techniques** | flow of liquids through micro-sized channels, EVs are captured by addressing different properties of EVs: immunoaffinity, size, density, *etc.* | - automation possible<br>- time-saving<br>- high purity<br>- suitable for small sample volumes | - special equipment required (very expensive)<br>- not routinely used, no standardization<br>- low sample capacity |

The “International Society for Extracellular Vesicles” recommends a three-step process to characterize EVs (Théry et al. 2018). The first step is the quantification of both the source of the EVs (e.g., blood) and the EV preparation itself. To measure the particle number, different techniques are available, for example nanoparticle tracking analysis (NTA), resistive pulse sensing (RPS), dynamic light scattering (DLS), flow cytometry for larger vesicles, and electron microscopy. The source of the EVs can be quantified by the amount of proteins, lipids, and RNA, for example. The second step requires the

detection of typical EV marker proteins and the absence of contaminants. The presence of at least one transmembrane or GPI-anchored protein and at least one cytosolic or periplasmic protein able to bind to membranes or lipids is required. For purity control, proteins that could be found in co-isolated contaminants should be absent (e.g., albumin or apolipoproteins in EV preparations from blood). Western blotting is the most common technique to characterize the protein composition of EVs, but especially mass spectrometry has become increasingly popular. The third step demands the characterization of single vesicles. Therefore transmission electron microscopy (TEM) is usually used, revealing a "cup-shaped" morphology due to the dehydrating conditions in the sample preparation process (Raposo et al. 1996). To preserve the native size and structure of the EVs, cryo-EM might be applied showing a naturally round shape (Raposo and Stoorvogel 2013). Other techniques include atomic force microscopy (AFM), NTA, or flow cytometry.

## 1.2. Parkinson's disease

### 1.2.1. Epidemiology

Parkinson's disease is the second most common neurodegenerative disease after Alzheimer's disease and was first described in 1817 by James Parkinson (James Parkinson 2002). It is a progressive disorder of the peripheral and the central nervous system, affecting mostly elderly people. People are usually 65 – 70 years old when the disease is diagnosed, and the prevalence is increasing with age (Rijk et al. 1995). It is estimated that 1% of people over the age of 60 worldwide are affected by PD (Tysnes and Storstein 2017) and that the prevalence of PD in men is modestly higher than in women in most populations (Tanner and Goldman 1996). There are several forms of parkinsonian syndromes: Idiopathic or sporadic PD, the largest group characterized by an unknown aetiology; genetic forms of PD with a Mendelian inheritance which account for approx. 5 – 10% of all PD cases (Corti, Lesage, and Brice 2011); atypical parkinsonian disorders such as dementia with Lewy bodies (DLB), multi system atrophy (MSA), progressive supranuclear palsy (PSP), and cortico-basal degeneration (CBD) and at last secondary (or symptomatic) parkinsonian syndromes, e.g. drug-induced, metabolic (e.g. M. Wilson),

inflammation, *etc.* Although just approx. 5 – 10% of all PD patients have inherited their disease, many of the sporadic PD patients have a positive family history. Patients with a monogenetic PD form are more likely to be affected earlier in their life than patients with sporadic PD. So far, at least 16 gene loci (PARK1-16) have been identified (reviewed by (Corti, Lesage, and Brice 2011)). *SNCA* (PARK1/PARK4) and *LRRK2* (PARK8) are the most common mutations causing autosomal-dominant PD. A gain of function mutation in the SCNA gene encoding for the protein αSyn, the driving pathology of PD, directly links with PD (Kim and Alcalay 2017). The most common genetic alterations in autosomal-recessive PD include *parkin* (PARK2), *PINK1* (PARK6), and *DJ-1* (PARK7) (reviewed by (Corti, Lesage, and Brice 2011)). The most frequent genetic alterations in early-onset PD (< 40 – 50 years) are mutations of the *parkin* gene at PARK2 (Hedrich et al. 2004). Mutation of the GBA gene (encoding for the lysosomal enzyme glucocerebrosidase, which is deficient in Gaucher's disease) is the most common genetic risk factor in PD (Riboldi and Di Fonzo 2019). The focus of this work lies on idiopathic (or sporadic) PD since it has a multifactorial aetiology and single disease-triggering genes are not known yet.

### 1.2.2. Pathophysiology

PD is counted among the extrapyramidal motor disorders. As the pathophysiological hallmark of PD, degeneration of dopaminergic neurons in the Substantia nigra, pars compacta (SNc) (a part of the basal ganglia) could be identified, leading to an impaired projection to the caudate nucleus and the putamen, which together form the striatum (Samii, Nutt, and Ransom 2004). Two separate pathways connect the striatum to the internal pallidal segments (GPi) and the substantia nigra, pars reticulata (SNr): a direct projection and an indirect projection via the external pallidal segments (GPe) and the subthalamic nucleus (STN) (Galvan and Wichmann 2008). The lack of the dopaminergic projection to the striatum results in overactivity of the indirect pathway and a decreased inhibition of the direct pathway, leading to a disinhibition of the STN and the GPi. In total, the inhibition of the thalamus increases, resulting in less input to the motor cortex leading to bradykinesia (Jankovic 2021).

The first motor symptoms typically occur, when 50 – 80% of the dopaminergic neurons have been destroyed (DeMaagd and Philip 2015). The histopathological correlate to the nigrostriatal degeneration is represented by the Lewy bodies (LB), intracellular cytoplasmic aggregates in neurons consisting of αSyn (Yasuda and Mochizuki 2010). Misfolded αSyn is more likely to form aggregates within the cells and dysregulated cellular clearance mechanisms, especially the ubiquitin-proteasome system, contribute to the formation and maintenance of the LBs (Del Tredici and Braak 2012; Olanow 2007). A hypothesis formulated by Braak postulates that the process of the LB formation begins in the lower brain stem, especially the dorsal motor nucleus of the vagus nerve before it continues to spread all over the brain like a falling row of dominos, including the medulla oblongata, pontine tegmentum, midbrain, forebrain and finally the cerebral cortex (Braak et al. 2003). Involvement of the enteric nervous system and the vagus nerve indicate, that there could exist a pathogen outside the CNS (which could not be identified yet), able to pass the mucosal barrier of the gastrointestinal tract and enter the vagus nerve, which could initiate the whole process of the LB formation (Braak et al. 2003). Studies could also identify risk factors associated with PD such as elevated cholesterol levels in the blood, high caloric intake, traumatic brain injury, and increased body mass index (reviewed by (Ascherio and Schwarzschild 2016)). Pesticides were among the first discovered risk factors for PD. In a prospective study by Ascherio et al from 2006 (CPS-IIN cohort), exposure to pesticides (5.7% of the participants) lead to a 70% higher incidence of PD compared to the absence of pesticide exposure. Similar findings were made in further studies (Ascherio et al. 2006). The observation of 4 people developing parkinsonism after using a drug containing 1-methyl-4-phenyl-1,2,5,6-tetrahydropyridine (MPTP), which is converted into a molecule similar to the herbicide paraquat supported pesticides as a risk factor (Langston et al. 1983). Other important pathophysiological contributors to PD include oxidative stress and mitochondrial dysfunction (see below), apoptosis, glutamate excitotoxicity (Lau and Tymianski 2010), and inflammation (De Virgilio et al. 2016), showing that the pathogenesis of PD is a complex process and is not fully understood yet.

### 1.2.3. Clinical presentation

The clinical presentation of PD consists of four cardinal symptoms: bradykinesia/akinesia, rigor, tremor at rest, and postural instability (Jankovic 2008). Depending on the expression of the motor symptoms three disease variants can be distinguished: tremor-dominant, akinetic-rigid, and Postural instability and gait difficulty (PIGD) (Thenganatt and Jankovic 2014). These subtypes can also change during the disease progression. Bradykinesia describes a slowness of movement e.g. shuffling steps, difficulties with fine motoric tasks, monotonic and hypophonic dysarthria, hypomimia, reduced blink frequency, and reduced arm swing while walking (Jankovic 2008). The resting tremor is often referred to as “pill-rolling” tremor with a frequency of 4 – 6 Hz. The clinical picture often begins with a unilateral resting tremor at the distal part of an extremity, spreading to the contralateral extremity when the disease progresses over time (Beitz 2014). Rigor refers to increased resistance to passive movements, apparent as “cogwheel” phenomenon when examining the joint range of motion. Postural instability increases the risk of falling due to the flexed neck and trunk posture (Jankovic 2008). Other motor symptoms, which often occur when the disease progresses include “freezing” (inability to initiate a movement), dysarthria and dysphagia, micrography, and a “shuffling” gait (Baumann 2012).

Another challenging therapeutic aspect of PD and often very burdensome for the patient are the non-motor symptoms (NMS). NMS can occur in all stages of the disease and can be divided into four domains: neuropsychiatric, autonomic, sensory, and sleep (Lim and Lang 2010). Different studies analysed, that 100% of all PD patients reported at least one NMS during their disease (Kim et al. 2013; Krishnan et al. 2011), but many NMS also occur during “normal” aging. Some of these NMS can precede the classical motor symptoms, such as REM sleep behaviour disorder (Olson, Boeve, and Silber 2000), constipation (Abbott et al. 2001), urinary incontinence and erectile dysfunction (Gao et al. 2007), orthostatic hypotension (Kaufmann et al. 2004), depression (Schuurman et al. 2002) and decreased olfactory function (hyposmia) (Ponsen et al. 2004). Other NMS include excessive daytime sleepiness, autonomic dysfunction, hallucinations, pain (Hely et al. 2008), and seborrheic dermatitis (Fischer et al. 2001). Cognitive dysfunction and dementia are

very common in PD especially when the disease progresses. A systematic review from 2005 on European and North American populations suggested a point-prevalence of dementia in PD between 25 and 30% (Aarsland, Zaccai, and Brayne 2005). PD patients have a six-times higher risk for (subcortical) dementia and 12 years after the initial diagnosis 60% of PD patients develop dementia (Aarsland, Beyer, and Kurz 2008). Major challenges about the NMS are the lower response to antiparkinsonian medication compared to the motor symptoms and the triggering of some of these symptoms due to the dopaminergic treatment (e.g., hallucinations as a side effect of dopamine agonists) (Fénelon et al. 2000).

### 1.2.4. Diagnosis

The diagnosis of PD is primarily based on the clinical presentation of the patient and requires both of the following symptoms: bradykinesia (or akinesia) and rest tremor or rigidity (Hughes et al. 1992). A positive response to a dopaminergic treatment (improvement of tremor, bradykinesia, and rigidity) is the most important supportive criterion. At the initial diagnosis, a conventional brain MRI should be performed to exclude structural abnormalities (e.g. hydrocephalus, tumor) (Chou 2021). The following additional imaging techniques are not used routinely and are reserved for unclear cases. DaTScan™ uses 123I-ioflupane, which binds to dopamine transporters to track dopaminergic nigrostriatal pathways (Stoessl, Lehericy, and Strafella 2014). Its main indication is the distinction between a tremor-dominant PD and an essential tremor, but it cannot discriminate between PD and atypical parkinsonian disorders like MSA or PSP (Chou 2021). [$^{18}$F]-fluorodeoxyglucose positron emission tomography (FDG-PET) can be used to assess regional cerebral glucose metabolism and [$^{18}$F]-DOPAL-6-fluoro-3, 4-dihydroxyphenylalanine ($^{18}$F-DOPA) PET shows a decreased striatal F-DOPA uptake in early PD (Teune et al. 2010). On suspicion of a familial PD, genetic analysis can be taken into consideration.

### 1.2.5. Treatment

The main goal in the management of PD is to alleviate the (non-)motor symptoms and to increase the quality of life. All pharmacological and non-pharmacological treatments (e.g., deep brain stimulation (DBS)) are just symptomatic therapies; so far (April 2022) there is no disease-modifying therapy available that could decelerate or stop the neurodegenerative processes (reviewed by (Radhakrishnan and Goyal 2018)). The most effective pharmacological therapy aims at the lack of dopamine due to the destruction of dopaminergic neurons, either by substitution of dopamine or stimulating dopaminergic receptors. Levodopa (or L-Dopa), a precursor of the endogenous dopamine able to pass the blood-brain-barrier, and its anti-parkinsonian effect was first discovered by Hornykiewicz and Birkmayer in 1961 and the benefit of high oral doses of levodopa could first be demonstrated in 1967 (Cotzias, Van Woert, and Schiffer 1967). Since then, levodopa became the “gold standard” in treating PD at all stages, usually administered with a dopa-decarboxylase inhibitor like benserazide or carbidopa to reduce the daily doses and the adverse effects due to decreased peripheral dopaminergic stimulation. Long-term usage of levodopa often leads to motor fluctuations and dyskinesia, complicating the therapy and limiting its potential (LeWitt 2015). Dopamine agonists like pramipexole or ropinirole show no fluctuation in the therapy's effect but are accompanied by severe side effects like hallucinations, psychosis, impulse control disorders, and daytime sleepiness (Radhakrishnan and Goyal 2018). Monoamine oxidase-B inhibitors (selegiline, rasagiline) can be used in patients with mild symptoms or in combination with Levodopa (Spindler and Tarsy 2021). Drugs of further choice include catechol O-methyltransferase (COMT) inhibitors, N-Methy-D-Aspartate (NMDA) receptor inhibitors, and anticholinergics (especially for tremor-dominant PD) (Beitz 2014). Supportive non-pharmacological treatments include physical activity and exercises, speech therapy, nutrition, and support groups (Beitz 2014). Patients with motor complications can benefit from surgical procedures like the deep brain stimulation (DBS) of either the subthalamic nucleus (STN) or internal pallidal segments (GPi) (Kalia, Sankar, and Lozano 2013). Other interventional treatments include MRI-guided focused ultrasound ablation, unilateral (sub)thalamotomy or pallidotomy, and the implantation of a drug pump (Chou and Tarsy 2022).

Gene therapy (reviewed by (Axelsen and Woldbye 2018)), neural transplantations to replace the dopamine-producing cells in the brain (Freed et al. 2001; Olanow et al. 2003), or drug delivery via EVs (Yang et al. 2021) are some of the recent investigational therapies still under research with partly promising results for the future.

## 1.3. Mitochondria and Parkinson's disease

### 1.3.1. Mitochondrial dysfunction in PD

The first discovery linking mitochondrial dysfunction and PD was made in the 1980s when drug addicts developed symptoms of parkinsonism after consuming a new synthetic heroin containing MPTP, an inhibitor of multiple complexes of the respiratory chain and selectively taken up by dopaminergic cells (Langston et al. 1983; Storch, Ludolph, and Schwarz 2004). Rotenone, an inhibitor of complex I of the respiratory chain in mitochondria, can also cause Parkinson-like symptoms (Greenamyre, Higgins, and Eller 1992). The observation of impaired respiratory chain function in post-mortem brain sections from PD patients supported the role of mitochondria in PD (Schapira et al. 1989). Monogenetic PD forms also exhibit mitochondrial involvement. Mutations in the αSyn gene (SCNA) can cause early-onset dominant PD (Polymeropoulos et al. 1997) and different organelles including mitochondria were identified inside Lewy bodies (Shahmoradian et al. 2019). Furthermore, αSyn accumulations could be detected in mitochondria reducing complex I function and increasing mitophagy *in vivo* (Chinta et al. 2010). Mutations in *Parkin* (PARK2) and *PINK1* (PARK6) can both result in autosomal recessive PD and both proteins (*Parkin* is an E3 ubiquitin ligase, *PINK1* = PTEN-induced putative kinase protein 1) are involved in mitochondrial quality control, regulation of mitochondrial homeostasis and mitophagy (reviewed by (Borsche et al. 2021)). The current model suggests the following: Under dysfunctional conditions, *PINK1* is stabilized on the outer mitochondrial membrane (despite being imported into mitochondria under healthy conditions) and phosphorylates diverse substrates (inter alia *Parkin*). *Parkin* is then recruited, translocated to the damaged mitochondria, activated, and finally initiates mitophagy (Pickrell and Youle 2015). Knocking down *PINK1* or *parkin* resulted in a reduced mitophagy, reduced clearance of damaged mitochondria, and their intracellular

accumulation (Wu et al. 2015). However, mitophagy is not the only mechanism for eliminating damaged mitochondria. Another mechanism consists of the formation of mitochondrial-derived vesicles (MDVs) that can carry damaged cargo, leading to its lysosomal degradation and elimination (Soubannier et al. 2012). Similar to their effect on mitophagy, the loss of *PINK1*- or *Parkin*-dependent vesicle trafficking mechanisms lead to an impaired ability of mitochondria to degrade damaged proteins resulting in mitochondrial dysfunction (McLelland et al. 2014). *PINK1* also has a direct effect on the respiratory chain function since loss-of-function mutations in *PINK1* diminish complex I activity (Morais et al. 2014). Another PD-linked gene, *LRRK2*, also impairs the *PINK1/Parkin*-dependent mitophagy (Bonello et al. 2019). And finally, DJ-1 which can cause an autosomal recessive form of PD in case of a mutation (Bonifati et al. 2003) directly translocates to mitochondria to reduce oxidative stress (Andres-Mateos et al. 2007).

### 1.3.2. Mitochondrial DNA damage in PD

Mitochondria are the only organelles in the human cell which contain their own DNA. It is located within the inner matrix of the mitochondrion and each mitochondrion possesses several copies of the mitochondrial genome (Keogh and Chinnery 2015). The 16,569 base-pairs (bp) form a closed circle of double-stranded DNA like in procaryotic cells, encoding for 37 genes, 2 rRNAs, and 22 tRNAs. This “equipment” allows the mtDNA to synthesize 13 peptides, subunits of the complexes I, III, IV, and V of the respiratory chain (reviewed by (Mishra and Chan 2014)). Due to the lack of histones and effective repair mechanisms, the mtDNA is susceptible to mutations as well as single- and double-strand breaks (Larsson and Clayton 1995; Shokolenko et al. 2009). One major cause of mtDNA damage are free radicals and active quinones, summarized as reactive oxygen species (ROS), that can emerge from respiratory chain dysfunction or auto-oxidation of dopamine (LaVoie and Hastings 1999). A strong link between mtDNA and PD involves the DNA polymerase γ (POLG). POLG is the only known mammalian DNA polymerase in mitochondria (encoded in the nuclear DNA (nDNA)), responsible for maintaining mtDNA homeostasis (Chan and Copeland 2009) and mutations in the POLG gene can cause inherited PD (Davidzon et al. 2006). Although no inherited mtDNA mutations in PD are

(yet) known, somatic alterations in mtDNA often occur during the disease process (Giannoccaro et al. 2017). Postmortem SN neurons from patients with sporadic PD exhibited a reduction in mtDNA copy numbers (Grünewald et al. 2016; Dolle et al. 2016; Pyle et al. 2016) and high levels of deleted mtDNA (Bender et al. 2006), although no increased mtDNA point mutational load was measured (Dolle et al. 2016). However, two other studies from 2012 and 2016 detected significantly higher somatic mtDNA mutation levels in SN neurons from early PD and incidental DLB patients (Lin et al. 2012; Coxhead et al. 2016). It was shown, that dopaminergic neurons are particularly susceptible to mtDNA damage since the dopamine metabolism drives the generation and accumulation of mtDNA mutations and deletions (Neuhaus et al. 2014). The “common deletion” is a 4,977-base-pair deletion located between the MT-ATP8 and MT-ND5 genes including four genes coding for complex I of the respiratory chain (MT-ND3, MT-ND4, MT-ND4L, and MT-ND5) (Ikebe et al. 1990). The mtDNA deletion load is usually measured by calculating the ratio of a frequently deleted gene (e.g., MT-ND4) and a commonly not deleted gene (e.g., MT-ND1) by using quantitative PCR (qPCR) (Müller-Nedebock et al. 2019). Cell-free circulating mtDNA (cf-mtDNA) in CSF was firstly analysed in AD patients (Podlesniy et al. 2013) and it was later revealed, that the level of cf-mtDNA in CSF from PD patients is also significantly lower than in controls (Pyle et al. 2015). Furthermore, it was discovered that *Parkin* has a direct effect on the mitochondrial genome by binding to TFAM, the mitochondrial transcription factor A, which modulates gene expression of the mtDNA (Kuroda et al. 2006). It is therefore postulated that *Parkin* has a neuroprotective effect on dopaminergic SN neurons, preserving mtDNA against mutagenic stress (Pickrell et al. 2015). Another focus of interest is the association between mtDNA haplogroups and the risk of PD: Multiple European haplogroups (including J, K, and U) have been linked to a reduced PD risk, although the results are not consistent and other groups could not confirm these findings (reviewed by (Müller-Nedebock et al. 2019)). Finally, it was shown recently that mtDNA levels in EVs decline with age (Lazo et al. 2021).

## 1.4. Biomarkers in neurodegenerative diseases

### 1.4.1. Definition “Biomarker”

The Biomarkers Definitions Working Group from the U.S. National Institutes of Health (NIH) defined the term “biomarker” in 2001 as follows: “A characteristic that is objectively measured and evaluated as an indicator of normal biological processes, pathogenic processes, or pharmacologic responses to a therapeutic intervention.” ('Biomarkers and surrogate endpoints: preferred definitions and conceptual framework' 2001). Since not all biomarkers are objectively measurable (e.g., histological or radiological findings) and the definition concentrates on pharmacological responses and lacks other treatments (e.g., surgery), another definition of biomarkers might be more suitable: “A biological observation that substitutes for and ideally predicts a clinically relevant endpoint or intermediate outcome that is more difficult to observe.” (Aronson and Ferner 2017). The most important advantage of biomarkers is that they can be measured more easily and repeatedly over some time instead of waiting for the final clinical endpoint, therefore allowing clinical trials to be completed in a shorter time and with fewer subjects (Aronson and Ferner 2017). Biomarkers can be used for a variety of applications. The most common application might be as a diagnostic tool (e.g., blood glucose levels or $HbA_{1c}$ for the diagnosis of diabetes mellitus). In this context, they can also be used as screening parameters (e.g., PSA for the diagnosis of prostate cancer). When it comes to cancer, biomarkers are often used for staging or classifying the extent of a tumor or to screen for metastases after cancer therapy (various tumor markers like calcitonin in medullary thyroid cancer) (Wu and Qu 2015). Other applications of biomarkers include the prediction of a disease prognosis (e.g. tumor shrinkage or growth after cancer therapy) and monitoring or predicting the clinical response to an intervention ('Biomarkers and surrogate endpoints: preferred definitions and conceptual framework' 2001). Regarding biomarkers in cancer, another popular term refers to “liquid biopsy”, i.e., parameters from biological fluids such as blood or urine instead of tumor tissue to detect, analyse and monitor cancer (Poulet, Massias, and Taly 2019). Therefore, EVs can serve as liquid biopsies for various cancer types. The first step in identifying a suitable biomarker is to understand the pathophysiology behind a disease respectively the

mechanisms of how an intervention works or affects the pathophysiology (cholesterol might serve as a biomarker for atherosclerosis since elevated blood cholesterol levels play a crucial role in the formation of plaques) (Aronson and Ferner 2017). The next step would be to create and establish a method to measure/observe the suggested biomarker in the most objective way possible (e.g., high interrater reliability or high test-retest reliability). Finally, the biomarker must be validated, often in a retrospective analysis: How strong is the linkage between the biomarker and the clinical endpoint? How reliable is the suggested biomarker in predicting the clinical endpoint (Aronson and Ferner 2017)?

### 1.4.2. EV-based biomarkers in PD

The main pathology behind PD as described above is the formation of Lewy bodies consisting of αSyn. Different studies reported lower αSyn levels in the CSF of PD patients compared to healthy controls (Hong et al. 2010; Mollenhauer et al. 2011). Since red blood cells and platelets also produce abundant αSyn, blood αSyn levels are inconsistent and not suitable as a biomarker (Shi et al. 2010). It was also shown that αSyn containing exosomes can pass the BBB and enter the circulatory system and that exosomal αSyn is relatively specific to the CNS, despite just a small portion of the total αSyn being enclosed in exosomes (Shi et al. 2014). The same study reported higher αSyn levels in neuronal-derived ($L1CAM^+$) exosomes in PD patients compared to healthy controls and an association with the disease severity (Shi et al. 2014). Exosomes filled with αSyn could also be detected in the CSF with decreased αSyn levels in PD patients compared to controls (Stuendl et al. 2016). Furthermore, higher levels of oligomeric αSyn and oligomeric αSyn/total αSyn were measured in exosomes isolated from saliva from PD patients in comparison with healthy controls (Cao et al. 2019). Tau is another protein associated with neurodegenerative diseases and can pass the BBB similar to αSyn via $L1CAM^+$ exosomes (Shi et al. 2016). In PD (but not in AD) tau levels in $L1CAM^+$ exosomes isolated from human plasma were reported to be higher in PD patients compared to controls and the $L1CAM^+$ exosomal tau levels correlated with the CSF tau levels (Shi et al. 2016). Mutations in the LRRK2 gene cause familial and late-onset sporadic PD and LRRK2-

positive exosomes were found in urine and CSF (although many other cell types apart from neurons like kidney epithelial cells secrete LRRK2) (Fraser et al. 2013). LRRK2 levels in urinary exosomes were reported to be higher in men than women, to be elevated in PD patients when compared with controls, and to correlate with the severity of cognitive impairment (Fraser et al. 2016). This gender difference in exosomal LRRK2 levels was also reported by another study (Ho et al. 2014). This study also postulated that the concentration of DJ-1 in urinary exosomes, another gene mutation that can cause autosomal-recessive PD, was 1.7-fold higher in male PD patients than in healthy controls and that its concentration increased with age. miRNAs in EVs are another possible target for biomarker research. The profiling of exosomal miRNA from CSF exosomes in PD and AD patients revealed 16 significantly upregulated (MiR-1, miR-19b-3p) and 11 significantly downregulated (miR-153, miR-409-3p, miR-10a-5p, let-7g-3p) miRNAs in PD (Gui et al. 2015). The exosomal transcripts including αSyn, tau, NFL, and DJ-1 also differed between AD and PD (Gui et al. 2015). Another study reported exosomal apolipoprotein A1 as a potential biomarker in PD: Plasma exosomes from PD patients at Hoehn and Yahr (HY) stages II and III were isolated and analysed for potential protein-based markers, showing decreased levels of exosomal apolipoprotein A1 in PD patients at HY stage III compared to stage II and a correlation with the disease progression (Kitamura et al. 2018).

## 1.5. Aims of the study

Based on previous findings of mtDNA deletions in PD, the suitability of mtDNA extracted from EVs as a biomarker for PD was tried to assess. Therefore, firstly a method had to be established to isolate EVs from human blood serum and CSF and to enrich the total serum EVs for neuronal-derived EVs. Secondly, another method had to be developed to extract DNA from the EV preparation with sufficient quality and quantity for quantitative real-time PCR (rtPCR). Thirdly, an existing PCR protocol for mtDNA using primers against the mitochondrial genes ND1 and ND4 had to be applied to the DNA preparations from serum and CSF samples from PD patients and controls, using samples from the biobank of the Clinic for Neurology Tübingen. The primary endpoint was defined as the ratio between the threshold values of ND4 and ND1 ($C_t$(ND4)/$C_t$(ND1)). Finally, a statistical

analysis of the obtained PCR data had to be carried out to answer the question of whether mtDNA in EVs can serve as a biomarker for PD.

# 2. Materials and Methods

## 2.1. Materials

### 2.1.1. Chemicals and Consumables

Most of the chemicals and consumables were purchased from Sigma-Aldrich (Merck KGaA, Darmstadt, Germany) and AppliChem GmbH (Darmstadt, Germany). Plastic consumables were purchased from Greiner Bio-One (Frickenhausen, Germany) and Eppendorf AG (Hamburg, Germany).

### 2.1.2. Solutions and Buffers

- Running buffer 10x
    - 151.5 g Tris-Base
    - 725 g glycine
    - 50 g SDS
    - fill up with distilled water to a total volume of 5 l
    - for use in Western Blot: dilute 1:10 in distilled water
- TBS 10x
    - 50 mM Tris-Base, pH = 7.4
    - 150 mM NaCl
    - dissolve in distilled water, adjust to pH = 7.5
    - for use in Western Blot: dilute 1:10 in distilled water and add Tween-20 to a concentration of 0.1%
- Stripping buffer
    - 50 g glycine
    - 1 g SDS (0.1%) or 10 ml 10% SDS solution
    - 10 ml Tween-20
    - fill up with distilled water to a total volume of 1 l and adjust pH = 2.2

### 2.1.3. Antibodies

Primary antibodies used for Western Blot and IP are listed in table 3.

***Table 3:*** *List of primary antibodies.*

| target | predicted target size | species | company | catalogue number | dilution |
|---|---|---|---|---|---|
| **CD9** | 25 kDa | mouse | Invitrogen, Thermo Fisher Scientific, Waltham, USA | MA1-19301 | 1:500 |
| **Monoclonal Anti-CD9-Biotin antibody** | 25 kDa | mouse | Sigma-Aldrich, Merck KGaA, Darmstadt, Germany | SAB4700094 | only used in IP |
| **CD63** | 26 kDa | rabbit | GeneTex, Alton Pkwy Irvine, USA | GTX37555 | 1:500 |
| **TSG101** | 46 kDa | mouse | GeneTex | GTX70255 | 1:500 |
| **Flotillin-1** | 48 kDa | mouse | BD Biosciences, San Jose, USA | 610820 | 1:500 |
| **L1CAM / CD171** | 200 kDa, cleavage products: 60 – 80 kDa | mouse | Thermo Fisher Scientific | UJ127 | 1:500 |
| | | mouse | Abcam, Cambridge, USA | ab80832 | 1:500 |
| **CD171 Monoclonal Antibody (eBio5G3 (5G3)), Biotin, eBioscience™** | | mouse | Thermo Fisher Scientific | 13-1719-82 | only used in IP |
| **Calnexin** | 90 kDa | rabbit | Enzo Life Sciences, Farmingdale, USA | ADI-SPA-860-F | 1:500 |
| **Vinculin** | 116 kDa | mouse | Sigma-Aldrich | V9131 | 1:20 000 |

Secondary antibodies for detection in Western Blots are listed in table 4.

***Table 4:*** *List of secondary antibodies.*

| target | company | catalog number | dilution |
|---|---|---|---|
| **Mouse IgG HRP Linked Whole Ab** | Sigma-Aldrich | NA931V | 1:5000 |
| **Rabbit IgG HRP Linked Whole Ab** | Sigma-Aldrich | NA934V | 1:5000 |

| | | | |
|---|---|---|---|
| **Rat monoclonal [H139-52.1] Anti-Mouse kappa light chain (HRP)** | abcam | ab99632 | 1:5000 |
| **IRDye® 800CW Goat anti-Mouse IgG (H + L)** | LI-COR | 926-32210 | 1:10 000 |
| **IRDye® 800CW Goat anti-Rabbit IgG (H + L)** | LI-COR | 926-32211 | 1:10 000 |

### 2.1.4. Commercial solutions and components

Commercial solutions and components are listed in table 5.

***Table 5:*** *List of commercial solutions and components.*

| solution / component | company |
|---|---|
| S-Monovette® 9ml Z | SARSTEDT AG & Co. KG, Nümbrecht, Germany |
| Millex-GP Syringe Filter Unit, 0.22 µm, polyethersulfone, 33 mm, gamma sterilized | Merck Millipore, Darmstadt, Germany |
| 14 mL, Open-Top Thinwall Ultra-Clear Tube, 14 x 95mm | Beckman Coulter, Krefeld, Germany |
| Dulbecco's Phosphate Buffered Saline | Sigma-Aldrich |
| Sepharose® CL-2B | Sigma-Aldrich |
| Telos column 15 ml | Kinesis, Wertheim, Germany |
| 20 µm polyethylene frits | Kinesis |
| NuPAGE LDS sample buffer 4x | Invitrogen™, Thermo Fisher Scientific |
| PageRuler™ Plus Prestained Protein Ladder, 10 to 250 kDa | Thermo Fisher Scientific |
| 4 – 12% gradient NuPAGE Bis-Tris-Gels | Invitrogen™, Thermo Fisher Scientific |
| Streptavidin Magnetic Beads (5 ml) | New England Biolabs, Ipswich, USA |
| Fluorescence Mounting Medium | Agilent Santa Clara, USA |
| LightCycler® 480 Multiwell Plate 96, white | Roche, Basel, Switzerland |
| LightCycler® 480 Sealing Foil | Roche |
| GeneRuler 1 kb Plus DNA-Leiter | Thermo Fisher Scientific |
| TriTrack DNA loading dye (6x) | Thermo Fisher Scientific |
| Qubit™ assay tubes | Invitrogen™, Thermo Fisher Scientific |
| cOmplete™, mini, EDTA-free protease inhibitor cocktail | Roche |

### 2.1.5. Commercial Kits

For the commercial kits used in this study refer to table 6.

***Table 6:*** *List of commercial kits.*

| kit | company |
|---|---|
| ExoQuick™ Exosome Precipitation Solution for Serum, Plasma and Tumor Ascites Fluid (5 ml) | System Biosciences, Palo Alto, USA |
| ExoQuick™-TC Exosome Precipitation Solution for Culture Media, Spinal Fluid and Urine (10 ml) | System Biosciences |
| RQ1 RNase free DNase | Promega GmbH, Mannheim, Germany |
| QIAamp DNA Micro Kit | QIAGEN, Hilden, Germany |
| Invitrogen™ Qubit™ dsDNA HS Assay Kit | Thermo Fisher Scientific |
| Quant-iT™ PicoGreen dsDNA reagent | Thermo Fisher Scientific |
| FastStart Essential DNA Green Master | Roche |
| Thermo Scientific™ Micro BCA™ Protein-Assay-Kit | Thermo Fisher Scientific |

### 2.1.6. Software

The software used in this project is listed in table 7.

***Table 7:*** *List of software.*

| software | company | application |
|---|---|---|
| MS Office Word | Microsoft | text writing |
| MS Office Excel | Microsoft | statistical analysis |
| EndNote X9 | Thomson Reuters | bibliography management |
| GraphPad Prism 8 | GraphPad Software Inc. | statistical analysis and graph creation |
| LightCycler® 96 software | Roche | rtPCR data |
| Image Studio Lite | LI-COR | Western Blot detection |
| ImageJ | National Institutes of Health | image analysis |

## 2.2. Methods

### 2.2.1. Test samples used for establishing the methods

#### 2.2.1.1. Blood serum

For the establishment of the methods, fresh serum from the author of this study was collected. Venous blood was drawn and collected in an S-Monovette® 9ml Z (SARSTEDT AG & Co. KG) containing a coagulation activator. After incubating for 45 min at room

temperature, the tubes were centrifuged for 10 min at 2000 x g. The supernatant was aspirated, and all samples were pooled together in a new bottle. The double amount of the recommended concentration of a protease inhibitor cocktail was added directly to the serum. The pooled serum preparation was aliquoted into 2 ml samples and stored until use at -80°C.

#### 2.2.1.2. Cerebrospinal Fluid

As test-CSF, old CSF samples from the biobank of the Hertie Institute could be used. These samples were stored at -80°C for a longer time and could not be used for ongoing studies at the moment or in the future. Partly because they were too old, poorly classified, or did not meet the criteria for nowadays studies. There were not just samples from PD patients, but also AD patients, healthy people, or patients with other brain conditions such as tumours. Since these samples were only used for trials and to test the methods, the condition of the donor was negligible.

### 2.2.2. EV Isolation Techniques

#### 2.2.2.1. Differential ultracentrifugation

##### 2.2.2.1.1. Serum samples

EVs were isolated from human serum using differential ultracentrifugation according to a protocol from (Thery et al. 2006) with some modifications. Frozen serum samples were thawed on ice and 1 ml of serum was diluted in PBS to a total volume of 12 ml. Samples were centrifuged for 30 min at 200 x g, the supernatant was transferred to an ultracentrifuge tube (Beckman Coulter) and centrifuged for 45 min at 12,000 x g. The supernatant was transferred to a new ultracentrifuge tube and EVs were pelleted at 110,000 x g for 2 hours. The supernatant was discarded, and the pellet was resuspended in a large volume of PBS (typical about 12 ml) and filtered through a 0.22-µm filter (Merck Millipore). The flow-through was collected in a new ultracentrifuge tube and centrifuged 70 min at 110,000 x g. The last centrifugation step described in the original protocol from Théry et al. 2006 (110,000 x g for 70 min) was omitted to prevent losing too many particles. All centrifugation steps were carried out at 4°C. The supernatant was removed,

and the pellet resuspended in 500 µl PBS for storage or in 50 µl of 20 mM HEPES buffer with 0.025% Tween, pH = 7.5 for NTA measurements. The ultracentrifugation steps were carried out in an OPTIMA XE ultracentrifuge (Beckman Coulter) with an SW 40 Ti swinging bucket rotor (Beckman Coulter)

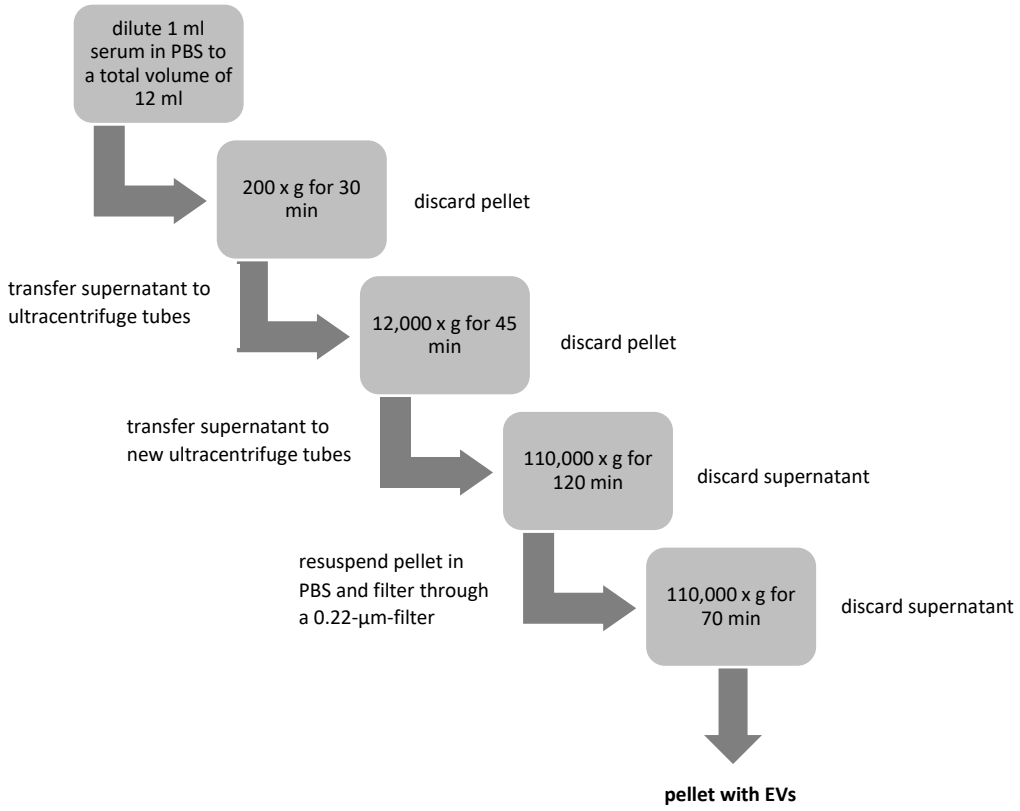


***Figure 2: Centrifugation steps for isolating EVs from serum samples.*** *Adapted from (Thery et al. 2006)).*

### 2.2.2.1.2. CSF samples

For EV isolation from CSF, centrifugation steps were replicated from a protocol from Strauss et al. 2010. CSF samples (1 ml) were thawed on ice and subjected to various centrifugation steps: 3500 x g for 10 min (two times), 4500 x g for 10 min, and 10,000 x g for 30 min. After each of these steps, the pellet was discarded, and the supernatant was transferred to a new tube for the next centrifugation steps. The remaining supernatant after the last step was filled in an ultracentrifugation tube and centrifuged for 60 min at 100,000 x g. The supernatant was discarded, and the pellet was washed with 2 ml PBS (because the smaller OPTIMA MAX tabletop ultracentrifuge (Beckman Coulter) was used) and again centrifuged at 100,000 x g for 60 min. After removing the

supernatant, the remaining pellet with the EVs was resuspended in a suitable buffer for downstream analysis (e.g., 50 µl of 20 mM HEPES buffer with 0.025% Tween, pH = 7.5 for NTA measurements). All centrifugation steps were performed at 4°C.

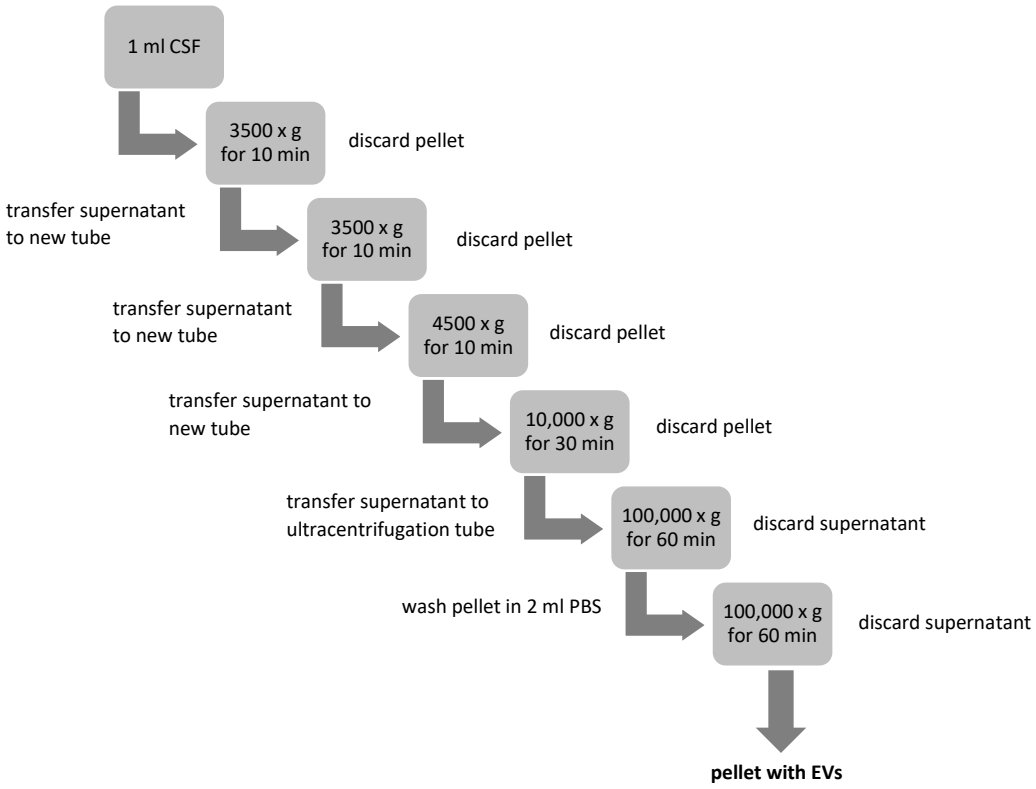


***Figure 3: Centrifugation steps for isolating EVs from CSF samples.*** *Adapted from (Strauss et al. 2010).*

### 2.2.2.2. Size-exclusion Chromatography

Size-exclusion chromatography makes use of the distinct size of EVs floating through a porous gel. Boing et al were the first who described this method in 2014 which was replicated in this study. Two washing steps with each 10 ml 0.32% tri-sodium-citrate in PBS removed the ethanol from the Sepharose CL-2B (Sigma-Aldrich). A 15-ml column (Kinesis) was filled with pre-washed Sepharose CL-2B and equilibrated

***Figure 4: Demonstration of the setup of the SEC.*** *Private photo.*

with a variable volume of 0.32% tri-sodium-citrate in PBS till the settled Sepharose reached a volume of 10 ml. A 20 µm polyethylene frit (Kinesis) was placed at the top of the stacked Sepharose and just as the last drops of the tri-sodium-citrate buffer had entered the frit, 1 ml serum was pipetted on the top of the frit. From this moment forward the flow-through was collected in 0.5 ml fractions. After the serum had completely entered the frit, 0.32% tri-sodium-citrate in PBS was added to the column to prevent the Sepharose from running dry. 26 fractions à 0.5 ml were collected in total and used for downstream analyses.

Due to the high dilution of proteins in the running buffer, the protein concentrations in the earlier fractions were too low to run on a gel for Western Blot. A tri-chloroacetic acid (TCA) precipitation was performed on these fractions to concentrate the existing proteins in a lower volume. One volume of TCA stock was added to 4 volumes of sample (e.g., 125 µl TCA to 500 µl sample) and the mixture was incubated 10 min on ice. Centrifugation was performed at 14,000 rpm for 5 min at 4°C. The supernatant was removed with great caution to leave the pellet intact. The pellet was washed with 200 µl ice-cold acetone before another centrifugation step at 14,000 rpm for 5 min at 4°C. The supernatant was discarded, the pellet again washed with 200 µl acetone and centrifuged at 14,000 rpm for 5 min. After removing the supernatant, the pellet was air-dried at room temperature by opening the lid of the tube and waiting 5 – 10 min. NuPAGE LDS sample buffer 4x (Invitrogen™, Thermo Fisher Scientific) was added to the pellet.

#### 2.2.2.3. ExoQuick™ Kit

ExoQuick™ (System Biosciences) is a precipitation solution based on polyethylene-glycol and is used as a commercial kit to enrich EVs in a sample. Preparation of the serum or CSF samples included thawing them on ice and spinning at 3000 x g for 15 min. The supernatant was kept for the following steps. 125 µl ExoQuick™ was added to 500 µl serum supernatant, the tube was inverted several times to ensure proper mixing and incubated for 1 h at 4°C. For CSF samples, 200 µl ExoQuick™ precipitation solution was incubated overnight at 4°C with 1 ml of CSF supernatant. After this incubation time, the tubes were centrifuged at 1500 x g for 30 min, the supernatant was removed, and the

tubes took a second spin at 1500 x g for 5 min. After discarding the remaining supernatant, the pellet was resuspended in different buffers depending on the downstream analysis (table 6).

***Table 8:*** *Buffers for resuspension of the ExoQuick™ pellet according to the downstream analysis.*

| Downstream analysis | Buffer | Volume of Buffer |
|---|---|---|
| **Western Blot** | NuPAGE LDS sample buffer | 100 µl |
| **Immunoprecipitation** | PBS + PIC | 500 µl |
| **DNA extraction** | molecular grade water + PIC | 100 µl |
| **NTA** | 20 mM HEPES buffer with 0.025% Tween, pH = 7.5 | - 50 µl for CSF<br>- 100 µl for serum |

#### 2.2.2.4. Immunoprecipitation

Immunoprecipitation (IP) is a method, that uses the specific interaction between an antibody and its antigen to isolate a target protein from a mixture of different proteins (Kaboord and Perr 2008). Due to the specific binding of an antibody to its antigen, the desired protein can be captured, and the antigen-antibody complex can be precipitated from the solution. For these precipitation steps, antibodies are normally attached to a solid support. Traditionally, antibodies are immobilized on Protein A and G agarose beads. After centrifugation, the antigen-antibody-bead complexes are enriched in the pellet and can be separated from the supernatant. Another possibility is the usage of magnetic beads. The tubes with the solution and the magnetic beads are attached to a static magnet and the magnetic beads are attracted by the magnetic fields and accumulate on the side of the tube closest to the magnet. The supernatant can now be easily removed with a pipet since the beads with the desired proteins stick on the side of the tube. The big advantage of this method is the cleaner separation of beads and supernatant because of the missing pellet. Without a pellet, contamination of the final sample with unwanted proteins from the supernatant can be reduced to a minimum. Furthermore, the loss of protein through accidentally disturbing the pellet can be reduced to a minimum. Since serum contains huge amounts of proteins and surface proteins of EVs account only for a very small portion of all these proteins, the magnetic beads were qualified for our purpose. But even when using magnetic beads, two different

approaches can be considered. On the one hand, you can incubate the antibodies with the beads at higher temperatures to bind the antibodies permanently to the beads. The antibody-bead complex can in the next step be incubated with the sample to pull down the corresponding proteins. On the other hand, you can make use of the streptavidin-biotin interaction, which is one of the strongest non-covalent bindings in nature. The tetramer protein streptavidin (MW = 25.8 kDa) was originally found in the hen egg white and can be purified from *Streptomyces avidinii* (Luong and Vashist 2019). Biotin (also known as vitamin B7) is an essential protein for the human body and serves as a cofactor for some carboxylases (Luong and Vashist 2019). Instead of coupling the antibodies directly to the beads, you can use biotinylated antibodies (commercial antibodies that are bound with their Fc part to biotin) and streptavidin magnetic beads (streptavidin that is attached to magnetic beads). It is now possible to capture the antibody-bound protein due to the strong interaction between streptavidin and biotin. This method is faster because when bringing streptavidin and biotin together, they react at a higher speed and the long step of binding the (pure) antibodies to the (pure) magnetic beads can be omitted. After trying both methods, we decided to go ahead with the streptavidin-biotin based method which is described in the following (also refer to the discussion section).

An IP-based method to isolate EVs makes use of surface markers on EVs which can be captured by antibodies. Eligible proteins are tetraspanins such as CD9 or CD81 or other transmembrane proteins like L1CAM. Since EVs from different fluids and organs differ in their surface protein profile, different subpopulations of EVs can be isolated by using different specific antibodies. This method was only applied to serum samples since the primary purpose was to isolate neuronal-derived EVs that are positive for L1CAM. EVs were isolated according to a protocol from (Mustapic et al. 2017) with a few modifications (visualised in figure 5). The first steps were identical to the isolation of EVs from serum using ExoQuick™ which is described above. The pellet after the last centrifugation step was resuspended in 500 µl PBS containing two times the suggested concentration of protease inhibitors. 4 µg of biotinylated antibody in a total volume of 50 µl 3% BSA in PBS was added to the suspension and incubated at 4°C for 1 h on a rotation mixer. Meanwhile, the streptavidin magnetic beads (New England Biolabs) had to be prepared: The

beads in the original tube were inverted several times to ensure proper mixing of the beads. 200 µl of the beads solution were transferred to a microcentrifuge tube, a magnet was applied to pull the beads to the side and the supernatant was removed. The beads were washed three times in total through resuspending in 1 ml binding buffer by pipetting up and down (20 mM Tris-HCl, pH = 7.5, 0.5 mM NaCl, 1 mM EDTA; recipe from the producer of the beads). After each washing cycle, the supernatant was removed. After the last washing step, the serum samples (with the biotinylated antibodies) were added to the washed streptavidin magnetic beads and the mixture was incubated for 30 min at 4°C with continuous mixing on a wheel. A magnet was subsequently applied, and the supernatant was removed. Three washing steps with each 1 ml 0.1% BSA in PBS, pH = 7.5 followed. Proper washing was ensured by inverting the tubes about 20 times or till the beads cluster had dissolved and by removing the supernatant after each washing cycle. After the last removal of the supernatant, the beads were resuspended in one of two different elution buffers: 100 µl 0.1 M glycine, pH = 2 for electron microscopy, and NTA analysis or 100 µl NuPAGE LDS sample buffer for Western blotting. The complete suspension (beads + elution buffer) was transferred to a new microcentrifuge tube. The tube was vortexed strongly for at least 30 s and centrifuged at 4500 x g for 10 min at 4°C to detach the EVs from the bead-antibody complex. The samples with NuPAGE LDS samples buffer were also boiled for 10 min at 95°C on a thermomixer with gentle shaking to reach a higher particle yield. A magnet was applied and the supernatant containing the EVs was transferred to a new tube. 15 µl 1 M Tris-HCl was added to the samples with glycine as the elution buffer to neutralize the sample. For a more detailed protocol please refer to the appendix.

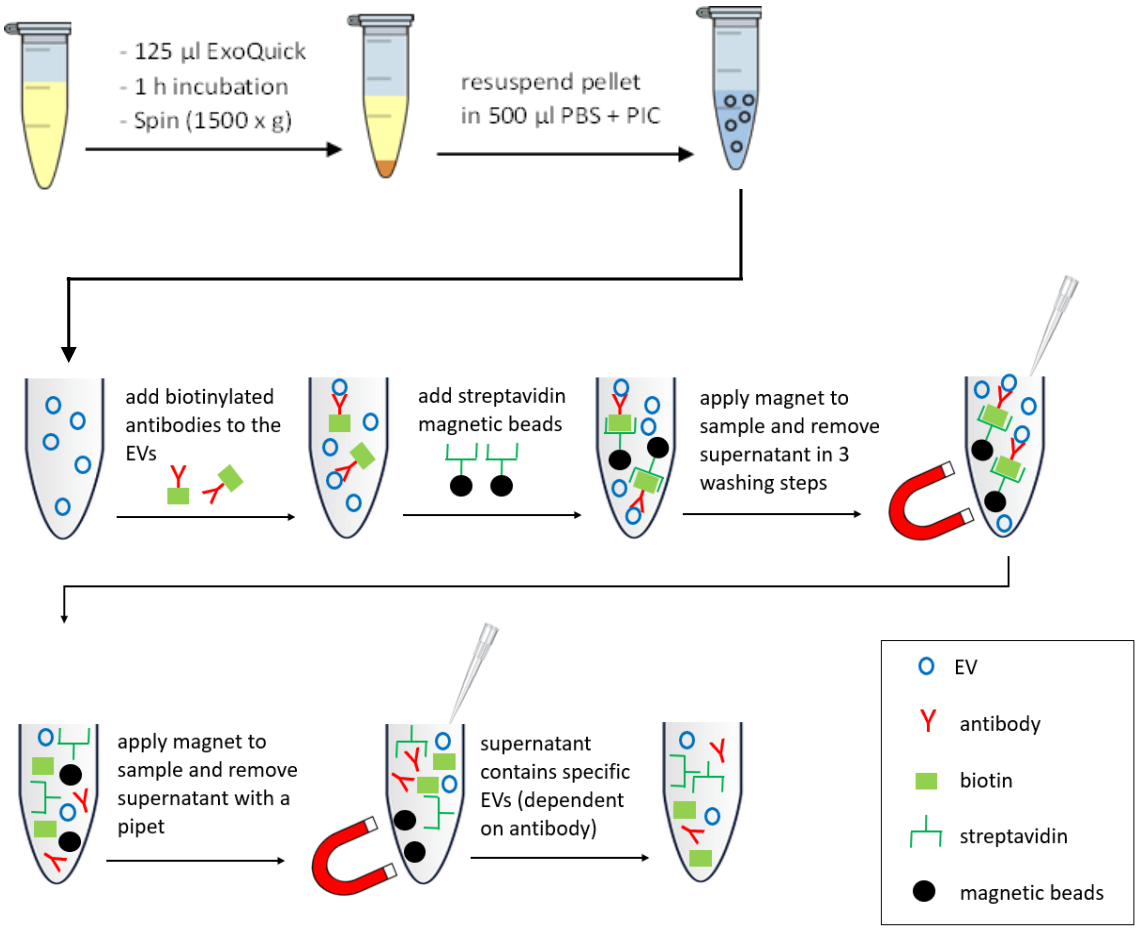


***Figure 5: Visualisation of the IP method to enrich an EV sample for a specific subpopulation of EVs depending on the antibody.*** *Adapted from (Mustapic et al. 2017).*

## 2.2.3. Characterization of EVs

### 2.2.3.1. Dynamic Light Scattering

DLS was performed on all samples but only the SEC samples are presented in the results part since the other samples were also analysed with NTA which provided better and more reliable results. Nevertheless, DLS is a good method to get a first impression of the size distribution of a sample. EVs from serum were analysed using SEC according to the protocol. 40 µl of each fraction was filled in a cuvette and analysed with a Zetasizer Nano ZS (Malvern Panalytical Ltd, Malvern, UK) 173° backscatter. Per sample, 3 runs à 15 single measurements were performed.

### 2.2.3.2. Nanoparticle Tracking Analysis

NTA was performed with a NanoSight NS300 (Malvern Panalytical Ltd) in the lab of Prof Anja Schneider at the DZNE in Bonn. UC, ExoQuick™, and IP samples were prepared in our lab, and samples were diluted in 20 mM HEPES buffer with 0.025% Tween, pH = 7.5. Dilutions varied between the samples depending on the suggested particle concentrations (table 7). A total volume of 400 µl was placed in a 2 ml tube and sent on cool pads to Bonn.

***Table 9:*** *List of samples for NTA with their buffers and dilutions.*

| method | fluid | volume | resuspension of the pellet / elution | final dilution | particle number in 1 ml |
|---|---|---|---|---|---|
| **UC** | CSF | 1000 µl | 50 µl HEPES-T | 10 µl sample in 390 µl HEPES-T | particle concentration x 200 |
| | serum (pure) | 1000 µl | 50 µl HEPES-T | 10 µl sample in 390 µl HEPES-T | particle concentration x 200 |
| **ExoQuick™** | CSF | 1000 µl | 50 µl HEPES-T | 10 µl sample in 390 µl HEPES-T | particle concentration x 200 |
| | serum (pure) | 500 µl | 100 µl HEPES-T | 5 µl sample in 395 µl HEPES-T | particle concentration x 3200 |
| **IP**<br>**- L1CAM**<br>**- CD9**<br>**- negative** | serum (in 500 µl PBS resuspended pellet of ExoQuick™) | 500 µl | 80 µl 0.1 M glycine in PBS + 20 µl 1 M Tris-HCl in PBS | 100 µl sample in 300 µl HEPES-T | particle concentration x 8 |

### 2.2.3.3. Electron Microscopy

Electron Microscopy was performed by Dr. Katharina Hipp at the Max-Planck Institute (MPI) in Tübingen. Samples were prepared according to the protocols and transferred on ice to the MPI. 4 µl of the samples were dropped on a grid that was prior taken to a

glow discharge unit making the surface of the grid negatively stained and more hydrophilic. The grid was pulled through a drop of water three times and the remaining fluid on the grid was soaked up with filter paper. This procedure was repeated using drops of 1% uranyl-acetate instead of water. Subsequently, one drop of 1% uranyl acetate was put on the grid, which was then incubated for 5 min at room temperature. The surplus fluid was soaked up and the grid was stored till performing the electron microscopy on the 120 kV Tecnai G2 Spirit BioTWIN (FEI Company, Hillsboro, USA).

#### 2.2.3.4. Western Blot

Samples were either resuspended in NuPAGE LDS sample buffer 4x (in a 1:4 dilution with PBS) or beads were eluted with a 1:4 dilution of the sample buffer in PBS or sample buffer was added to the sample (to a final 1:4 dilution). Samples were heated for 5 min at 95°C and loaded on 10- or 20-wells 4 – 12% gradient NuPAGE Bis-Tris-Gels (Thermo Fisher Scientific, Waltham, USA). An electrophoresis tank was filled with running buffer, the chamber with the gel was set into the tank, and proteins were separated for about 90 min at 100 V. Proteins were transferred to nitro-glycerine membranes using the iBlot 2 Dry Blotting System (Thermo Fisher Scientific). For total protein staining, the membranes were overlaid with Ponceau S solution (AppliChem GmbH) and placed on a shaker for 10 minutes. Incubation of the membranes with 5% milk in TBS-T for 1 h was used for blocking before the membranes were incubated with primary antibodies (diluted in 5% milk) overnight at 4°C on a roller. Unbound primary antibodies were removed by washing 6 times à 5 min with TBS-T the next day before incubating for 2 hours with the secondary antibody at room temperature on a roller (diluted in 5% milk). Depending on the primary antibody either fluorescence-labelled secondary anti-rabbit or anti-mouse antibodies (LI-COR, Bad Homburg, Germany) or HRP secondary antibodies (Sigma-Aldrich) were used. For special questions and to distinguish between the signal of the primary antibody and the heavy chain of IgG immune globulins an anti-Kappa light chain antibody (HRP coupled) (Abcam) was used. After a second washing step bands were detected depending on the type of the secondary antibody: For fluorescence-labelled secondary antibodies, membranes were scanned on the Odyssey® CLx Imaging System (LI-

COR). For HRP secondary antibodies membranes were incubated for 1 min with Amersham ECL Western Blotting Detection Reagent (GE Healthcare, Freiburg, Germany) before developing films using the film processor SRX-101A (Konica Minolta, Langenhagen, Germany).

#### 2.2.3.5. Bicinchoninic acid (BCA) Assay

Protein concentrations were measured with the BCA assay. Starting from a bovine serum albumin (BSA) stock solution with a concentration of 2 mg/ml, a dilution series was prepared according to the manufacturer's instructions with a protein concentration range between 0 µg/ml and 2000 µg/ml. 25 µl of the prepared BSA solutions were pipetted in each well of a 96-well plate in triplicates and 25 µl of the (diluted) sample was added (also in triplicates = 3 wells for each sample and each dilution). The master mix was prepared according to the manufacturer's instructions and 200 µl were added to each well. The plate was incubated for 30 min at 37°C and the optical density respectively absorption was measured at 563 nm in a plate reader. A standard curve was drawn with the measured data, plotting the absorption against the BSA concentration. The protein concentration in each well can be calculated with the following mathematical formula:

$$protein\ concentration\ [\frac{\mu g}{ml}] = \frac{absorption}{slope\ of\ the\ standard\ curve} * dilution\ factor$$

### 2.2.4. DNA analysis

#### 2.2.4.1. DNase digestion

To remove extra-vesicular DNA and other DNA contaminations in the sample, non-vesicular DNA was digested with the RQ1 RNase-free DNase (Promega GmbH). The DNase digestion was set up as follows: 70 µl sample, 10 µl 10x reaction buffer, 10 µl RNase free DNase (1 unit/µl). The digestion took place at 37°C for 30 minutes before adding 10 µl of RQ1 DNase Stop Solution for a total volume of 100 µl and incubating at 65°C for 10 minutes to inactivate the DNase.

#### 2.2.4.2. DNA extraction

DNA from EVs (and supernatant) was extracted using the QIAamp DNA Micro Kit (QIAGEN) according to the manufacturer's instructions with a few modifications (according to a protocol from (Thakur et al. 2014)): 100 µl of 100% ethanol instead of 50 µl was added to the sample in step 7 of the instruction and 30 µl AE buffer was used for the elution of the QIAamp MinElute columns in the last step. For more detail refer to the appendix. The Qubit™ fluorometer 3 (Invitrogen™, Thermo Fisher Scientific) confirmed the DNA concentrations in the samples. It was handled according to the manufacturer's instructions by using the Invitrogen™ Qubit™ dsDNA HS Assay Kit (Thermo Fisher Scientific) with 5 µl of sample volume as input.

#### 2.2.4.3. PicoGreen Staining of EV-associated DNA

DNA in EVs was stained with PicoGreen following a protocol published by Fernando et al. 2017: EVs isolated from 500 µl serum or 1 ml CSF using ExoQuick™ and from 500 µl serum with the IP method (antibody: anti-L1CAM) were resuspended in 100 µl ultrapure water and all samples except the IP samples were treated with 10 µl RNase-free DNase (Promega GmbH). 100 µl of the remaining supernatant from serum and CSF was kept and also treated with 10 µl DNase. After the DNA digestion was completed, 3 µl Quant-iT™ PicoGreen dsDNA reagent (Thermo Fisher Scientific) was added to each sample. They were incubated for 1 hour at RT. 100 µl of the sample were centrifuged (1500 rpm, 10 min) on slides using a Cellspin cytocentrifuge (Tharmac GmbH, Waldsolms, Germany). Slides were air-dried before mounting the samples with Fluorescence Mounting Medium (Agilent Santa Clara) and coverslips. Samples were analysed with Zeiss fluorescence microscope Axio Imager Z1 with Apotome 2 (Carl Zeiss AG, Oberkochen, Deutschland).

#### 2.2.4.4. Agarose Gel Electrophoresis

Agarose was added to TBS to produce a 3% agarose solution (3 g agarose in 100 ml TBS). The suspension was boiled up in a microwave and cooled down to approx. 60°C. 2 – 3 µl ethidium bromide was added per 10 ml gel solution and the mixture was filled in a

chamber with a casting frame on one side. After solidifying, the casting frame was removed and the gel was put in an electrophoresis unit with TBE running buffer. One volume loading dye 6x was added to five volumes sample. The samples were vortexed and loaded on the gel. The first chamber was filled with a DNA ladder (1 µg). The gel was run at 150 V for about 90 min and finally, the gel was visualized under UV light.

#### 2.2.4.5. rtPCR

Real-time PCR (rtPCR) was performed using the LightCycler® system by Roche with SYBR Green as the detection format. Two primers amplified a short part of the ND1- and ND4-gene of the mitochondrial DNA and a third primer (ACTB) amplified a segment of the human β-actin gene which is localized on the nuclear genome (base sequences for the β-actin primers were taken from (Fernando et al. 2017)). Information about the primers and the amplified segments can be found in table 10:

***Table 10:*** *Primer for rtPCR.*

| Gene | Sequence | | Amplicon length |
|---|---|---|---|
| **ND1** | forward | 5' – CCC TAA AAC CCG CCA CAT CT – 3' | 69 bp |
| | reverse | 5' – GAG CGA TGG TGA GAG CTA AGG T – 3' | |
| **ND4** | forward | 5' – CCA TTC TCC TCC TAT CCC TCA AC – 3' | 84 bp |
| | reverse | 5' – CAC AAT CTG ATG TTT TGG TTA AAC TAT ATT T – 3' | |
| **ACTB** | forward | 5' – GCC AGG GCT TAC CTGG TAC ACT – 3' | 76 bp |
| | reverse | 5' – GTC ACA CTT GGC CTC ATT TTT – 3' | |

For rtPCR, one PCR Mix for each primer pair (forward + reverse) was prepared according to table 11.

***Table 11:*** *Composition of the PCR Mix for ONE DNA sample.*

| Reagent | Volume |
|---|---|
| Water, PCR grade | 2 µl |
| PCR Primer (1:10 dilution) | 1.4 µl<br>- 0.7 µl forward-primer<br>- 0.7 µl reverse-primer |
| Master Mix | 6.6 µl |
| Total volume | 10 µl |

Primers were diluted 1:10 in molecular-grade water (separate for forward and reverse) before adding them to the PCR Mix. All reagents were mixed before pipetting 10 µl of the PCR Mix in each well of a 96-well plate. In every well, 3.3 µl of the DNA sample was added to a total volume of 13.3 µl per well. The multiwell plate was sealed with sealing foil and centrifuged at 600 x g for a few seconds. The plate was loaded into the LightCycler® 96 instrument (Roche) and the PCR reaction was started. For the settings of the PCR cycles refer to the appendix. Results were analysed with the LightCycler® 96 software.

### 2.2.5. Data analysis and statistics

Data and statistical analysis were performed with Microsoft Office Excel 2019 software (Microsoft, Redmond, USA) and GraphPad Prism® 8 software (GraphPad Software Inc., San Diego, USA). The Student's two-sided t-test was performed on normally distributed, independent data sets. A p-value < 0,05 was considered significant. Values are given as mean + standard deviation (SD).

## 2.3. Ethics

The study was approved by the Ethics Committee of the University of Tübingen (199/2011BO1 for samples from the biobank of the Hertie Institute for Clinical Brain Research (HIH) Tübiinigen and 586/2018B02). Participants gave written informed consent according to the Helsinki Declaration.

# 3. Results

## 3.1. Characterization of EVs

### 3.1.1. Electron Microscopy

TEM images taken from EV samples isolated with different techniques revealed the presence of round vesicle-like structures with sizes between 25 and 120 nm. Total EVs from 500 µl serum respectively 1000 µl CSF were isolated using the ExoQuick™ kit and the pellets were resuspended in 100 µl PBS. For L1CAM$^+$ EVs, the IP method with biotinylated anti-L1CAM antibodies and magnetic beads was applied. The EVs were eluted from the beads with 100 µl of 0.1 M glycine in PBS (pH = 2). Especially EVs from serum and CSF isolated with ExoQuick™ showed an average particle size of around 35 nm with very few particles bigger than 50 nm. Only in samples of the IP method with anti-L1CAM antibodies, bigger particles up to 120 nm could be found, but the majority of vesicles had sizes of approx. 60 nm (figure 1C). The number of EV-like particles under the microscope differed highly between the samples. While ExoQuick™ samples of CSF and serum had to be diluted 1:5 respectively 1:10 to obtain a good picture, no dilution was required for the L1CAM$^+$ EVs, and the concentration of these particles was even without dilution much lower compared to total serum and CSF EVs. Also, the purity of the preparations

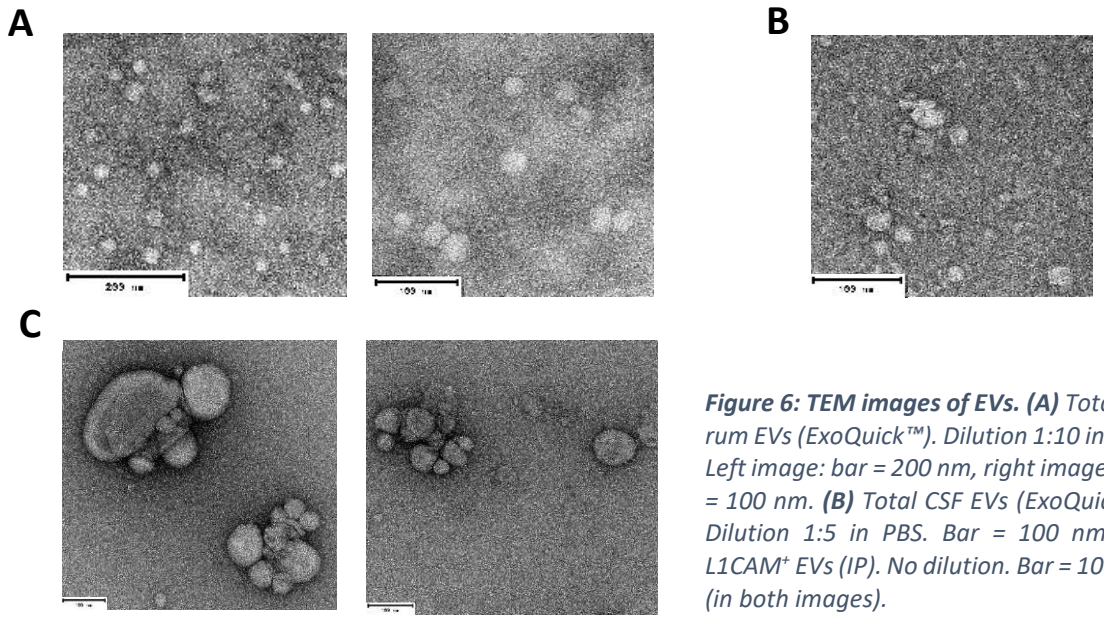


***Figure 6: TEM images of EVs. (A)*** *Total serum EVs (ExoQuick™). Dilution 1:10 in PBS. Left image: bar = 200 nm, right image: bar = 100 nm.* ***(B)*** *Total CSF EVs (ExoQuick™). Dilution 1:5 in PBS. Bar = 100 nm.* ***(C)*** *L1CAM$^+$ EVs (IP). No dilution. Bar = 100 nm (in both images).*

differed widely between the samples: While EVs samples isolated with ExoQuick™ (especially serum) were quite impure with a large amount of very small particles and a high background signal, the IP samples displayed much fewer contaminants.

### 3.1.2. Nanoparticle Tracking Analysis

NTA is a method to measure the size distribution of particles and the particle number in a solution. NTA was performed on almost all isolation techniques. All measured samples revealed particles in a size between 10 and 150 nm with different peaks and particle concentrations. UC from serum and CSF demonstrated a wide range of particle sizes with multiple peaks and much lower particle concentrations in comparison with the ExoQuick™ preparations (all particle numbers standardized to 1 ml sample). The difference between both methods was most obvious in serum samples: ExoQuick™ obtained 112-times more particles/ml than UC. Similar to the results from the UC samples, CSF particles isolated with ExoQuick™ presented a wide range of sizes, while serum particles isolated with ExoQuick™ were concentrated in two major peaks at about 50 and 100 nm. The most homogenous particle population was obtained with the IP method. Especially the usage of the anti-L1CAM-antibody to capture $L1CAM^+$ vesicles displayed one major peak at the size of 110 nm and a smaller peak at around 75 nm. By using an anti-CD9-antibody (a more general vesicle marker), fewer particles were isolated. In summary, ExoQuick™ from serum outranked all other isolation methods in particle yield (mean = 8,5 x $10^{11}$ particles in 1 ml serum, n = 3), followed by the IP from serum with antibodies against L1CAM (mean = 2.37 x $10^9$ particles in 1 ml serum, n = 5) and ExoQuick™ for CSF (mean = 2 x $10^9$ particles in 1 ml CSF, n = 3). UC on the other side resulted in much lower particle yields (UC serum mean = 5.58 x $10^8$ particles in 1 ml serum, n = 1; UC CSF mean = 1.6 x $10^9$ particles in 1 ml CSF, n = 1). Regarding the purity and homogeneity of the isolated particles, UC provided the widest range of particles with multiple peaks, followed by the ExoQuick™ kit with a quite heterogeneous particle population as well. The antibody-based IP methods showed very clear peaks with fewer background signals. Both results also fit the EM images taken from the IP method. Figure 6 provides an

overview of the size distribution profiles and particle concentrations from the NTA measurements.

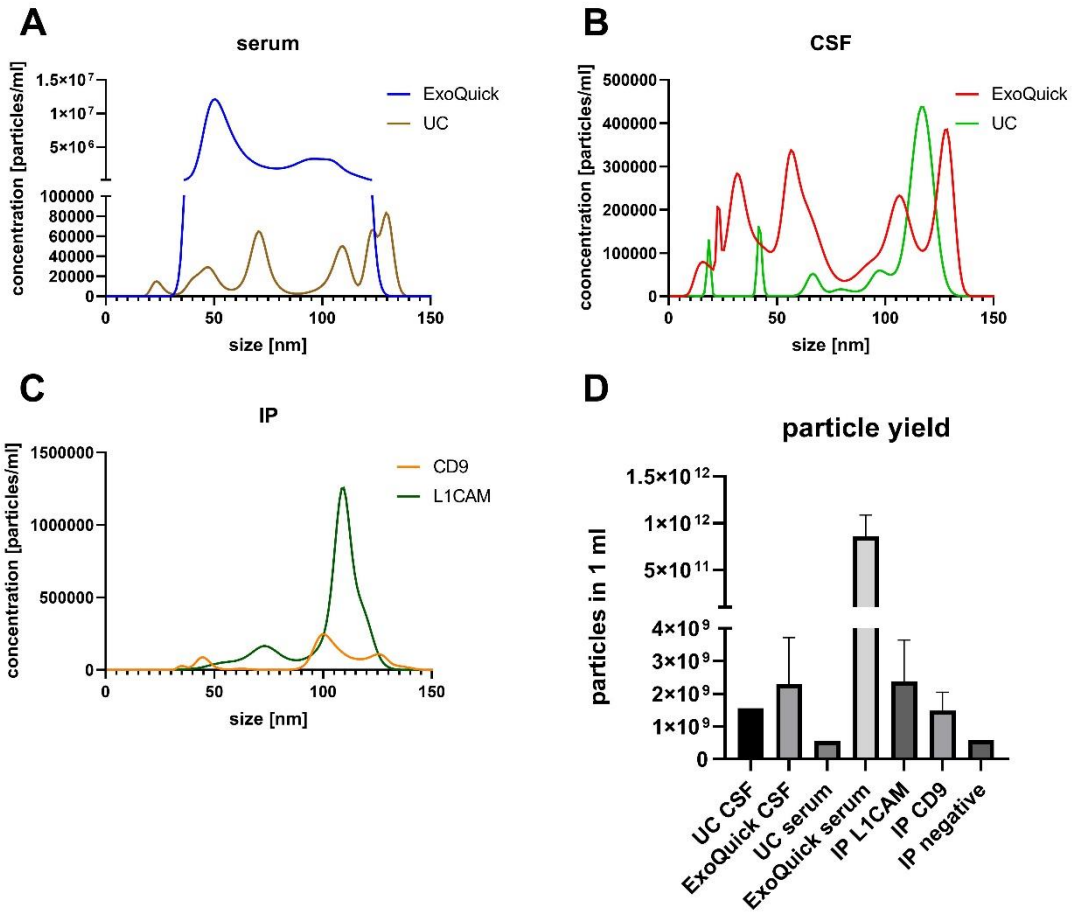


***Figure 7: NTA measurements of EV samples. (A)*** *Size distribution profiles of EVs isolated from 500 µl serum (each) using UC (brown line) and ExoQuick™ (blue line) showed multiple peaks in the UC preparation and two peaks at about 50 nm and 100 nm in the ExoQuick™ preparation. Also note the huge difference between the particle concentrations with approx. 112-times more particles per ml in the ExoQuick™ preparation than in the UC.* ***(B)*** *Size distribution profile of EVs isolated from 1000 µl CSF (each) using ultracentrifugation (green line) and ExoQuick™ (red line) displayed multiple peaks between 0 and 150 nm with one major peak in the UC sample at about 120 nm. The ExoQuick™ sample contained approx. 2.5-times more particles/ml than the UC sample.* ***(C)*** *Size distribution profile of EVs isolated from 500 µl serum using immunoprecipitation with antibodies against L1CAM (green line) and CD9 (orange line) showed a more homogenous particle population then the other isolation techniques with a major peak at about 115 nm in the L1CAM sample. The L1CAM sample contained approx. 3.5-times more particles/ml then the CD9 sample.* ***(D)*** *Comparison of the particle yields obtained by different isolation methods. ExoQuick™ serum outranked all other isolation methods followed by ExoQuick™ CSF and IP L1CAM with similar concentrations. Bar represents the absolute particle number in 1 ml fluid.* ***Annotation:*** *Particles were measured with a cut-off value of 140 nm. Values are given as mean ± SD.*

### 3.1.3. Western Blot

Western Blot analysis of EV samples allows the detection of EV marker proteins respectively the absence of contaminants. As cited above, the International Society for Extracellular Vesicles (ISEV) recommended in its positional paper from 2018 (Théry et al. 2018) to prove the presence of EVs and the absence of contaminants by detecting at least one protein of the following five categories (categories 4 and 5 not for all EVs):

***Table 12: Requirements for the characterization of EVs on a protein basis according to the ISEV.*** *Adapted from (Théry et al. 2018).*

| | **Application** | **Definition** | **Examples** |
|---|---|---|---|
| **Category 1** | for all EVs | transmembrane or GPI-anchored proteins as indicators for the lipid-bilayer structure of EVs | CD9, CD63, CD81, LAMP1/2, L1CAM (CD171) |
| **Category 2** | for all EVs | cytosolic proteins enclosed by the lipid bilayer with the ability to bind to lipids or membrane proteins | TSG101, Flotillin-1/-2, HSC 70, HSP90AB1, actin, tubulin |
| **Category 3** | for all EVs | absence of contaminants (non-EV structures), that are often co-isolated with EVs | apolipoprotein A1/2, albumin, uromodulin (in urinary EVs) |
| **Category 4** | for specific subpopulations of EVs (e.g., small EVs) | absence of proteins associated with other intracellular compartments than the plasma membrane or endosomes (e.g., endoplasmic reticulum, Golgi apparatus, nucleus, mitochondria) | nucleus: histones, mitochondria: cytochrome c, endoplasmic reticulum: calnexin |
| **Category 5** | for the functional component of EVs | secreted or luminal proteins that can bind to specific receptors on the EV surface | cytokines/growth factors, extracellular matrix proteins (e.g., collagen) |

Figure 7 summarizes the most important findings of the Western Blot experiments. EVs isolated with ExoQuick™ both from serum and CSF revealed the presence of different EV marker proteins: TSG101 (44 kDa), Flotillin-1 (47 kDa), and L1CAM (200 – 250 kDa). CD63 (26 kDa), another common marker protein for EVs, was only measurable in serum EVs and the signal was very weak and unstable (not repeatable in all Western blots) (figure 7B). On the one hand, it was not possible to detect calnexin, a marker for the

endoplasmic reticulum, in the EV preparations. On the other hand, calnexin could not be detected in serum supernatant either, suggesting that the antibody was not working sufficiently. The supernatants which remained after the isolation of EVs from CSF and serum served as a negative control and showed the absence of the aforementioned proteins although TSG101 and Flotillin-1 still emitted a faint signal but at a much longer exposure time. The strength of the bands can serve as an indicator for the amount of proteins loaded on the gel under the condition, that the same exposure times and detection mediums were applied to the samples. This is best seen in the TSG101 band. As a general EV marker protein, it can be found in serum and CSF EVs. Despite the double volume of CSF (1000 µl) used for the EV isolation with ExoQuick™ compared to the volume of serum (500 µl), the much stronger band in the serum EV sample implies a higher number of particles in this sample, an observation also emphasized by the NTA measurements. Nevertheless, the L1CAM band in the CSF EV sample is slightly stronger than in the serum EV sample. This higher L1CAM/TSG101 ratio in CSF EVs could indicate the enrichment of L1CAM in neuronal-derived EVs from CSF. Due to the capturing of L1CAM with an anti-L1CAM-antibody in the IP, L1CAM is highly expressed in these samples (figure 7A). Furthermore, also TSG101, Flotllin-1, CD63, and CD9 were detectable in the IP-L1CAM-samples. As a negative control, the same protocol as for $L1CAM^+$ EVs was followed with the difference, that no anti-L1CAM antibodies were added to the sample and the beads. No bands accounting for EV marker proteins were observed in these samples. In conclusion, the IP method makes it possible to enrich samples for different proteins (e.g., L1CAM) that cannot be found in the negative control; and the $L1CAM^+$ EVs also bear other EV marker proteins. Instead of an anti-L1CAM antibody to capture $L1CAM^+$ EVs, CD9 as a common EV marker can be used to capture CD9-expressing EVs. The direct comparison of $L1CAM^+$ and $CD9^+$ EVs (figure 7C) showed, that L1CAM, TSG101, and CD9 could be detected in both samples. The stronger L1CAM band in the $L1CAM^+$ EV sample seems plausible, but even the CD9 band is (despite the same sample input) more dominant in the $L1CAM^+$ EVs than in the $CD9^+$ EVs.

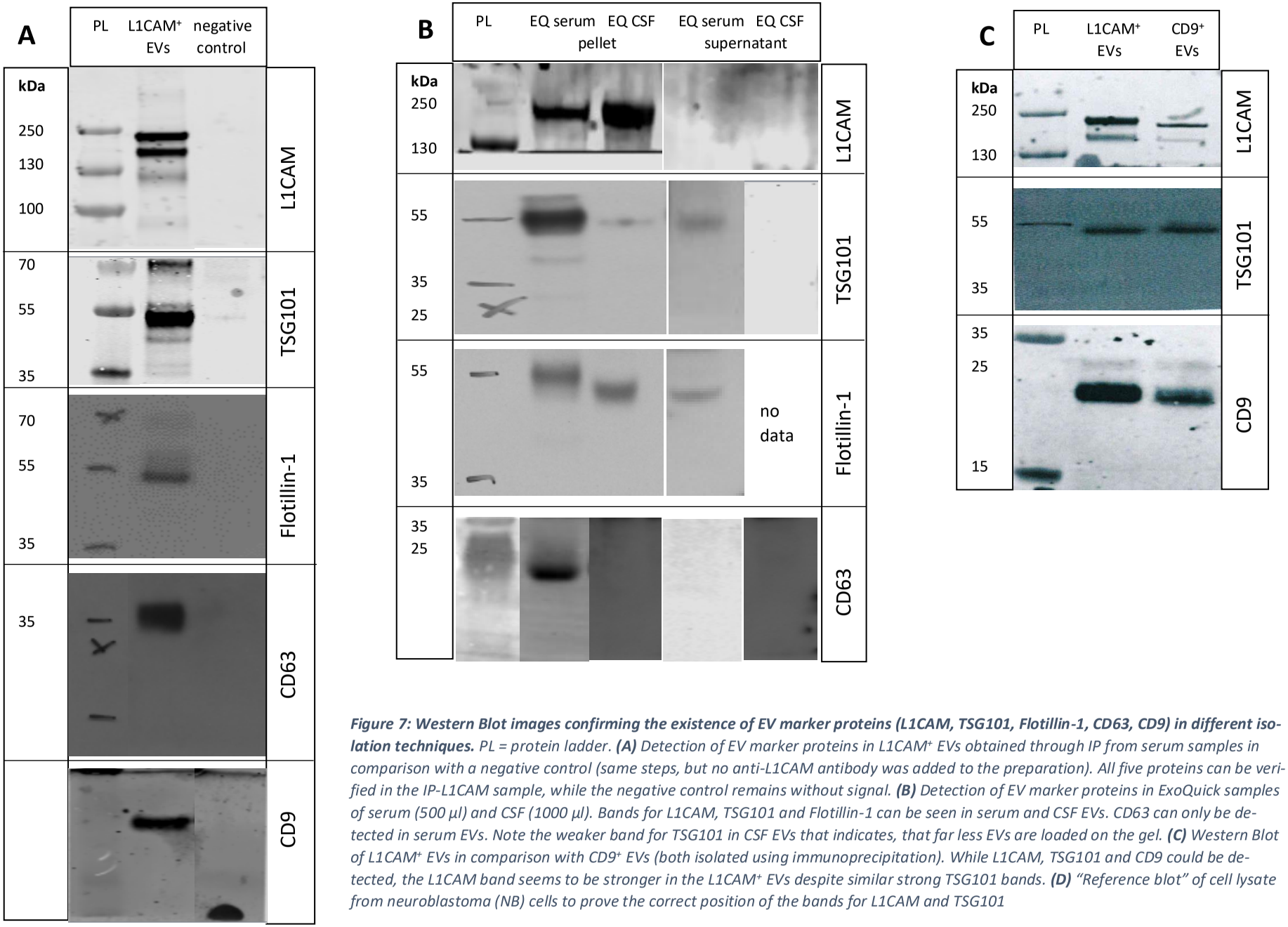


***Figure 7: Western Blot images confirming the existence of EV marker proteins (L1CAM, TSG101, Flotillin-1, CD63, CD9) in different isolation techniques.*** *PL = protein ladder.* ***(A)*** *Detection of EV marker proteins in L1CAM+ EVs obtained through IP from serum samples in comparison with a negative control (same steps, but no anti-L1CAM antibody was added to the preparation). All five proteins can be verified in the IP-L1CAM sample, while the negative control remains without signal.* ***(B)*** *Detection of EV marker proteins in ExoQuick samples of serum (500 µl) and CSF (1000 µl). Bands for L1CAM, TSG101 and Flotillin-1 can be seen in serum and CSF EVs. CD63 can only be detected in serum EVs. Note the weaker band for TSG101 in CSF EVs that indicates, that far less EVs are loaded on the gel.* ***(C)*** *Western Blot of L1CAM+ EVs in comparison with CD9+ EVs (both isolated using immunoprecipitation). While L1CAM, TSG101 and CD9 could be detected, the L1CAM band seems to be stronger in the L1CAM+ EVs despite similar strong TSG101 bands.* ***(D)*** *"Reference blot" of cell lysate from neuroblastoma (NB) cells to prove the correct position of the bands for L1CAM and TSG101*

### 3.1.4. Enrichment of L1CAM in neuronal-derived EVs

The whole concept of isolating neuronal-derived EVs as a subpopulation of all EVs is based on the specific enrichment of L1CAM at the surface of neuronal-derived EVs. When comparing total serum and total CSF EVs one would expect a higher expression of L1CAM in CSF exosomes than in serum EVs. Nevertheless, L1CAM should still be detectable in serum exosomes, because neuronal-derived exosomes can pass the BBB and can be found circulating in the blood. Considering the much higher number of total EVs in serum than in CSF, the number of EVs loaded on Western Blot must be standardized to examine the L1CAM expression. Due to a lacking possibility of exactly quantifying the number of EVs in a sample in the institute, the TSG101 band was taken as a reference. As mentioned above, TSG101 is a common EV marker and is found on EVs of variable origin. The intensity of the TSG101 band can be used as an indicator for the number of EVs loaded in the Western Blot (exemplary demonstrated in figure 8A). The quotient of the intensity of the L1CAM band divided through the intensity of the TSG101 band can serve as a rough idea about the enrichment of L1CAM in the EV preparation. The higher this quotient, the higher the enrichment of L1CAM in the sample. This procedure was applied in ExoQuick™ samples to compare total CSF and serum EVs. The relative intensity of TSG101 and L1CAM bands were measured in three independent Western Blots with 14 different serum and 14 different CSF samples using the free software ImageJ. The L1CAM/TSG101 ratio was significant higher in CSF EVs compared to serum EVs (serum EVs mean = 0.8557, SD = 0.126, n = 14; CSF EVs mean = 2.968, SD = 1.480, n = 14; **** $p < 0.0001$, Student's two-sided t-test) (figure 8B). L1CAM is a transmembrane protein that is especially expressed on neurons and plays a crucial role in neuronal differentiation (Salinas et al. 2008). To prove, that L1CAM is expressed on neuronal cells and to verify the localization of the L1CAM band for the other Western Blot experiments, lysate from a mouse brain cortex was run on a Western Blot and stained with an anti-L1CAM antibody as a positive control. The band at approx. 250 kDa represents the protein L1CAM and fit to the L1CAM band in the EV samples (figure 8C).

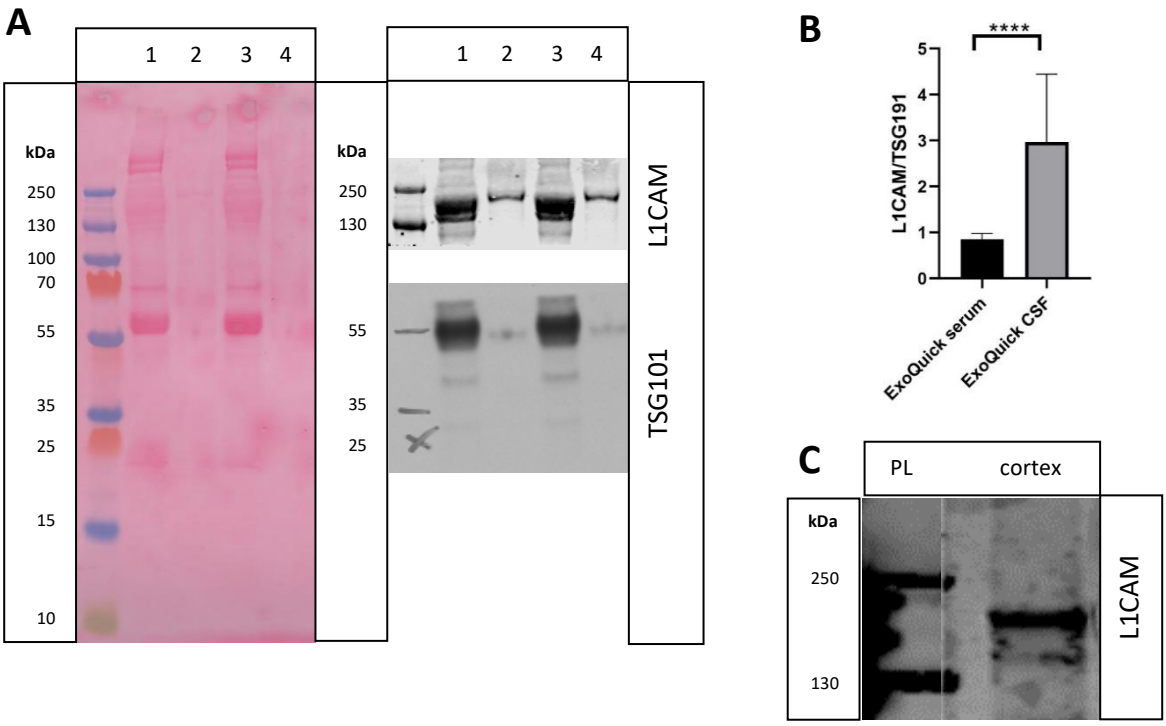


***Figure 9: Enrichment of L1CAM in neuronal-derived CSF EVs compared to serum EVs. (A)*** *Comparison of serum EVS (1, 3) and CSF EVs (2, 4) isolated with ExoQuick™. The Ponceau staining (left side) shows the difference in the protein composition between two serum and CSF EVs samples. The relative intensity of the TSG101 and L1CAM bands in the Western Blot (right side) were used to calculate the L1CAM/TSG101 ratio.* ***(B)*** *In CSF EVs, a significant higher L1CAM/TSG101 ratio can be measured compared to serum EVs (n = 14, **** p < 0.0001, Student's two-sided t-test). Values are given as mean ± SD.* ***(C)*** *Positive L1CAM staining in a lysate from a mouse brain cortex after incubating with an anti-L1CAM antibody in Western Blot (PL = protein ladder).*

## 3.2. Size-Exclusion-Chromatography

This isolation method is based on the flow of a viscous mobile phase (in our experiment the serum sample diluted in buffer) through a porous stationary phase (Sepharose CL-2B). Smaller particles like proteins and antibodies enter the pores in the Sepharose where they are trapped and elute later while bigger particles (like VLDL and HDL) cannot enter the small pores and are carried away through the flow of the mobile phase resulting in an elution in the earlier fractions. This separation method allows the enrichment of particles according to their sizes. Further advantages of this method include the efficient removal of proteins and lipids which elute in different fractions than the EVs with little overlap and the gentle treatment of EVs which preserves their integrity and functionality. To prove the elution of proteins, a BCA assay was performed on all 26 fractions. Figure 9B shows the protein concentrations of the 26 fractions à 0.5 ml. The protein

concentration increased from fraction 1 to 18 (with hardly any proteins in the first 7 fractions), reached its maximum in the 18$^{th}$ fraction, and decreased in the later fractions. All 26 fractions were still not enough to remove all the proteins from the column. This measurement was also supported by SDS page and subsequent Copper staining revealing the increase of the loaded protein amount from fraction 1 to 18 (equal volumes of each fraction were loaded) (figure 9A).

To confirm the size distribution of the particles in the different fractions, DLS measurements of selected fractions were performed. Fractions were chosen according to the literature that proclaims the vesicle peak in fractions 8 and 9 (Böing et al. 2014). Figure 9D summarizes the average size of the fractions 7 to 11 of one SEC experiment with 500 µl serum. As expected, the size of the isolated particles decreased from the earlier to the later fractions because larger particles elute earlier than smaller particles (also presented in figure 9E with the average sizes of the fractions from three replicates). Considering the average size of exosomes as a subpopulation of EVs between 40 and 160 nm, fractions 9, 10, and 11 show the strongest enrichment of exosomes. The comparison of this data with the protein concentrations in figure 9B suggests, that this method can successfully separate most of the proteins from the vesicles, resulting in a very clean and pure sample. Western Blot was performed to detect EV marker proteins in the sample. Despite several tries, CD63 and TSG101 could not be detected in any SEC fraction. Nevertheless, a distinct signal was obtained for L1CAM presented in figure 9C. The strongest L1CAM bands could be detected in the 10$^{th}$, 11$^{th}$, and 12$^{th}$ fraction, the same fractions that contain most of the EVs measured in the DLS. Interestingly, the later fractions with a much higher protein concentration did not emit a signal for L1CAM, indicating that L1CAM is a specific marker for EVs. These findings underline the use of anti-L1CAM-antibodies to capture EVs and strengthen together with the L1CAM/TSG101 quotient from the ExoQuick™ serum and CSF samples the expression of L1CAM on neuronal-derived EVs.

To complete the characterization of EVs obtained by SEC, TEM was performed on fraction 9. Round vesicle-like structures could be identified on the TEM images with diameters ranging from 30 nm to 80 nm (figure 9F).

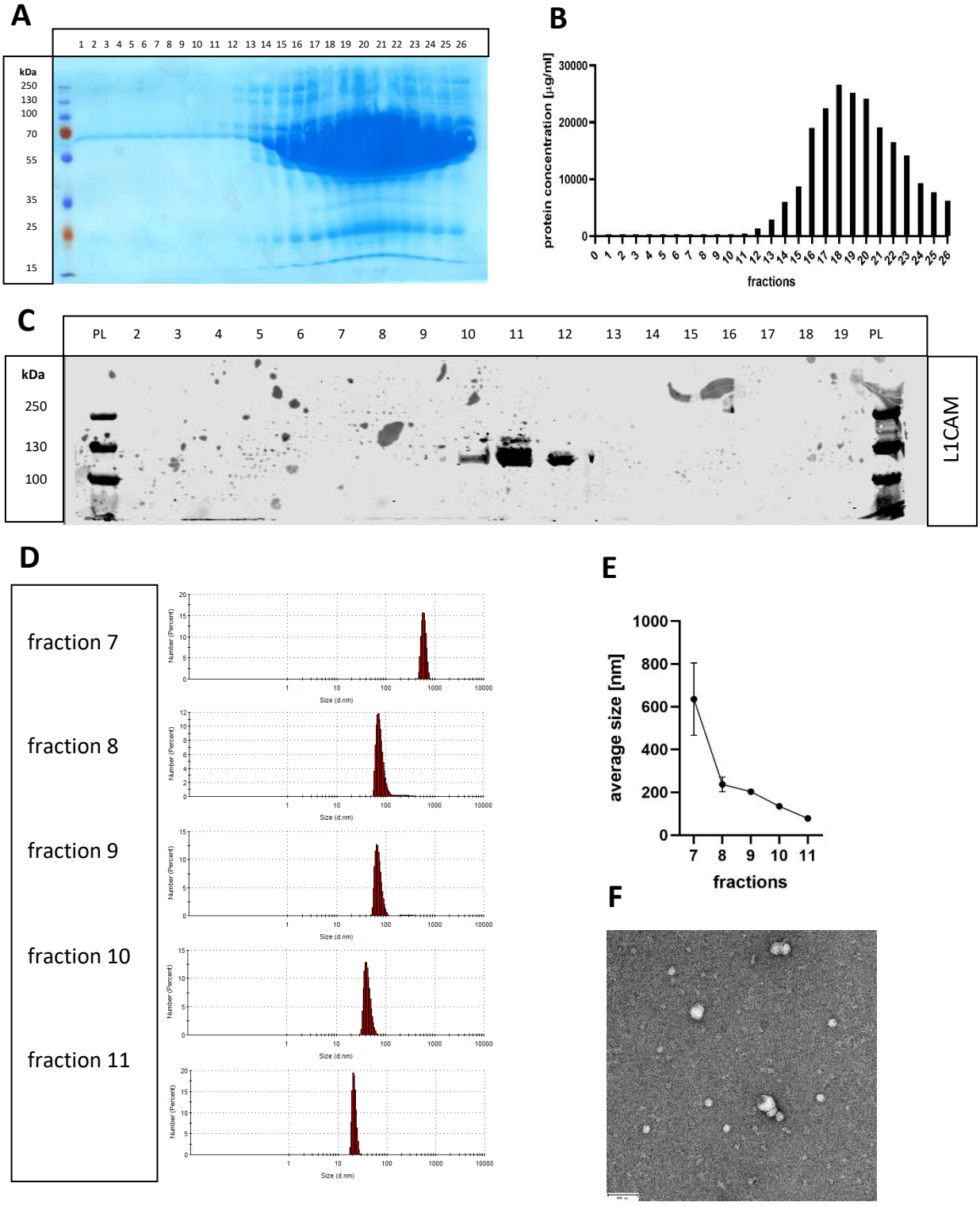


***Figure 10: Characterization of EVs isolated with SEC. (A)*** *Copper staining of a SDS gel with the 26 fractions obtained in one SEC from 500 µl serum (the numbers 1-26 in the upper bar stand for the fractions).* ***(B)*** *Correlation between protein concentration (measured with BCA assay) and SEC fraction. The protein concentration increases with the fractions and reaches its peak in the 18$^{th}$ fraction before decreasing again.* ***(C)*** *Western Blot with fractions 2 – 19 with a staining against L1CAM. Bands are only visible in fractions 10, 11 and 12 (PL = protein ladder).* ***(D)*** *Size distribution profile of different SEC fractions measured with DLS. The higher the fraction the smaller the particle size. Particles with a diameter of 100 nm have their peak in fractions 8 und 9.* ***(E)*** *Average size of particles in fractions 7 – 11 from 3 SEC experiments.* ***(F)*** *Electron microscopy image of the 9$^{th}$ fraction. Bar = 100 nm.*

## 3.3. Validation and Efficiency of rtPCR

Quantitative real-time PCR (rtPCR) was performed on DNA extracted from EVs on multiple occasions. Essentially three primers were of interest for this study: ND1 and ND4 as markers for the mtDNA and ACTB (encoding for β-actin) as a marker for the nuclear genome. The $C_t$ value (cycle threshold), the main parameter in rtPCR experiments, is defined as the number of reaction cycles that are necessary for the fluorescent signal to pass the threshold. The threshold is usually defined as the specific signal intensity of the reaction that exceeds the background signal.

There are many different methods to prove the efficiency (E) of an rtPCR. One possibility is to run the rtPCR with a serial dilution of the original DNA sample (normally using 10-fold dilutions steps) and draw a standard curve through the $C_t$ values. When plotting the $C_t$ values against the logarithm of the targeted concentrations, a linear curve with a negative slope is expected. For a 100% efficiency, the slope must be -3.33 in a 10-fold dilution series (Svec et al. 2015). The efficiency is 100% when the number of DNA templates doubles in every PCR cycle. For the aforementioned three primers, four dilutions of an original DNA test sample (0.1, 0.01, 0.02, and 0.001) were prepared and standard curves were fitted through the resulting $C_t$ values shown in figure 11. Linear regression calculations resulted in a slope of -2.836 for ND1 (Y-intercept: 15.40), -3.020 for ND4 (Y-intercept: 14.92) and -3.270 for ACTB (Y-intercept: 22.99). All three slopes come close to the ideal slope of -3.3, indicating high efficiency.

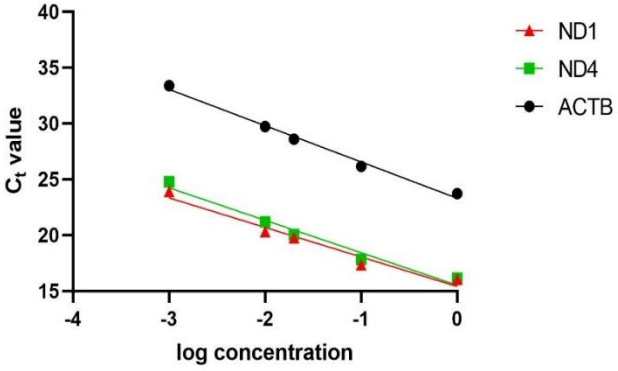


***Figure 11: Standard curves of rtPCR primers.*** *$C_t$ values are plotted against DNA concentrations in a serial dilution (logarithmic scale) for three primers: ND1, ND4 and ACTB. Standard curves were calculated with simple linear regression: slope ND1: -2.836, slope ND4: -3.020, slope ACTB: -3.270. A slope of -3.3 is associated with a 100% efficiency of the rtPCR.*

Knowing the slope, the efficiency can be also calculated by this equation (Kubista et al. 2006):

$$E = 10^{-\left(\frac{1}{slope}\right)} - 1$$

By fitting the slopes in this equation, the efficiencies are 1.25 for ND1, 1.14 for ND4, and 1.02 for ACTB.

Another possibility to assess the purity of the reaction and whether there is one specific amplified DNA product or additional off-target amplicons, or contaminants provides the analysis of the melting peaks. A melting curve measures the fluorescence emitted from the amplified products when gradually raising the temperature. In the beginning, the fluorescence decreases with increasing temperatures. When the temperature reaches a

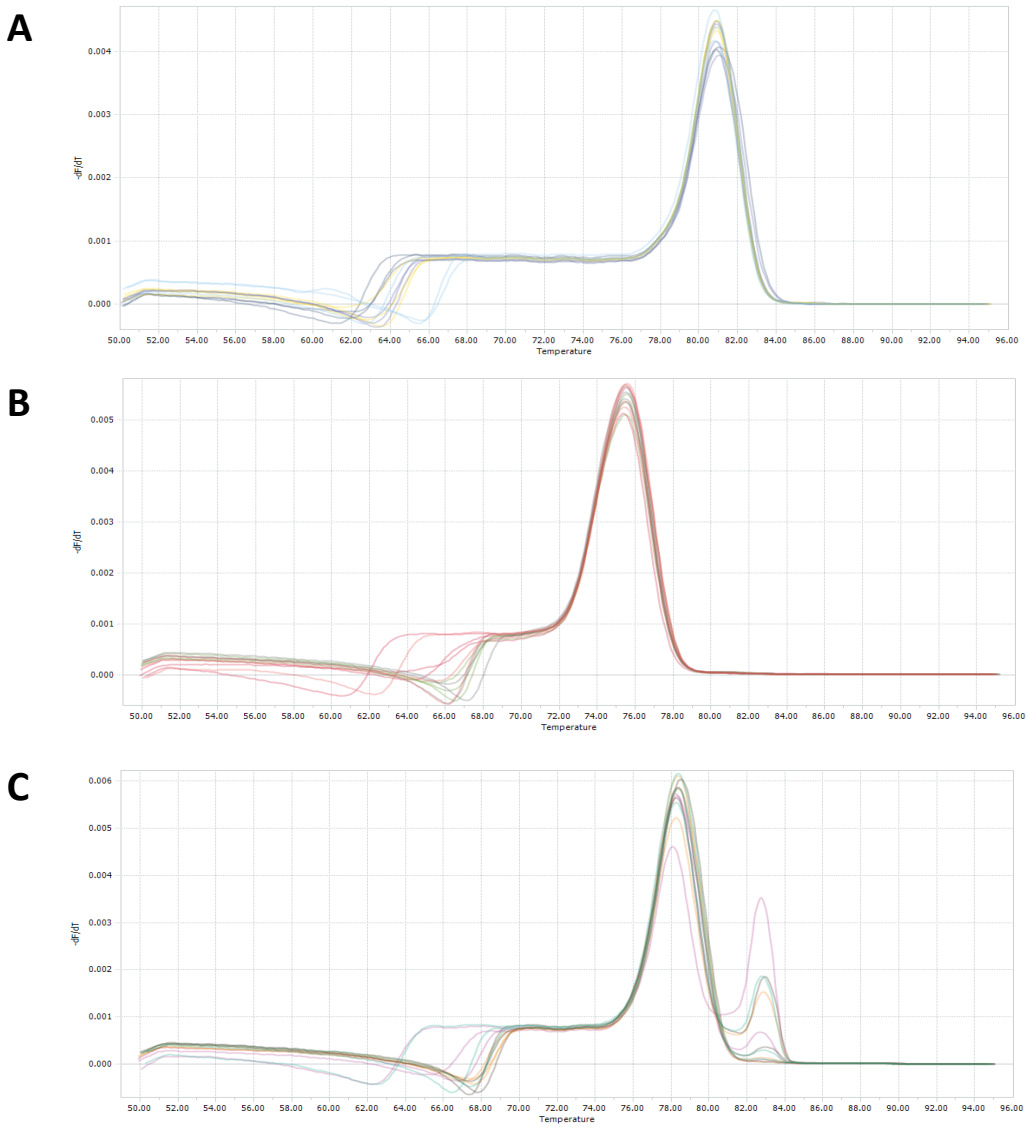


***Figure 12: Melting peaks of the rtPCR using different primers. (A)*** *Primer against ND1.* ***(B)*** *Primer against ND4.* ***(C)*** *Primer against ACTB. While ND1 and ND4 showed a single melting peak indicating a single pure amplified DNA product, ACTB exhibited two peaks.*

certain point, the double-stranded DNA breaks apart, the dye is released and the fluorescence drops abruptly (Kubista et al. 2006). This process is visualized as a melting peak. A single melting peak stands for a single specific amplified DNA product. The melting peaks for the primers ND1, ND4, and ACTB are shown in figure 12.

In the rtPCR, the amplified DNA products are measured by fluorescence, but they can also be run on conventional gel electrophoresis to visualize the bands presented in figure 11. The rtPCR DNA amplicons were loaded on a 3% agarose gel and left there at 150 V for 90 min. All three samples exhibited a band with the expected size of the amplified DNA sequence: 69 bp for ND1, 84 bp for ND4, and 76 bp for ACTB. The amplicon of the ACTB primer showed an additional smaller and fainter band at about 275 bp.

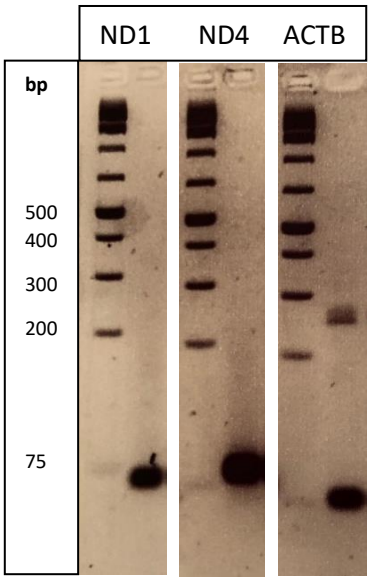


***Figure 13: Gel electrophoresis of rtPCR products.*** *The amplified products of ND1, ND4 and ACTB from the rtPCR were put on 3% agarose gel and run at 150 V for 90 min. For ND1 and ND4, the shown bands fit to the expected size of the amplicon (ND1: 69 bp, ND4: 84 bp). For ACTB, the lower band is the expected amplicon (76 bp), the upper band and approx. 275 bp an additional, most likely contaminating or off-target product.*

## 3.4. Analysis of DNA in EVs

### 3.4.1. PicoGreen staining of EV-associated DNA

PicoGreen is a fluorescent dye that preferably binds to double-stranded DNA (dsDNA) and is often used for the quantification of dsDNA. Nevertheless, it is also able to permeate cell membranes without prior permeabilization (Ashley et al, 2005). It is therefore suitable to stain mtDNA in mitochondria, but also to stain DNA in EVs which are also surrounded by a lipid bilayer. EV preparations from serum and CSF using ExoQuick™ and IP with anti-L1CAM antibodies (only with serum samples) were incubated with

PicoGreen, centrifuged on slides, air-dried, and observed under the microscope. The microscopy images revealed the presence of fluorescent green dots that indicate the presence of dsDNA. Due to the prior treatment with DNase, most of the extra-vesicular DNA should have been degraded making the dsDNA inside the EVs mainly responsible for the signal. This observation was underlined by the declining density of fluorescent EVs after dilutions and the absence respectively a much lower number of fluorescent particles in the supernatant samples that were also treated with DNase. The same applied to EVs obtained via IP although the image appeared different with a predominant number of small particles (< 500 nm) and a smaller number of big green dots (1 – 5 µm).

***Table 13: Microscopy images of EVs from serum and CSF stained with PicoGreen to visualize dsDNA inside EVs*** *(bar = 10 µm).*

| | | | |
|---|---|---|---|
| **ExoQuick™ from serum** | **pellet** | | |
| | no dilution | 1:3 dilution | 1:30 dilution |
| | 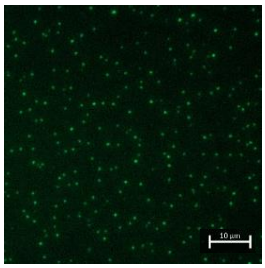 | 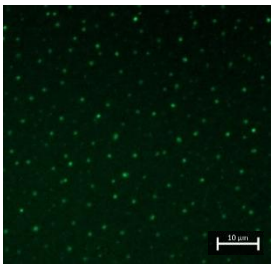 | 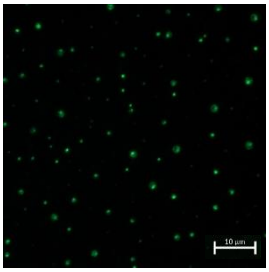 |
| | **supernatant** | | |
| | 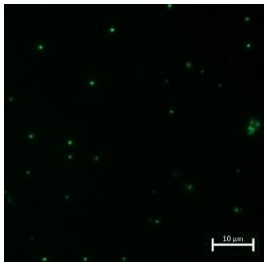 | | |
| **ExoQuick™ from CSF** | **pellet** | **supernatant** | |
| | 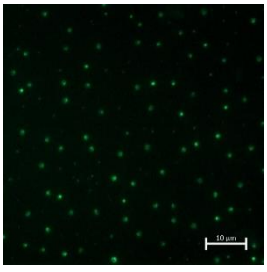 | 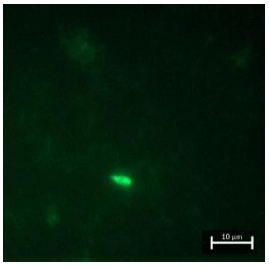 | |

| | | |
|---|---|---|
| **L1CAM$^+$ EVs (IP)** | 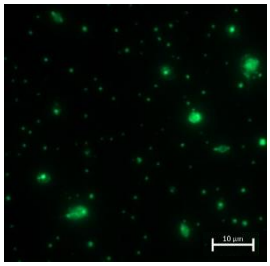 | 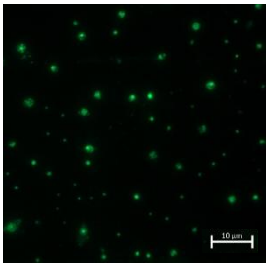 |

### 3.4.2. Characterization of the DNA composition in EVs

#### 3.4.2.1. Effect of DNase treatment

Since cfDNA consists of vesicular and non-vesicular DNA, it is a crucial step to remove extra-vesicular DNA from the sample in order to leave only vesicular DNA behind. For this purpose, 10 µl of DNase (10 units) was added to 100 µl of the sample according to the manufacturer's instructions. For bigger sample sizes (like 500 µl supernatant), the volume of the DNase and the other reagents was scaled up. DNase treatment was performed on EV preparations from serum and CSF isolated with the ExoQuick™ kit. It was not applied to EVs isolated with the IP method, because the majority of the contaminating non-vesicular cfDNA should have been removed in the multiple washing steps before, and since the amount of DNA was very low anyway, additional loss of DNA had to be avoided at any cost to run the rtPCR. Quantitative PCR measurements of the mitochondrial genes ND1 and ND4 provide the most reliable method to assess the effect of the DNase treatment on serum and CSF EVs.

*Note: DNA concentrations were measured in different settings (pellet, supernatant, eluate). The "native" DNA concentrations cannot be compared properly since the pellet, for example, contains "concentrated" DNA and the measured DNA concentration depends on the resuspension volume while the supernatant in contrast is not concentrated. To reflect this situation, DNA concentrations were normalized to 1 µl serum or CSF and the numbers do not show the "native" DNA concentrations.*

**Serum EVs:** $C_t$ values of ND1 and ND4 revealed no significant difference between samples before and after DNA digestion (ND1: serum EVs with DNase mean = 20.471, SD = 1.572, n = 10; serum EVs without DNase mean = 19.995, SD = 1.579, n = 6; p = 0.5676,

Student's two-sided t-test; ND4: serum EVs with DNase mean = 20.843, SD = 1.486, n = 10; serum EVs without DNase mean = 20.352, SD = 1.576, n = 6; p = 0.5411, Student's two-sided t-test) (figure 13B). However, when measuring the DNA concentrations in the serum EV samples, the DNase treatment resulted in a significantly lower DNA concentration (serum EVs with DNase mean = 0.116 ng/µl serum, SD = 0.033, n = 3; serum EVs without DNase mean = 0.365 ng/µl serum, SD = 0.105, n = 3; * p = 0.0174, Student's two-sided t-test) (figure 13A). The $C_t$ values alone are not quite meaningful since they strongly depend on the DNA concentration in the sample. Therefore, a more accurate parameter would be the ratio of the $C_t$ values of ND1 respectively ND4 and the DNA concentration. Using this calculation, the difference between the DNase treatment and the absence of the DNase treatment in serum EVs becomes highly significant (ND1: *$C_t$(ND1)/DNA concentration:* with DNase mean = 176.5, SD = 13.55, n = 10; without DNase mean = 54.78, SD = 4.326, n = 6; **** p < 0.0001, Student's two-sided t-test; ND4: *$C_t$(ND4)/DNA concentration:* with DNase mean = 179.7, SD = 12.81, n = 10; without DNase mean = 55.76, SD = 4.318, n = 6; **** p < 0.0001, Student's two-sided t-test).

**CSF EVs:** In contrast to serum EVs, the DNase treatment had a significant effect on the mtDNA in CSF EVs, resulting in higher $C_t$ values for ND1 and ND4 in the DNase treatment group compared to the group without DNase treatment (ND1: CSF EVs with DNase mean = 30.71, SD = 0.601, n = 3; CSF EVs without DNase mean = 26.71, SD = 0,199, n = 3; ** p = 0.0014, Student's two-sided t-test; ND4: CSF EVs with DNase mean = 32.28, SD = 1.301, n = 3; CSF EVs without DNase mean = 27.33, SD = 0.323, n = 3; ** p = 0,0061, Student's two-sided t-test) (figure 13B).

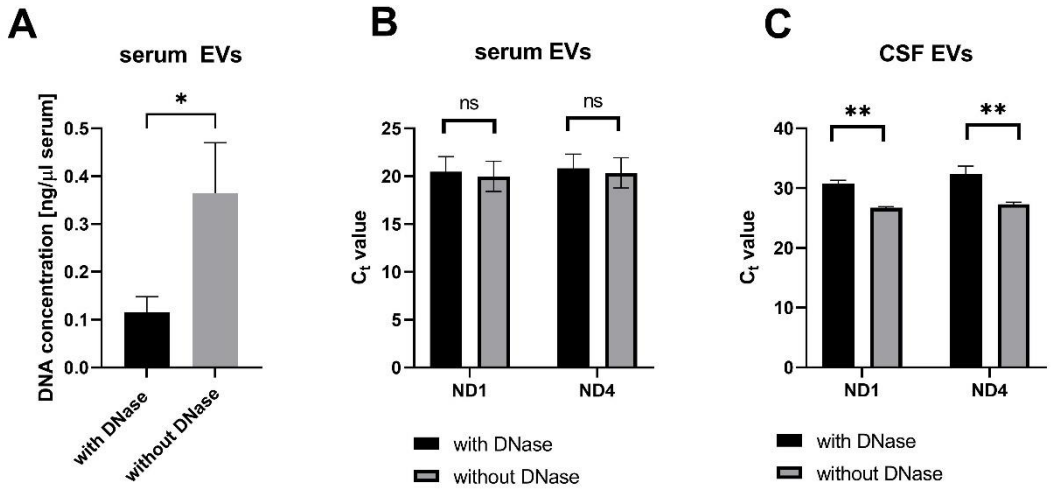


***Figure 14: Effect of DNase treatment on EV samples. (A)*** *The adding of 10 units DNase to an ExoQuick™ serum pellet containing the EVs shows a significant decline of the DNA concentration compared to the absence of the DNase. The mean DNA concentration decreases from 1.823 ng/µl without DNase to 0.577 ng/µl with DNase (n = 3, * p < 0.05, Student's two-sided t-test).* ***(B)*** *The DNase treatment has no significant effect on the $C_t$ values of the mitochondrial genes ND1 and ND4. The $C_t$ values are slightly lower without DNase than with DNase, but the difference is neglectable and not significant (ND1: n = 6 and 10, p > 0.05, Student's two-sided t-test; ND4: n = 6 and 10, p > 0.05, Student's two-sided t-test).* ***(C)*** *In CSF EVs, the DNase treatment leads to significant higher $C_t$ values for ND1 and ND4 (ND1: n = 3, ** p < 0.01, Student's two-sided t-test; ND4: n = 3, ** p < 0.01, Student's two-sided t-test). Values are given as mean ± SD.*

### 3.4.2.2. DNA in serum EVs

DNA concentrations were measured in all ExoQuick™ serum and CSF samples from the patients and controls in the cohort as well as in the IP samples containing L1CAM$^+$ EVs. The DNA concentrations of the cohort samples are listed below. The results which are presented in this section refer to the test serum and CSF samples that were used for establishing the methods. According to the previous results, 10 µl of DNase (10 units) were added to the in 100 µl molecular-grade water resuspended pellet as well as the supernatant (the volume of DNase was scaled up according to the volume of the sample). Figure 14A shows the mean DNA concentration of EVs isolated from serum samples using the ExoQuick™ kit (the measured concentration values were normalized to 1 µl serum): In the pellet samples (containing the expected EVs), a mean DNA concentration of 0.055 ng/µl serum was measured, ranging from 0.011 ng/µl serum to 0.153 ng/µl serum (SD = 0.045, n = 15), whereas the DNA concentration in the supernatant with mean 1.771 ng/µl serum (ranging from 0.480 ng/µl serum to 5.460 ng/µl serum, SD =

1.821, n = 12, ** p = 0.001, Student's two-sided t-test) was significantly higher. A contrary picture was observed when looking at the $C_t$ values of ND1, ND4, and ACTB in the rtPCR (figure 14B). Despite lower DNA concentrations in serum pellet samples compared to supernatant, the $C_t$ values were significantly lower in the pellet samples containing the EVs implicating higher mtDNA and nDNA amount (ND1: pellet mean = 20.53, SD = 1.238, n = 16; supernatant mean = 28.51, SD = 4.153, n = 11; **** p < 0.0001, Student's two-sided t-test; ND4: pellet mean = 21.04, SD = 1.195, n = 16; supernatant mean = 30.64, SD = 3.454, n = 11; **** p < 0.0001, Student's two-sided t-test; ACTB: pellet mean = 31.31, SD = 1,900, n = 3; supernatant mean = 40.29, SD = 0, n = 1; too few replicates for statistical analysis). The ratio of the $C_t$ values and the DNA concentrations resulted in even bigger differences between the pellet and the supernatant group (ND1: *$C_t$(ND1)/DNA concentration*: pellet mean = 373.341, SD = 22.50, n = 16; supernatant mean = 16.099, SD = 2.345, n = 11; **** p < 0.0001, Student's two-sided t-test; ND4:

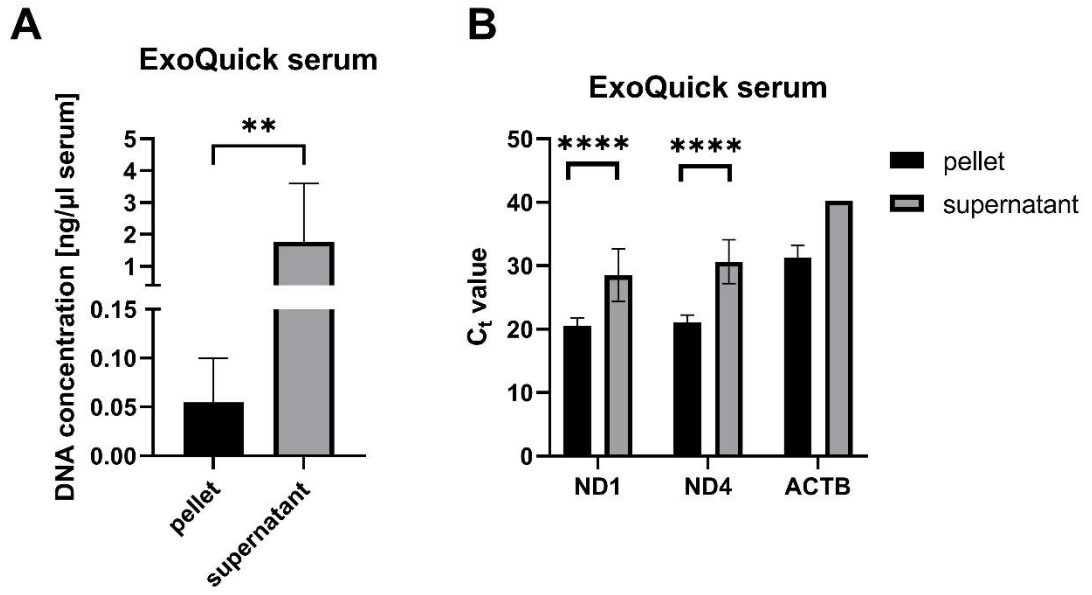


***Figure 15: Characterization of the DNA composition in serum EVs. (A)*** *Mean DNA concentrations of ExoQuick™ samples from 500 µl serum. The supernatant has a 32.2-times higher DNA concentration than the pellet with the EVs (pellet: n = 15, supernatant: n = 12; ** p < 0.01, Student's two-sided t-test).* ***(B)*** *rtPCR with primers against ND1, ND4, and ACTB in ExoQuick™ serum samples. The $C_t$ values in the serum pellet samples are significantly lower for all three amplicons compared to the supernatant although a higher total DNA concentration was measured in the supernatant (ND1 and ND4: pellet: n = 14, supernatant: n = 11, **** p < 0.0001, Student's two-sided t-test; ACTB: pellet: n = 3, supernatant: n = 1). When putting the $C_t$ values in relation to the DNA concentrations, the difference between both groups is even bigger. Values are given as mean ± SD.*

*$C_t$(ND4)/DNA concentration:* pellet mean = 382.591, SD = 21.73, n = 16; supernatant mean = 17.301, SD = 1.950, n = 11; **** p < 0.0001, Student's two-sided t-test; ACTB: *$C_t$(ACTB)/DNA concentration:* pellet mean = 569.273, SD = 34.55, n = 3; supernatant mean = 22.750, n = 1; too few replicates for statistical analysis).

#### 3.4.2.3. DNA in CSF EVs

EVs from CSF isolated with the ExoQuick™ kit were subjected to the same experiments and measurements as the serum EVs. Figure 15A presents the mean DNA concentration of EVs isolated from CSF samples (the measured concentration values were again normalized to 1 µl CSF). With 0.0217 ng/µl CSF, the DNA concentration in CSF EVs (pellet from ExoQuick™ kit) was about half as low than in serum EVs (0.055 ng/µl) with a minimum of 0.005 ng/µl CSF and a maximum of 0.039 ng/µl CSF (SD = 0.010, n = 15). Similar to the serum samples, significant higher DNA concentrations were measured in the CSF supernatant (CSF supernatant mean = 0.263 ng/µl, SD = 0.067, n = 4; **** p < 0.0001, Student's two-sided t-test). The DNA concentration data was very inconsistent, and some values had to be excluded from the analysis. The rtPCR with primers against ND1, ND4, and ACTB revealed also no significant difference between the CSF pellet and the supernatant as presented in figure 15B (ND1: pellet mean = 30.71, SD = 0.601, n = 2; supernatant mean = 31.92, SD = 1.153, n = 2; p = 0.319, Student's two-sided t-test; ND4: pellet mean = 32.28, SD = 1.301, n = 2; supernatant mean = 33.34, SD = 0.672, n = 2; p = 0.454, Student's two-sided t-test, ACTB: pellet mean = 38.37, SD = 0.240, n = 2; supernatant mean = 39.84, n = 1; too few replicates for statistical analysis). However, after normalizing the $C_t$ values to the mean DNA concentrations of the CSF pellet and supernatant, both groups differed significantly for ND1 and ND4 (ND1: *$C_t$(ND1)/DNA concentration*: pellet mean = 1414.977, SD = 27.70, n = 2; supernatant mean = 121.350, SD = 4.382, n = 2; *** p = 0.0002, Student's two-sided t-test; ND4: *$C_t$(ND4)/DNA concentration:* pellet mean = 1492.166, SD = 59.96, n = 2; supernatant mean = 126.749, SD = 2.554, n = 2; *** p = 0.001, Student's two-sided t-test; ACTB: *$C_t$(ACTB)/DNA concentration:*

pellet mean = 1768.203, SD = 11.08, n = 2; supernatant = 151.483, n = 1; too few replicates for statistical analysis).

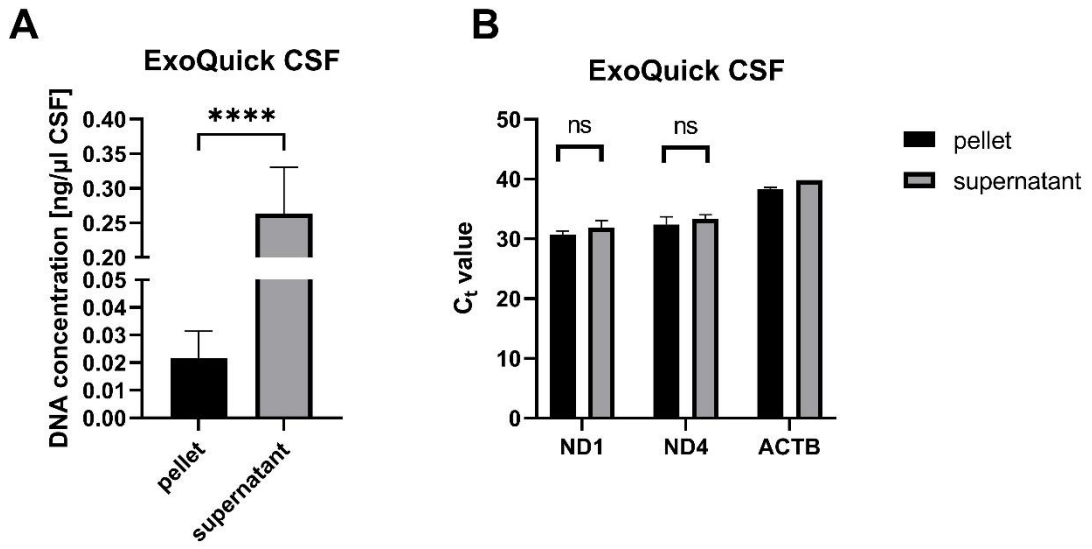


***Figure 16: Characterization of the DNA composition in CSF EVs. (A)*** *Mean DNA concentrations of ExoQuick™ samples from 500 µl CSF. The supernatant has a 12.1-times higher DNA concentration then the pellet with the EVs, but the difference is highly significant (pellet: n = 15, supernatant: n = 6; **** p > 0.0001, Student's two-sided t-test).* ***(B)*** *rtPCR with primers against ND1, ND4, and ACTB in ExoQuick™ CSF samples. The $C_t$ values in the CSF pellet samples for all three primers differ not significantly from the supernatant (ND1 and ND4: pellet: n = 2, supernatant: n = 2; p > 0.05, Student's two-sided t-test; ACTB: pellet: n = 2, supernatant: n = 1). Values are given as mean ± SD.*

### 3.4.2.4. DNA in L1CAM$^+$ EVs

A little bit lower DNA concentration than in serum EVs were detected in the IP samples using a biotinylated anti-L1CAM-antibody. A mean DNA concentration of 0.041 ng/µl serum (range = 0.061 ng/µl, SD = 0.021, n = 16) was measured on the Qubit™ Fluorometer. Compared to a negative control in which no antibody at all was used, there was no significant difference between both samples (negative control = 0.049 ng/µl serum, SD = 0.035, range = 0.136, n = 13; p = 0.4437, Student's two-sided t-test). It is important to note, that neither in the L1CAM$^+$ EV sample nor in the negative control a DNase was added to the sample to avoid too much DNA loss. To determine the difference in the amount of mtDNA and nDNA between both samples, rtPCR with primers for ND1 and ND4 for the mtDNA and ACTB for the nDNA was performed. Despite a significant difference in the $C_t$ values for ND1 and ND4 between L1CAM$^+$ EV samples and negative

controls, the $C_t$ values were lower in the negative control indicating a higher mtDNA quantity in the negative control compared to the L1CAM$^+$ EVs enriched sample (ND1: L1CAM$^+$ EVs mean = 22.39, SD = 0.7201, n = 14; negative control mean = 21.58, SD = 0.6044, n = 13; ** p = 0.0042, Student's two-sided t-test; ND4: L1CAM$^+$ EVs mean = 23.00, SD = 0.9172, n = 14; negative control mean = 22.01, SD = 0.7903, n = 13; ** p = 0.0062, Student's two-sided t-test). No significant difference was observed in the $C_t$ values for ACTB, but in contrast to ND1 and ND4, $C_t$ values for ACTB were higher in the negative control (ACTB: L1CAM$^+$ EVs mean = 31.84, SD = 1.937, n = 12; negative control mean = 32.16, SD = 1.639, n = 11; p = 0.680, Student's two-sided t-test). The ratio of the $C_t$ values of ND1/ND4/ACTB and the DNA concentration revealed a bigger difference between L1CAM$^+$ EVs and the negative control (ND1: *$C_t$(ND1)/DNA concentration*: L1CAM$^+$ EVs mean = 552.9, SD = 17.78, n = 14; negative control mean = 443.7, SD = 12.43, n = 13; **** p < 0.0001, Student's two-sided t-test; ND4: *$C_t$(ND4)/DNA concentration:* L1CAM$^+$ EVs mean = 567.8, SD = 22.65, n = 14; negative control mean = 452.5, SD = 16.25, n = 13; **** p < 0.0001, Student's two-sided t-test; ACTB: *$C_t$(ACTB)/DNA concentration:* L1CAM$^+$ EVs mean = 786.2, SD = 47.83, n = 12; negative control mean = 661.1, SD = 33.69, n = 11; **** p < 0.0001, Student's two-sided t-test). In summary, it can be said that the DNA concentrations on the one hand and the "pure" $C_t$ values on the other hand revealed no difference between L1CAM$^+$ EVs and the negative control. On the other hand, when calculating the ratio of the $C_t$ value and the DNA concentration, significant higher mtDNA and nDNA quantities could be found in the L1CAM$^+$ EVs compared to the negative control. Due to the inconsistent results, this method was not applied to the cohort samples and instead only total serum EVs were isolated by using the ExoQuick™ kit.

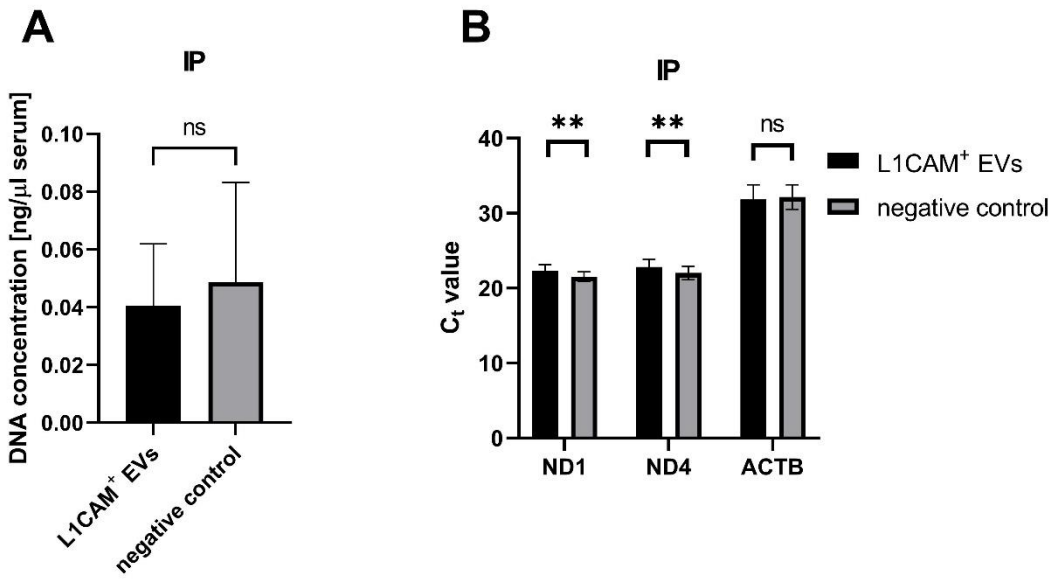


***Figure 17: Characterization of the DNA composition in L1CAM⁺ EVs compared to negative controls. (A)*** *Mean DNA concentrations of IP samples. There is no significant difference between the L1CAM⁺ EVs and the negative control (L1CAM⁺ EVS: n = 16, negative control: n = 13, p > 0.05, Student's two-sided t-test). Also note the considerably lower DNA concentrations compared to serum EVs.* ***(B)*** *rtPCR of ND1, ND4 and ACTB in IP samples. A significant difference in the $C_t$ values of ND1 and ND4 between L1CAM⁺ EVs and a negative control (without anti-L1CAM antibody) was observed, but with lower $C_t$ values in the negative control group (ND1: L1CAM⁺ EVs: n = 14, negative control: n = 13, ** p < 0.01, Student's two-sided t-test; ND4: L1CAM⁺ EVs: n = 14, negative control: n = 13, ** p < 0.01, Student's two-sided t-test). ACTB showed no difference between both groups (L1CAM⁺ EVs: n = 12, negative control: n = 11, p > 0.05, Student's two-sided t-test). Values are given as mean ± SD.*

## 3.5. Analysis of the cohort

### 3.5.1. Description of the cohort

The cohort consisted of 35 PD patients and 35 age- and gender-matched healthy controls. More details for both groups provide table 1.

***Table 14: Characteristics of the cohort.***

| | | **PD patients** | **controls** |
|---|---|---|---|
| **total** | | 35 | 35 |
| **mean age** (sample picking) | | 64.343 years | 64 years |
| **sex** | **male** | 21 | 21 |
| | **female** | 14 | 14 |
| **age of onset** | | 56.030 years | - |
| **samples** | | - 35 x serum (à 500 µl)<br>- 30 x CSF (à 400 µl) | 35 x serum (à 500 µl) |

More exactly, the PD cohort consisted of 29 patients with idiopathic PD, one patient with a genetic PD (*PINK1* (PARK6)), two patients with a mitochondriopathy, and three patients with PSP-P. In the following, all patients are referred to as PD patients.

There was one serum sample from each PD patient available, and from 30 of the 35 PD patients, also a CSF sample was available (5 PD patients only had serum samples). Of the 35 healthy controls, only serum samples were accessible (figure 17).

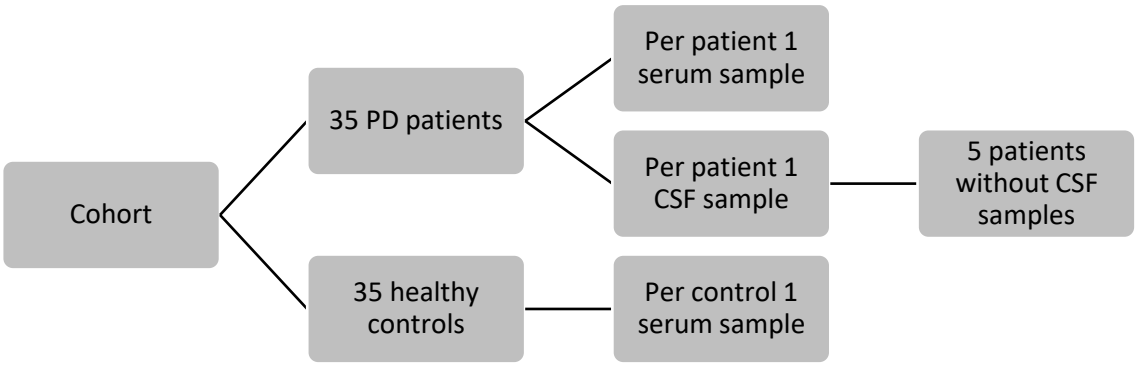


***Figure 18: Structure of the cohort.*** *From 5 PD patients only serum samples were available. From all controls only serum samples (and no CSF) were available.*

Total EVs from serum and CSF were isolated using the ExoQuick™ kit and DNA was analysed regarding the mitochondrial genes ND1 and ND4 with rtPCR. The $C_t$ values of ND1 and ND4 and especially the ratio $C_t$(ND4)/$C_t$(ND1) represented the primary endpoint. Furthermore, protein and DNA concentrations were measured in every sample and the ratio of the $C_t$ values of ND4 respectively ND1, and the DNA concentration was calculated. For statistical analysis, the results from the serum samples of the PD patients and the controls were compared and the results from the serum samples of the PD patients and the CSF samples of the same PD patients (figure 18).

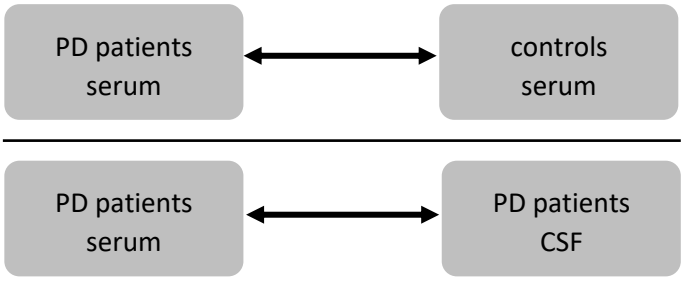


***Figure 19: Illustration of the two major comparisons for statistical analysis.*** *Serum EVs from controls were not compared to the CSF EVs from patients.*

### 3.5.2. Serum EVs

Total EVs were extracted from serum from PD patients and healthy controls. Since no method to measure the number of particles in the EV preparation was available, the protein concentration served as a rough indicator for isolation efficiency. Both groups did not differ significantly in protein concentration (serum patients mean = 58.48 mg/ml, SD = 9.706, n = 30; serum controls mean = 60.43, SD = 18.87, n = 30; p = 0.6164, Student's two-sided t-test; Note: n is 30 (and not 35), because 5 patient and 5 control serum samples were not measured). There was also no difference in the DNA concentrations of both groups measurable (serum patients mean = 0.5176 ng/µl, SD = 0.3992, n = 35; serum controls mean = 0.5522 ng/µl, SD = 0.3939, n = 35; p = 0.7161, Student's two-sided t-test) (figure 19A). Furthermore, the primary endpoint $C_t$(ND4)/$C_t$(ND1) in serum revealed no significant difference between the PD patients and the controls (serum patients mean = 1.048, SD = 0.025, n = 33; serum controls mean = 1.047, SD = 0.017, n = 35; p = 0.837, Student's two-sided t-test) (figure 19B). In conclusion, this parameter could not be used to distinguish between PD patients and healthy controls based on serum EVs. Serum samples from two patients showed unusual high $C_t$ values for ND1 and ND4 which exceeded all other values. Since both values were increased, the ratio (ND4/ND1) was similar to the others. Statistical analysis (robust nonlinear regression (ROUT test)) was performed to identify outliers and the $C_t$ values for ND1 and ND4 for the serum samples of the patients with the IDs 17846 and 17949 were removed. This explains n = 33 for serum samples from PD patients when $C_t$ values are included in the further calculations. As an alternative to the ND4/ND1 ratio, the quotient of the $C_t$ values of ND1 respectively ND4 and the DNA concentration was calculated and showed no difference between both groups ($C_t$(ND1)/DNA concentration: serum patients mean = 60.41, SD = 45.01, n = 33; serum controls mean = 55.05, SD = 35.91, n = 35; p = 0.5879, Student's two-sided t-test; $C_t$(ND4)/DNA concentration: serum patients mean = 63.30, SD = 47.00, n = 33; serum controls mean = 57.68, SD = 37.89, n = 35; p = 0.5885, Student's two-sided t-test) (figure 19C). Also the two patients with mitochondriopathy did not differ from the rest of the cohort or from the healthy controls.

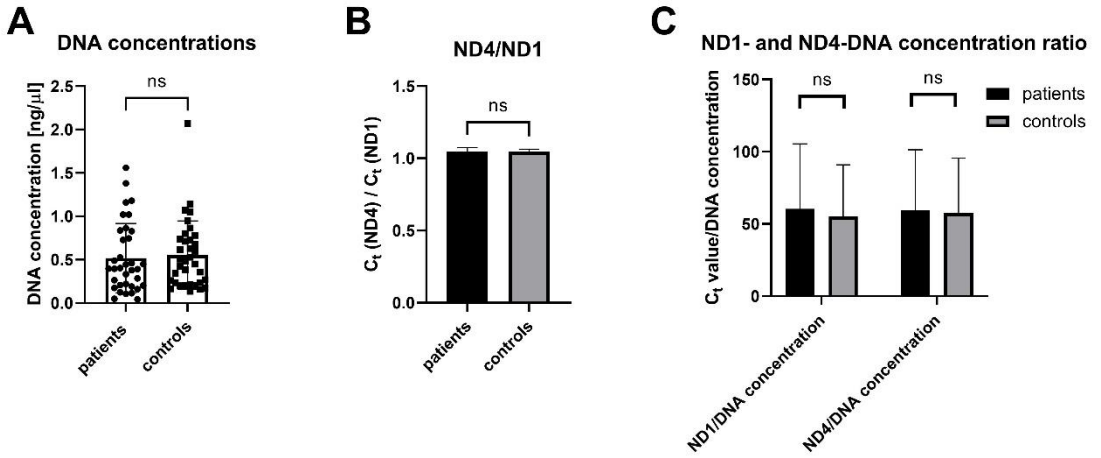


***Figure 20: Results of the serum samples from PD patients and healthy controls of the cohort.*** *Starting volume was 500 µl each.* ***(A)*** *Comparison of the DNA concentrations measured in the serum EVs samples from patients and controls. Both groups have similar DNA concentrations with a wide range (patients: range = 1.518 ng/µl, n = 35; controls: range = 1.935 ng/µl, n = 35) and an insignificant difference (p > 0.05, Student's two-sided t-test).* ***(B)*** *Primary endpoint was the ratio of the $C_t$ values of ND4 and ND1. This ratio does not differ significantly between serum EVs from patients and controls (patients: n = 33, controls: n = 35; p > 0.05, Student's two-sided t-test) and therefore cannot be used to distinguish between PD patients and controls.* ***(C)*** *The quotient of the $C_t$ values of ND1 or ND4 and the DNA concentration can serve as an alternative endpoint. But also with this parameter, no significant difference between serum EVs from patients and controls can be found (patients: n = 33, controls: n = 35; $C_t$(ND1)/DNA concentration: p > 0.05, $C_t$(ND4)/DNA concentration: p > 0.05, both Student's two-sided t-test). Values are given as mean ± SD.*

### 3.5.3. CSF EVs

Since no CSF samples from healthy controls were available, the main focus lied on the comparison between serum and CSF samples from the same PD patients. Since CSF and serum EVs represent different EV populations with distinguished features and since PD mainly affects the brain, the comparison between both EV populations can lead to new findings. The 5 patients with only serum and no CSF samples (ID13314, ID14333, ID17553, ID22424, ID31779) were omitted from the statistical analysis. In conclusion, 30 PD patients with their serum and CSF samples were compared. As described above, CSF contains much less EVs than serum in the same starting volume. This could explain partly the almost 187-times higher mean protein concentration in the serum samples of the PD patients compared to the CSF samples of the same patients (serum patients mean = 58.270 mg/ml, SD = 10.34, n = 25; CSF patients mean = 0.312 mg/ml, SD = 0.277, n = 30; **** p < 0.0001, Student's two-sided t-test) (figure 19A). Other reasons include the

lower concentration of albumin and lipoproteins in the CSF. Contrary to the protein concentration, the DNA concentration in both groups behaves the other way round: The mean DNA concentrations in the CSF samples was 1.4-times higher than in the serum samples of the PD patients (serum patients mean = 0.448 ng/µl, SD = 0.367, n = 30; CSF patients mean = 0.6479 ng/µl, SD = 0.344, n = 30; * p = 0.033, Student's two-sided t-test) (figure 19B). This finding seems contrary to the DNA concentrations measured in the "test samples" above and will be tackled in the discussion section. Nevertheless, the DNA concentrations in both groups differed widely and had a large overlap area. Despite slightly higher DNA concentrations in the CSF EV samples, the $C_t$ values for ND1 and ND4 were much lower in the serum EVs samples (ND1: serum patients mean = 19.59, SD = 0.981, n = 28; CSF patients mean = 30.48, SD = 1.734, n = 30; **** p < 0.0001, Student's two-sided t-test; ND4: serum patients mean = 20.57, SD = 1.114, n = 28; CSF patients mean = 32.88, SD = 2.323, n = 30; **** p < 0.0001, Student's two-sided t-test) (figure 19D). In other words: Although the CSF EV preparations contained a little bit more DNA than serum EV preparations, they possessed less mtDNA, because the $C_t$ values for the mitochondrial genes ND1 and ND4 were higher. But more important than the "pure" $C_t$ values is the ratio of the $C_t$ values of ND4 and ND1. When comparing serum EVs and CSF EVs from the same patients, a significant difference in the $C_t$(ND4)/$C_t$(ND1) ratio between both groups could be detected with a slightly higher value in the CSF group (serum patients mean = 1.047, SD = 0.026, n = 30; CSF patients mean = 1.079, SD = 0.046, n = 30; ** p = 0.0016, Student's two-sided t-test) (figure 19C). The difference in the ND4/ND1 ratio between serum and CSF EVs could indicate, that these two EV populations differ in their mtDNA composition. Another perspective on this subject provides the matching of the ND4/ND1 ratio for each person separate: In 21 of 30 PD patients (70%) the ND4/ND1 ratio in the CSF EVs was higher than in the serum EVs, while in the other 9 of 30 patients (30%), the ND4/ND1 ratio in the CSF EVs was lower than in the serum EVs (figure 19E). Not significant on the other hand was the difference between the $C_t$(ND1)/DNA concentration respectively $C_t$(ND4)/DNA concentration ratio between serum and CSF samples (ND1/DNA concentration: serum patients mean = 66.94, SD = 45.69, n = 28; CSF patients mean = 60.33, SD = 29.32, n = 30; p = 0.512, Student's two-

sided t-test; ND4/DNA concentration: serum patients mean = 70.04, SD = 47.76, n = 28; CSF patients mean = 65.09, SD = 31.21, n = 30; p = 0.640, Student's two-sided t-test).

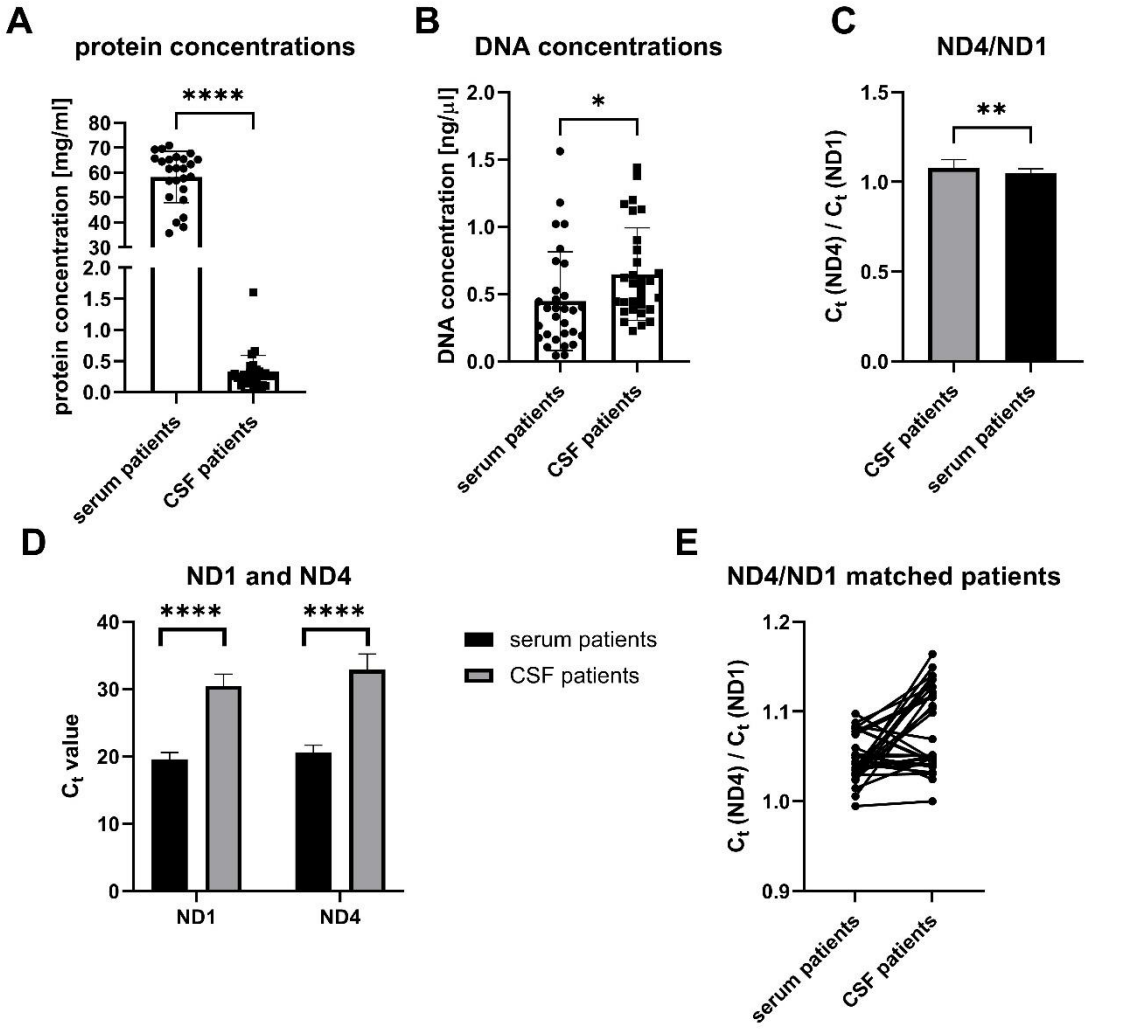


***Figure 21: Results of the CSF samples from the patients compared to their serum samples.*** *CSF and serum were taken from the same patients. Starting volume was 500 µl for serum samples and 400 µl for CSF samples.* ***(A)*** *Comparison of the protein concentrations in serum and CSF samples from the PD patients. Serum samples have a 187-times higher protein concentration than CSF samples (serum patients: n = 25, CSF patients: n = 30).* ***(B)*** *DNA concentrations shows a slightly higher value in the CSF samples than in the serum samples but with a wide range (serum patients: range = 1.518 ng/µl, n = 30; CSF patients: range = 1.215, n = 30).* ***(C)*** *The primary endpoint ($C_t$(ND4)/$C_t$(ND1)) differs significantly between serum and CSF EVs from the same patients (serum: n = 30, CSF: n = 30; ** p < 0.005, Student's two-sided t-test).* ***(D)*** *Comparison of the absolute $C_t$ values between both groups. Significant lower $C_t$ values for ND1 and ND4 can be found in the serum EVs compared to the CSF EVs (serum: n = 30, CSF: n = 30; **** p < 0.0001 for ND1 and ND4 each, Student's two-sided t-test).* ***(E)*** *Illustration of the ND4/ND1 ratio in serum and CSF samples of each patient separately. The two points linked with a line stand for one person. The line connects the ND4/ND1 ratio in serum EVs (left) and CSF EVs (right) in one patient and illustrates the direction in which both samples differ. 70% of the patients (21 of 30) show a higher ND1/ND4 ratio in CSF EVs than in serum EVs. On the other hand, 30% of the patients (9 of 30) behave the other way round with lower ND4/ND1 ratios in CSF EVs than in serum EVs. All values are given as mean ± SD.*

# 4. Discussion

## 4.1. Characterization of EVs

### 4.1.1. Total serum and CSF EVs

Characterization of EVs requires a three-step process according to the ISEV as described above (Théry et al. 2018). The first step involves the quantification of the EV preparation and the source. For the quantification of the EV preparations, NTA was performed to measure particle yield and size distribution. NTA measurements of the ExoQuick™ samples revealed the predominantly small size of the EVs and the high "background signal". Serum EVs from ExoQuick™ exhibited their peak at a size of about 50 nm and CSF EVs from ExoQuick™ presented multiple peaks between 50 and 130 nm. Particle yields from ExoQuick™ samples outranked the other isolation techniques and a compromise had to be found between purity and particle gain. Since the main focus of this study lies on DNA analysis, a higher particle yield seemed to be preferable to gain enough material for the measurements. The quantification of the EV source (serum or CSF) was largely skipped since slots for NTA measurements were rare (they had to be sent to Bonn) and the mean protein concentration of serum and CSF is widely known (serum: 61 – 81 g/l, CSF: 15 – 45 mg/dl). The second step according to the ISEV requires the detection of EV marker proteins and the absence of contaminants. This was done by Western blotting with the following target proteins: CD63, TSG101, Flotillin-1, and L1CAM. Except for CD63, all three proteins could be detected in serum and CSF EVs. CD63 and L1CAM are tetraspanins (category 1 according to ISEV), TSG101 and Flotillin-1 are cytosolic proteins (category 2). Also, calnexin, a protein associated with the endoplasmic reticulum and Golgi apparatus (category 4) could not be detected in the EV preparations (but also not in the supernatant). However, the absence of common proteins, which are often co-isolated with EVs, was not measured (partly because the Western blot experiments were performed before the positional paper was published). Especially serum is a mixture of abundant types of proteins and staining against albumin or apolipoprotein A1/2 would have been sensible to evaluate the extent of contaminating proteins. Nevertheless, when loading serum EV samples on a Western blot and staining the gel with Ponceau or Copper, a

prominent band at just over the 55 kDa protein ladder band was visible which could – with some probability – represent albumin. This is another indicator, that many serum proteins were co-isolated with the EVs when using the ExoQuick™ kit. This finding is consistent with other studies that compared different isolation techniques (Tang et al. 2017; Helwa et al. 2017). They compared different isolation techniques and took the ratio of particle number and protein concentration as an indicator of the purity of a sample. They reported a significantly higher particle-to-protein ratio in the UC samples (= higher purity) than in the ExoQuick™ samples (Tang et al. 2017). The third and last step requires the characterization of single vesicles, in this case by TEM. The majority of the total serum and CSF EVs isolated with the ExoQuick™ kit had sizes smaller than 50 nm in TEM. According to the nomenclature of the ISEV, the correct term for these particles would be “small EVs” (< 100 nm) (Théry et al. 2018). In accordance with the NTA measurements, TEM images of ExoQuick™ serum and CSF EVs came along with a high background signal. In summary, most of the requirements of the ISEV were fulfilled. Although the isolation process with ExoQuick™ provides many advantages (easy to handle, time-saving, high particle yield, EV marker detectable, little sample volume sufficient), the biggest disadvantage remains the co-isolation of other proteins resulting in an unclean sample.

Different studies have also investigated the stability of EVs themselves and the stability of DNA in EVs. One study with serum EVs from 2016 concluded, that EVs are quite stable when exposed to different environments: EV markers in Western blot were stable at 4°C for at least 168 h (= 7 days), at room temperature for at least 48 h, and at -80°C for at least 5 freeze-thaw-cycles (Jin et al. 2016). The same study also reported, that exosomal DNA is stable for at least one week at 4°C, for at least one day at room temperature, and also after multiple freeze-thaw cycles (Jin et al. 2016). Another group reported, that TSG101 was still detectable in EV samples after 3 months when stored at 4°C, -20°C, and -80°C, and even after 30 days at 37°C. However, they suggested that EVs are more stable when stored at -80°C (Kalra et al. 2013). The serum samples used for the test experiments were freshly drawn and stored at -80°C for max. one month. However, the test

CSF samples were quite old, and despite being stored at -80°C, a decline of EV marker proteins and DNA has to be assumed.

### 4.1.2. Immunoprecipitation

Basically, two different IP methods exist, that were applied to EVs: The first method directly couples antibodies to (magnetic) beads by incubating the beads with the antibodies on a shaking incubator at 37°C for 24 h (first described by (Tauro et al. 2012), adapted for L1CAM$^+$ EVs by (Shi 2014)). After this procedure, the antibodies are linked covalently to the beads and can be added to the sample. The second method adds a biotinylated antibody (e.g., anti-L1CAM) directly to the sample and traps the antigen-antibody-complexes with streptavidin magnetic beads profiting from the strong interaction between biotin and streptavidin (first described by (Fiandaca et al. 2015), modified by (Mustapic et al. 2017)). Both methods were tried out and allowed the isolation of L1CAM$^+$ EVs. Several reasons made us use the second method: It took only one day to isolate the EVs and not three days like the first method; the overall protein, particle, and DNA yield was higher; and it was overall cheaper. The crucial part and biggest disadvantage of the first method lies in the coupling of the antibodies directly to the beads. Firstly, the coupling efficiency is difficult to measure so it remains unclear how many antibodies are coupled to the beads. Secondly, the antibodies are incubated at 37°C for 24 h with the beads, and considering the fragility of protein structures, one can assume that such a long time at 37°C could damage the antibodies. Nevertheless, also the second method with biotinylated antibodies has its problem. BSA was added to the washing solution (0.1%) and to the antibody (3%) to prevent and block non-specific bindings of proteins and particles to the beads (Bonifacino, Gershlick, and Dell'Angelica 2016). Although multiple washing steps were performed to get rid of obsolete proteins and BSA it cannot fully be excluded that some BSA remained in the final preparation and that it interfered with the protein concentration measurements and the Western blot. BSA has a molecular weight of approx. 66 kDa and in Western blots of IP samples a corresponding band could be observed (similar to serum samples which contained abundant human albumin). Another obstacle in Western blots of IP samples was the IP-antibody itself. In the final step of this method,

SDS and heat were applied to the sample to separate the antibody-bound proteins (in this case antibody-bound EVs) from the magnetic beads. The beads stayed at the side of the tube due to the magnetic force, but not just the desired protein was detached from the beads, also the antibody was separated from the beads and appeared in the final solution. The typical IgG antibody consists of two light chains (à 25 kDa) and two heavy chains (à 50 – 55 kDa) and has a total molecular weight of approx. 150 – 160 kDa (Schroeder and Cavacini 2010). Because the IP sample was boiled in the last step to detach the proteins respectively EVs from the beads, most of the antibodies from the IP should have split into heavy and light chains and they should appear as 25 and 50 kDa bands in the Western blot. IgG also denatures irreversibly at temperatures higher than 65°C (Mainer et al. 1999; Indyk, Williams, and Patel 2008). The biotinylated anti-L1CAM and anti-CD9 antibodies used for the IP were produced in mice and the primary and secondary antibodies were selected to originate from another species than mouse (e.g., rat, goat). Nevertheless, cross-reactions between antibodies of different species are possible, especially when abundant antibodies are loaded on the gel (Erickson, Lewis, and Fisher 1993; Mao et al. 2021). That is per se not a big problem, but it can get problematic when the expected size of a target protein is close to the molecular weight of a heavy or light chain. In this case, the band from the target protein and the band from the heavy or light chain cannot be distinguished. Therefore, a specific secondary antibody that only recognizes the kappa light chain of the primary antibody was used, especially for TSG101 due to the similar molecular weight to the heavy chain. The same approach was applied to the serum EV samples since serum also contains abundant antibodies.

Two different antibodies were used for IP: CD9 as a common EV marker and L1CAM as a (potential) marker for neuronal-derived EVs. Paradoxically, although $L1CAM^+$ EVs only represent a small subpopulation of all EVs (Mustapic et al. 2017), the particle yield in the NTA measurements was higher and the bands for L1CAM, TSG101, and CD9 were stronger compared to the $CD9^+$ EVs. The reason for this finding might be the worse efficiency of the anti-CD9 antibody to capture EVs. As negative control to prove the specific binding of $L1CAM^+$ or $CD9^+$ EVs to the beads, IP samples with no antibody but the same

starting material and the same steps were used. As an alternative negative control, an unspecific antibody like IgG could have been added to the sample instead of L1CAM or CD9.

### 4.1.3. Neuronal-derived EVs

After the discovery that CSF EVs can pass the BBB and can be found in the peripheral circulation, many attempts have been made to isolate this specific subpopulation of neuronal-derived EVs. Results from *in vitro* cultured neuronal cells suggested L1CAM as a marker for neuronal-derived EVs (Fauré et al. 2006; Kenwrick, Watkins, and De Angelis 2000; Lachenal et al. 2011). Shi et al were the first to use L1CAM to capture neuronal-derived EVs (Shi 2014). Multiple other studies followed using L1CAM as a marker for neuronal-derived EVs. This method was also supported by the observation, that typical neuronal proteins (e.g., αSyn) were enriched in L1CAM$^+$ EVs compared to CD81$^+$ EVs (Mustapic et al. 2017). However, a recent study from 2021 postulated, that L1CAM is not associated with plasma or CSF EVs at all (Norman et al. 2021). Several reasons lead to their conclusion: L1CAM is also expressed outside the brain and not neuron-specific; there is also a soluble extracellular form of L1CAM which is not associated with EVs and can be captured by anti-L1CAM antibodies; when performing SEC, L1CAM was enriched in different fractions than EVs. Furthermore, the detection of higher αSyn levels in L1CAM$^+$ EVs could be explained by a non-specific binding of soluble αSyn to the anti-L1CAM antibody. In conclusion, the authors do not recommend using L1CAM as a marker for neuronal-derived EVs (Norman et al. 2021). So far there is no suitable marker for neuronal-derived EVs available.

Despite doubt about the suitability of L1CAM and the IP experiments carried out before this last paper was published, some findings in this study still support L1CAM as a marker for neuronal-derived EVs. Firstly, the L1CAM signal in CSF EVs was stronger than in the serum EVs despite an overall lower protein concentration and particle number in the CSF samples. After standardising to the intensity of the TSG101 band as a common EV marker found in neuronal-derived and CSF EVs (Mustapic et al. 2017), the relative intensity of the L1CAM band was still higher in the CSF EVs. This observation suggests that

L1CAM is enriched in CSF EVs. Secondly, in the SEC experiment, L1CAM could be detected in the same fractions as the EVs: The EV peak was observed in the fractions 8 – 11 and L1CAM could be measured in the fractions 10 – 12. Both groups overlap indeed, nevertheless in the fractions 8 and 9 with vesicles the size of 100 – 200 nm, no L1AM signal was obtained. However, the topic remains controversial and future studies on $L1CAM^+$ neuronal-derived EVs must address this problem.

## 4.2. DNA composition in EVs

The first evidence of genetic information embedded in EVs came up in 2007 when it was discovered that exosomes from mouse and human mast cell lines contain functional mRNA and miRNA (Valadi et al. 2007). After transferring the exosomal RNA originating from the mouse cell line to human cells, new mouse proteins were detected in the human cells. A similar observation was made in exosomes from Glioblastoma tumour cells containing mRNA and miRNA, which could transfer their genetic information to recipient cells (Skog et al. 2008). The same study also suggested using the genetic information in EVs for diagnostic and therapeutic purposes. Double-stranded DNA was firstly discovered in exosomes in 2011: amplified oncogenes (c-Myc) and retrotransposon RNA transcripts were found in tumour exosomes (Balaj et al. 2011). The existence of dsDNA was later proven by other studies (Thakur et al. 2014; Kalluri and LeBleu 2016). Their findings also suggested that the exosomal DNA reflects the mutational status of the donor cells indicating the potential use of this parameter as a circulating biomarker (“liquid biopsy”) in tumours (Thakur et al. 2014). And finally, mtDNA could be detected in exosomes from Glioblastoma and Astrocyte cells (Guescini et al. 2010). However, not all cfDNA is associated with EVs/exosomes. A study from 2017 showed, that 93% of all amplifiable cfDNA in human plasma was located in plasma exosomes measured by droplet digital PCR (ddPCR) (Fernando et al. 2017). This observation also necessitates the use of a DNase to degrade the extra-vesicular cfDNA. Confocal microscopy of PicoGreen stained DNA in exosome preparations revealed, that a large proportion of plasma cfDNA was associated respectively localized in exosomes. Even after adding DNase to the sample, the DNA remained inside the exosomes indicating that exosomal DNA is protected from the DNase

due to the surrounding lipid bilayer (Fernando et al. 2017). Our PicoGreen staining experiments suggest a similar conclusion: The serum and CSF EV preparations ("pellet") exhibited a much higher number and density of the green fluorescent dots compared to the supernatant. Even when taking into consideration, that the serum and CSF EV preparations were highly concentrated because a small pellet from original 500 µl serum or 1000 µl CSF was resuspended in only 100 µl volume while the remaining supernatant was not concentrated at all, the signal is still stronger in the EV samples. (To compare both samples in the right way, the number of green dots in the supernatant sample would have to be multiplied by 5 (serum) or 10 (CSF), but as seen in the serum sample, the 1:30 dilution of the EV preparation still emits a stronger signal than the supernatant.) This difference was even more obvious in the CSF sample because there was almost no stained DNA in the supernatant present. Furthermore, the DNA inside EVs was protected from the DNase, because the DNase (added to the serum and CSF EV and supernatant samples) could not eradicate the DNA signal in the EV preparations. The positive signal in the DNase-treated supernatant could have two reasons: Firstly, the amount of DNase added to the supernatant might not have been sufficient to digest all remaining DNA. Secondly, many EVs could still be present in the supernatant protecting the DNA from being degraded. As expected, the number and density of the green fluorescent dots in the L1CAM$^+$ EV sample were much lower than in the serum EV sample since only a subpopulation of the total serum EVs was isolated. Nevertheless, the existence of dsDNA in EVs is still under investigation and different studies come to contradictory results. A recent extensive work from 2019 postulated, that dsDNA is not natively present in small EVs and exosomes, and the coexistence of dsDNA is more likely an indicator of insufficient purification (Jeppesen et al. 2019). However, dsDNA can be associated with larger vesicles.

The effect of the DNase treatment happened to be inconsistent between serum and CSF EV samples. While a clear and significant decline of the total DNA concentration in serum EVs after DNase treatment could be measured, no significant effect was found in the rtPCR for mtDNA. A possible explanation therefore could be, that cf-mtDNA only makes up a small part of the total cfDNA (Szilágyi et al. 2020), meaning that the effect of the

DNase should be most apparent in the nDNA that stands for the majority of the cfDNA. Therefore, the decline in the total DNA concentration and the absence of a DNase effect in mtDNA after the DNase treatment would make sense. A quantitative PCR for the nDNA would be helpful to prove this theory, but it was not performed in this study. In contrast to the serum EVs, the DNase had a significant effect on the $C_t$ values of ND1 and ND4 in the CSF EVs, but the sample size was also very small. In harmony with these results and the procedures described in the literature, DNase was added to all serum and CSF EV samples in the following experiments and also in the cohort samples.

DNA concentrations and compositions were examined in total serum and CSF EVs isolated with the ExoQuick™ kit as well as in L1CAM$^+$ EVs. Due to the multiple measurements and parameters, table 15 provides a short overview of the most important data:

***Table 15: Overview of the results of the DNA measurements in EVs.***

| **Total serum EVs** | | | **pellet** | **supernatant** | **p-value (t-test)** |
|---|---|---|---|---|---|
| | **DNA concentration** | | 0.055 ng/µl serum | 1.771 ng/µl serum | ** |
| | **$C_t$ value** | **ND1** | 20.53 | 28.51 | **** |
| | | **ND4** | 21.04 | 30.64 | **** |
| | | **ACTB** | 31.31 | 40.29 | - |
| | **$C_t$/DNA concentration** | **ND1** | 373.341 | 16.099 | **** |
| | | **ND4** | 382.591 | 17.301 | **** |
| | | **ACTB** | 569.273 | 22.750 | - |

| **Total CSF EVs** | | | **pellet** | **supernatant** | **p-value (t-test)** |
|---|---|---|---|---|---|
| | **DNA concentration** | | 0.022 ng/µl CSF | 0.263 ng/µl CSF | **** |
| | **$C_t$ value** | **ND1** | 30.71 | 31.92 | ns |
| | | **ND4** | 32.28 | 33.34 | ns |
| | | **ACTB** | 38.37 | 39.84 | - |
| | **$C_t$/DNA concentration** | **ND1** | 1414.977 | 121.350 | *** |
| | | **ND4** | 1492.166 | 126.749 | *** |
| | | **ACTB** | 1768.203 | 151.483 | - |

| **IP** | | **L1CAM$^+$ EVs** | **negative control** | **p-value (t-test)** |
|---|---|---|---|---|
| | **DNA concentration** | 0.041 ng/µl serum | 0.049 ng/µl serum) | ns |

| | | | | | |
|---|---|---|---|---|---|
| | **$C_t$ value** | **ND1** | 22.39 | 21.58 | ** |
| | | **ND4** | 23.00 | 22.01 | ** |
| | | **ACTB** | 31.84 | 32.16 | ns |
| | **$C_t$/DNA concentration** | **ND1** | 552.9 | 443.7 | **** |
| | | **ND4** | 567.8 | 452.5 | **** |
| | | **ACTB** | 786.2 | 661.1 | **** |

A common method to analyse rtPCR results is the $\Delta\Delta C_t$ method which calculates the difference between the expression of a housekeeping gene and the gene of interest. However, this method was not quite suitable for these experiments since defining a housekeeping gene for DNA in EVs is difficult and not standardised, and the goal was to measure the difference in the overall (mt)DNA quantity between pellet and supernatant respectively between L1CAM$^+$ EVs and negative controls and not primarily the difference in the expression of different genes. Since the $C_t$ value represents the number of cycles required for the fluorescence to exceed the background signal (= threshold), this value depends on the quantity of DNA loaded for the reaction. To reflect this situation, the ratio of the $C_t$ value and the DNA concentration was calculated and introduced as a new parameter. The higher the copy number of a gene, the lower the $C_t$ value for this gene and the other way round. DNA concentrations were measured with the Qubit™ fluorometer. However, biological replicates often exhibited a wide range of values, especially when measuring as low concentrations as in this case. For future experiments, a digital PCR (dPCR) could provide more precise and more reliable results because it makes the exact quantitation of target molecules possible (Kanagal-Shamanna 2016). The principle behind dPCR is the creation of millions of separate units by diluting and partitioning the original sample that contain all the necessary components for a “normal” PCR and additionally either one DNA particle or no DNA particle. Every single unit can be seen as a “micro-PCR” and the quantitation is binary (either reaction or no reaction) (Kanagal-Shamanna 2016). Two types of dPCR are used frequently: Either by creating millions of droplets of a water-in-oil emulsion (every droplet serves as a PCR unit) (Nakano et al. 2003) or by using a chip with microchannels (Azuara et al. 2012). This technique would allow the absolute quantitation of the number of copy numbers of a single DNA

fragment (e.g., gene) and could provide a more detailed insight into mtDNA copy numbers and deletions.

The only extensive study about the DNA composition of EVs was published by Fernando et al in 2017 (and their results were never proven by other studies). They measured the DNA concentration in plasma exosomes isolated with UC and sucrose gradient and compared it to the DNA concentration in the remaining supernatant and the native plasma. They reported a mean DNA concentration of 7 ng/ml plasma in native plasma, 5 ng/ml plasma in exosomes, and 0.6 ng/ml plasma in the supernatant (Fernando et al. 2017). Since they used 500 µl plasma instead of serum, another EV isolation method, and a different kit for the DNA extraction, a direct comparison between their data and the data presented in this study is not possible. Nevertheless, the reported DNA concentrations in this paper were lower than the measured DNA concentrations in this study (total serum EVs: 0.055 ng/µl serum (study: 0.005 ng/µl plasma), serum supernatant: 1.771 ng/µl serum (study: 0.0006 ng/µl plasma)) and in contrast to the paper, DNA concentrations were higher in the supernatant than in the EV preparations. This could indicate a contamination of the EV sample with non-vesicular DNA or an overall higher EV isolation efficiency (particle yields with the ExoQuick™ kit should be higher than with UC and sucrose gradient as used in the study). The same situation was observed in the CSF with overall lower DNA concentrations than in serum, but also with lower DNA concentrations in the CSF EV samples compared to the supernatant. No comparative values for the DNA concentration in CSF EVs and supernatant could be found in the literature. These findings seem to stand in contrast with the PicoGreen staining experiment. Since DNA measurements with the Qubit™ fluorometer often displayed a large range of values (especially for so low values like in this case) and a high standard deviation, rtPCR was regarded to provide a more accurate measurement. And although lower DNA concentrations were measured in serum and CSF EVs compared to the supernatant, higher copy numbers of ND1, ND4, and ACTB (lower $C_t$ values) were measured in the EV samples (highly significant in serum EVs, not significant in CSF EVs). This circumstance (lower $C_t$ values despite lower DNA concentrations) was also reflected in the $C_t$ value-DNA concentration ratio which was significantly higher in serum and CSF EVs compared to the

supernatant. For ND1 and ND4 this suggests the conclusion that mtDNA is enriched in the EV preparations. For ACTB, a nuclear gene, there is no simple conclusion to draw despite similar efficiency rates of the rtPCR. Firstly, it must be considered, that nDNA should make up the largest part of the total cfDNA (see above). However, overall higher $C_t$ values were measured in EV samples and supernatant. This could indicate that a large proportion of the cf-nDNA (including ACTB) was degraded by the DNase, but only a much smaller part of the cf-mtDNA, because it might have been protected inside the lipid bi-layer of the EVs. Furthermore, this hypothesis could also match the observations made in the DNase experiment (at least in serum EVs): The decline in the DNA concentration in the samples with DNase despite no significant difference in the $C_t$ values for ND1 and ND4 between DNase and no DNase samples could also implicate, that mtDNA is enriched in EVs where it is protected from degradation. Secondly, ACTB is just one gene among many others, and it cannot be fully excluded, that this gene is enriched in EVs while other nuclear genes are more abundant in the supernatant. Nevertheless, it remains unclear why also ACTB seems to be enriched in the EV preparations and further investigations would be required to solve this problem.

Beside serum and CSF samples, also IP samples with L1CAM$^+$ EVs and negative controls have been subjected to DNA measurements. The DNA concentrations between both groups did not differ significantly. On the one hand, the “native” $C_t$ values for ND1 and ND4 were lower in the negative control, but on the other hand, the normalization to the DNA concentration revealed for all three primers higher values in the L1CAM$^+$ EV group indicating a higher number of copy numbers of these genes. The origin of the DNA in the negative control in which no antibody at all was used could lie in an unspecific binding of DNA fragments to the beads (special magnetic beads can also be used for DNA extraction) which are then eluted in the sample. A possible solution for this problem could be the addition of a DNase because most of the unspecific bound DNA should be non-vesicular and therefore accessible for DNA degradation. This step was omitted in this experiment to avoid too much DNA loss, but it could help in the future to avoid the contamination of the EV samples with unspecific bound DNA. The original plan was to use this method for the serum cohort samples to isolate neuronal-derived EVs and use

their DNA for the calculation of the ND4/ND1 ratio. Due to the insufficient enrichment of (mt)DNA in L1CAM EVs compared to the negative controls, this plan was rejected, and instead, total serum EVs were used for the measurements. Furthermore, the prices for the materials need in the IP (beads, antibodies, …) were quite high and not suitable for a higher number of samples.

Summing up, mtDNA was enriched in total serum and CSF EVs compared to the supernatant justifying their usage for the cohort samples.

The remaining question concerns the biological role of mtDNA in EVs or to put it differently: What is the purpose of cf-mtDNA? Recent studies underline the role of mitochondria in innate immunity and the release of mtDNA into the cytosol or outside the cell as a mechanism to protect the nuclear genome (West et al. 2015; West and Shadel 2017; Wu et al. 2019). In this context, the cGAS-STING signalling pathway seems to be important. It was shown, that cGAS can detect cytoplasmic DNA fragments either from a bacterial respectively viral origin (Chen, Sun, and Chen 2016) or endogenous mtDNA (White et al. 2014). Stress to the mtDNA (e.g., a viral infection, chemotherapeutic drugs, *etc.*) can lead to an escape of mtDNA fragments into the cytosol where it is detected by cGAS. cGAS then activates and promotes STING signalling, which promotes a type I interferon response, resulting in an improved (antiviral) resistance of the cell and underlining the role of mitochondria in the innate immunity (West et al. 2015). It was also reported that the release of mtDNA into the cytosol enhances the repair of the nuclear genome, suggesting the role of mtDNA as a sentinel for genotoxic stress (Wu et al. 2019). But the presence of mtDNA is not limited to the cytosol, it can also be detected in the extracellular space (as shown in this study). A study from 2017 discovered that extracellular mtDNA can affect neighbouring immune cells and that neutrophil extracellular traps – involved in anti-bacterial response and sterile inflammations – contain mtDNA (Wang et al. 2015; Lood et al. 2016). Transferred to mitochondrial dysfunction and mtDNA deletions in PD, the question comes up whether more mtDNA is shipped out from damaged cells (e.g., dopaminergic SN neurons in PD) than healthy cells. The results of the cohort would suggest no (see below), but a comparison of mtDNA in CSF EVs from PD patients and healthy controls would be necessary to answer this question.

## 4.3. Cohort results

The basis of the usage of the ND4/ND1 ratio as a potential biomarker in PD lies in the discovery of a 4,977 bp deletion ("major arc deletion") (figure 22). This "common" deletion was first discovered in mtDNA extracted from muscle tissue in patients with mitochondrial myopathies (Holt, Harding, and Morgan-Hughes 1988). It was later reported that this deletion was also found in brain sections of PD patients: A higher mtDNA deletion load was found in the striatum of four of five PD patients compared to controls although also in the striatum of aged controls, deleted mtDNA was detectable but to a lesser degree (Ikebe et al. 1990). Furthermore, when looking at different parts of the brain, the proportion of deleted mtDNA was higher in the striatum (part of the basal ganglia and involved in the pathophysiology of PD) than in the cerebral cortex (Ikebe et al. 1990). Another study also found deleted mtDNA in the striatum of PD patients as well as controls, but the proportion of mutant mtDNA to normal mtDNA was in the parkinsonian striatum approx. 16-times higher than in the control striatum (5% vs. 0.3%) (Ozawa et al. 1990). A more recent study concluded that total mtDNA deletions and rearrangements (not limited to the common deletion) could be found in the SN of patients with PD, MSA, DLB, and AD compared to age-matched controls and that these changes

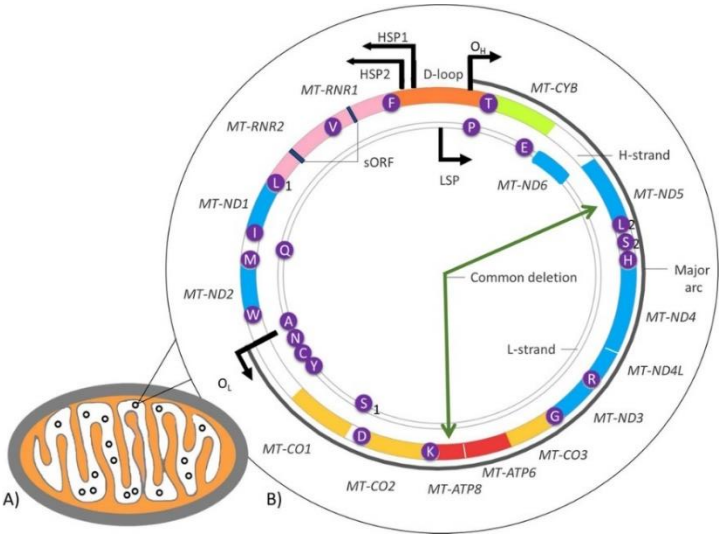


***Figure 22: Visualisation of the mitochondrial genome and the common deletion (between the green arrows).*** *The common deletion is a 4,977-bp deletion located between the MT-ATP8 and MT-ND5 gene. Several genes are enclosed by this deletion, including four genes coding for complex I of the respiratory chain (MT-ND3, MT-ND4, MT-ND4L, and MT-ND5).*

in the mtDNA were also increased in other parts of the brain (Dolle et al. 2016). In contrast, the point mutational load in the neuronal mtDNA was not increased ((Dolle et al. 2016). The same method to detect major arc deletions in mtDNA (N4/ND1) as in this study was also applied to fibroblasts from *LRRK2* carriers with either PD or not PD and healthy controls (Ouzren et al. 2019). They discovered a significant difference in the ND4/ND1 ratio between the three groups with the highest mtDNA deletion levels in *LRRK2* carriers with PD and an association between the somatic mtDNA deletion levels and PD (Ouzren et al. 2019). However, the link between the common deletion and PD is questioned by other researchers and the increased mtDNA deletion load could not be replicated in all studies: A study that performed Southern blot and PCR from SN tissue from PD patients and controls postulated, that the deletion is more likely to be age-related rather than contributing to the pathogenesis of the disease (Mann, Cooper, and Schapira 1992). Other researchers reported that the common deletion in PD patients is not increased at all compared to controls (Kösel et al. 1997). A study from 2002 showed, that mtDNA deletions accumulate primarily in neurons but not glial cells and that the mtDNA deletion load is the highest in the SN and other midbrain regions, but they did not find an association of the common deletion with nigral neurodegeneration (Zhang et al. 2002). Other studies followed a different approach and analysed the total burden of mtDNA deletions. Two studies reported significantly higher mtDNA deletion levels in single dopaminergic SN neurons in PD patients (Dolle et al. 2016) and in cholinergic neurons (Bury et al. 2017). Other studies only found a reduction of mtDNA copy numbers in SN neurons from idiopathic PD patients (Grünewald et al. 2016) or an overall higher level of deleted mtDNA in SN neurons in aged people and PD patients (Bender et al. 2006). Bender et al. also were the first to use the ND4/ND1 ratio to measure the common deletion. Last but not least, the ND4/ND1 ratio was also explored as a biomarker for bipolar disorder respectively schizophrenia (Kakiuchi et al. 2005), and thyroid cancer (Jiang et al. 2020). To sum up, the topic remains controversial with partly contradictory findings.

The study aimed to examine whether the ND4/ND1 ratio from DNA inside serum and CSF EVs could serve as a biomarker for PD. Since it was not possible to gain DNA from neuronal-derived $L1CAM^+$ serum EVs in sufficient quality and quantity and since the

controversy about L1CAM as a potential marker for neuronal-derived EVs continues, only total serum EVs extracted with the ExoQuick™ kit from PD patients and age-and gender-matched healthy controls as wells as total CSF EVs from PD patients were analysed. CSF samples from healthy controls would have been interesting too, but it was very hard to get them, so we gave up on these samples. The three remaining groups (total serum EVs from PD patients, total serum EVs from controls, and total CSF EVs from the same PD patients) also allowed for some interesting comparisons.

While the measured DNA concentrations in all three groups differed widely with a huge standard deviation and a large overlapping area, the $C_t$ values were quite homogenous within the groups with a little standard deviation (except for two values in the serum EV groups which had to be excluded). While some differences between the groups were expected (e.g., similar DNA and protein concentrations in serum EV samples from PD patients and controls or a much higher protein concentration in the serum EV samples compared to the CSF EV samples), it stands out, that the mean DNA concentration in the CSF EV samples was significantly higher than the mean DNA concentration in the serum EV samples. In the test samples which were analysed to establish the methods, the ratio between serum and CSF EVs was the other way round. This can partly be explained by the fact, that very old CSF samples were used that otherwise would have been discarded. As mentioned above, DNA in EVs seems to be quite stable when stored at -80°C, but nevertheless, a reduction of the DNA quantity over a longer period seems to be likely. Furthermore, despite the higher mean DNA concentration in CSF EVs, the $C_t$ values in this group were significantly higher than in the serum EV group, indicating that in total more mtDNA was enriched in the serum EVs compared to the CSF EVs. Unfortunately, no significant difference in the ND4/ND1 ratio between total serum EVs from PD patients and controls could be measured, also when normalized to the DNA concentration. Biomarkers from serum would be the most convenient since drawing blood is a less-invasive procedure, does not require special equipment, and is everywhere accessible. CSF biomarker would require a lumbar puncture, an invasive and painful procedure that requires a specialist and that is associated with the risk of severe complications, and the obtained volume is usually smaller. A significant difference could be calculated when the

ND4/ND1 ratios of total serum EVs and total CSF EVs from the same PD patients were compared. The ND4/ND1 ratio was significantly lower in the CSF EVs. However, the relation between the ratios in serum and CSF EVs was not consistent: 70% of the PD patients exhibited higher ND1/ND4 ratios in CSF EVs than in serum EVs and in 30% of the PD patients, the direction was the other way round. These findings clarify that the mtDNA composition of CSF EVs differed significantly from the mtDNA composition of serum EVs. Since no difference in the ND4/ND1 ratio in serum EVs from PD patients and controls was found, CSF EVs might be more suitable as a biomarker: Firstly, neuronal-derived EVs that have passed the BBB make up only a small part of the total serum EVs. When analysing total serum EVs they could get lost in the abundant other serum EVs. Secondly, the isolation of neuronal-derived EVs remains controversial, and as long as L1CAM is not validated as a marker for neuronal-derived EVs or as long as no other reliable marker is discovered, CSF EVs come closest to the brain. Thirdly, the main pathophysiological process plays in the brain that stands in a direct neighbourhood with the CSF, so changes in the brain should affect the CSF in an early stage making CSF EVs a suitable candidate for biomarkers. Nevertheless, also a difference in the ND4/ND1 ratio in CSF EVs between PD patients and controls would be hard to find because neurons are not the only cells secreting EVs and the mtDNA deletion was so far mainly observed in neurons from the SN and the striatum, but they only represent a tiny proportion of all cerebral neurons. So even if there were a mtDNA deletion in the patient's brain, it could get covered by the other EVs. What is missing in this experiment is a real positive control to prove that the method is functioning properly and can detect the common mutation. Another missing topic concerns the comparison between CSF EVs from PD patients and healthy controls. But before using these precious samples, the method should be tried and tested more to ensure proper results.

# 5. Conclusion

This study followed two main goals: Firstly, to establish a method to isolate EVs from serum and CSF, to characterize these EVs regarding their protein composition, particle size, and appearance under TEM, and to create a method to extract DNA from these particles. Secondly, to apply these methods to a cohort consisting of PD patients and healthy controls to examine, whether mtDNA in EVs could serve as a biomarker for PD. The isolation and characterization of EVs were successful: After trying different methods (UC, SEC), a commercial kit (ExoQuick™) was used to isolate EVs from serum and CSF. Characterization by TEM, NTA, and Western Blot revealed the typical characteristics of EVs. Also, the isolation of (potential) neuronal-derived $L1CAM^+$ EVs from serum was possible, although the method turned out to be unsuitable for the cohort samples. Total serum and CSF EVs showed the enrichment of mtDNA justifying their usage for the cohort samples. The cohort consisted of 35 PD patients with serum and CSF samples and 35 healthy controls with serum samples. The primary endpoint was the ratio of the mitochondrial genes ND4 and ND1 in DNA from total serum and CSF EVs to detect a common deletion previously found in PD patients. While no difference could be detected between serum EVs from PD patients and controls, the comparison of serum EVs and CSF EVs from the PD patients revealed a significant difference making CSF EVs a potential biomarker for PD although further research is required.

# 6. Summary

## 6.1. English

Parkinson's disease (PD) is the second most common neurodegenerative disease after Alzheimer's disease and affects 150 000 – 250 000 people in Germany. Although the disease is not curable yet, great progress has been made in the past few years to treat the symptoms and improve the quality of life of these patients. However, reliable biomarkers to detect the disease in an early stage before the first symptoms occur are so far unavailable. Mitochondrial dysfunction and mitochondrial DNA (mtDNA) damage could be detected in many PD patients, but their analysis requires either post-mortem brain sections, a brain biopsy, or CSF. Extracellular vesicles (EVs) are a potential new source of biomarkers. They are nanoparticles made of a lipid bilayer and can be found in serum and CSF and can also pass the blood-brain barrier. EVs carry mtDNA making them suitable for genetic analysis.

In this work, different EV isolation methods from serum and CSF were tested and corresponding protocols were established (ultracentrifugation, size-exclusion chromatography, precipitation techniques). A commercial kit (ExoQuick™) was chosen for the downstream analysis as the most promising method. EVs were characterized by their appearance, their size, and their protein composition. Extravesicular DNA was digested, and DNA was extracted from the EV preparation and characterized by PCR showing enrichment of mtDNA in these samples. Furthermore, an immunoprecipitation technique was modified to use the transmembrane protein L1CAM as a potential marker for neuronal-derived EVs in serum, but this method turned out to be unsuitable for the downstream analysis.

A cohort with 35 PD patients (serum and CSF samples) and 35 healthy controls (only serum samples) was built to assess the suitability of mtDNA in EVs as a biomarker for PD. The primary endpoint was the ratio of two mitochondrial genes (ND4 and ND1) as an established parameter to detect deletion in the mtDNA. EVs from the serum and CSF samples were isolated using the ExoQuick™ kit, their DNA was extracted, and gene expression was measured by using quantitative real-time PCR. The ND4/ND1 ratio showed

no difference between serum EVs from PD patients and controls, but a significant difference could be observed when comparing serum and CSF EVs from the PD patients. mtDNA deletion measured with the ND4/ND1 ratio in serum EVs did not turn out to be a reliable biomarker for PD. However, CSF EVs might serve as better biomarkers and further research is required to explore their promising potential.

## 6.2. German

Morbus Parkinson ist die zweithäufigste neurodegenerative Erkrankung hinter Morbus Alzheimer und betrifft 150 000 – 250 000 Menschen in Deutschland. Obwohl die Erkrankung bisher nicht heilbar ist, wurden in den letzten Jahren große Fortschritte gemacht was die Behandlung der Symptome und die Verbesserung der Lebensqualität betrifft. Nichtsdestotrotz fehlen bisher immer noch zuverlässige Biomarker, um die Krankheit in einem frühen Stadium zu erkennen bevor die ersten Symptome auftreten. Eine Dysfunktion der Mitochondrien und Schaden an der mitochondrialen DNA (mtDNA) wurden in Parkinson-Patienten entdeckt, jedoch erfordern derartige Untersuchungen entweder Gehirnschnitte von verstorbenen Parkinson-Patienten, eine Hirnbiopsie oder Liquor. Extrazelluläre Vesikel (EVs) stellen neue potentielle Biomarker dar. EVs sind Nanopartikel, die aus einer Lipiddoppelschicht bestehen und im Serum und im Liquor zu finden sind, aber auch die Blut-Hirn-Schranke überwinden können. EVs transportieren mtDNA im Innern, die für genetische Untersuchungen genutzt werden kann.

In dieser Arbeit wurden verschiedene Techniken zur Isolierung von EVs erprobt und entsprechende Protokolle etabliert (Ultrazentrifugation, Größenausschluss-Chromatographie, Fällungs-Techniken). Als vielversprechendste Methode wurde ein kommerziell erhältliches Kit (ExoQuick™) für die nachfolgenden Untersuchungen ausgewählt. EVs wurden anhand ihres Aussehens, ihrer Größe und ihrer Protein-Zusammensetzung charakterisiert. Extravesikuläre DNA wurde verdaut und die verbliebene DNA aus der EV-Probe extrahiert und mittels PCR charakterisiert. Darin zeigte sich eine Anreicherung von mtDNA in diesen Proben. Zusätzlich wurde eine Immunfällung-Methode modifiziert, um das Transmembran-Protein L1CAM als potentiellen Marker für EVs im Serum zu

verwenden, die von neuronalen Zellen abstammen. Diese Methode zeigte sich allerdings ungeeignet für die nachfolgenden Untersuchungen.

Eine Kohorte bestehend aus 35 Parkinson-Patienten (Serum- und Liquor-Proben) und 35 gesunden Kontrollpersonen (nur Serum-Proben) wurde aufgebaut, um herauszufinden, ob sich mtDNA als Biomarker für M. Parkinson eignen könnte. Der Quotient aus zwei mitochondrialen Genen (ND4 und ND1) – ein etablierter Parameter, um Deletionen in der mtDNA nachzuweisen – bildete den primären Endpunkt der Studie. EVs aus Serum und CSF wurden mithilfe des ExoQuick™ Kits isoliert, die entsprechende DNA extrahiert und die Genexpression mittels quantitativer real-time PCR gemessen. Der ND4/ND1-Quotient zeigte keinen Unterschied zwischen den Serum-EVs der Parkinson-Patienten und der Kontrollen, jedoch konnte ein signifikanter Unterschied zwischen den Serum-EVs und den Liquor-EVs der Parkinson-Patienten festgestellt werden. Der ND4/ND1-Quotient aus Serum-EVs, um Deletionen in der mtDNA zu messen, stellte sich somit nicht als zuverlässiger Biomarker für M. Parkinson heraus. EVs aus Liquor könnten dagegen eher als Biomarker in Frage kommen, es braucht jedoch mehr Forschung, um ihr Potential auszuloten.

# 7. References


Aarsland, D., M. K. Beyer, and M. W. Kurz. 2008. 'Dementia in Parkinson's disease', *Curr Opin Neurol*, 21: 676-82.

Aarsland, D., J. Zaccai, and C. Brayne. 2005. 'A systematic review of prevalence studies of dementia in Parkinson's disease', *Mov Disord*, 20: 1255-63.

Abbott, R. D., H. Petrovitch, L. R. White, K. H. Masaki, C. M. Tanner, J. D. Curb, A. Grandinetti, P. L. Blanchette, J. S. Popper, and G. W. Ross. 2001. 'Frequency of bowel movements and the future risk of Parkinson's disease', *Neurology*, 57: 456-62.

Alvarez-Erviti, L., Y. Seow, A. H. Schapira, C. Gardiner, I. L. Sargent, M. J. Wood, and J. M. Cooper. 2011. 'Lysosomal dysfunction increases exosome-mediated alpha-synuclein release and transmission', *Neurobiol Dis*, 42: 360-7.

Alvarez-Erviti, L., Y. Seow, H. Yin, C. Betts, S. Lakhal, and M. J. Wood. 2011. 'Delivery of siRNA to the mouse brain by systemic injection of targeted exosomes', *Nat Biotechnol*, 29: 341-5.

Andres-Mateos, E., C. Perier, L. Zhang, B. Blanchard-Fillion, T. M. Greco, B. Thomas, H. S. Ko, M. Sasaki, H. Ischiropoulos, S. Przedborski, T. M. Dawson, and V. L. Dawson. 2007. 'DJ-1 gene deletion reveals that DJ-1 is an atypical peroxiredoxin-like peroxidase', *Proc Natl Acad Sci U S A*, 104: 14807-12.

Aronson, J. K., and R. E. Ferner. 2017. 'Biomarkers-A General Review', *Curr Protoc Pharmacol*, 76: 9.23.1-9.23.17.

Ascherio, A., H. Chen, M. G. Weisskopf, E. O'Reilly, M. L. McCullough, E. E. Calle, M. A. Schwarzschild, and M. J. Thun. 2006. 'Pesticide exposure and risk for Parkinson's disease', *Ann Neurol*, 60: 197-203.

Ascherio, A., and M. A. Schwarzschild. 2016. 'The epidemiology of Parkinson's disease: risk factors and prevention', *Lancet Neurol*, 15: 1257-72.

Axelsen, T. M., and D. P. D. Woldbye. 2018. 'Gene Therapy for Parkinson's Disease, An Update', *J Parkinsons Dis*, 8: 195-215.

Azuara, D., M. M. Ginesta, M. Gausachs, F. Rodriguez-Moranta, J. Fabregat, J. Busquets, N. Pelaez, J. Boadas, S. Galter, V. Moreno, J. Costa, J. de Oca, and G. Capellá. 2012. 'Nanofluidic digital PCR for KRAS mutation detection and quantification in gastrointestinal cancer', *Clin Chem*, 58: 1332-41.

Bakhti, M., C. Winter, and M. Simons. 2011. 'Inhibition of myelin membrane sheath formation by oligodendrocyte-derived exosome-like vesicles', *J Biol Chem*, 286: 787-96.

Balaj, L., R. Lessard, L. Dai, Y. J. Cho, S. L. Pomeroy, X. O. Breakefield, and J. Skog. 2011. 'Tumour microvesicles contain retrotransposon elements and amplified oncogene sequences', *Nat Commun*, 2: 180.

Baumann, C. R. 2012. 'Epidemiology, diagnosis and differential diagnosis in Parkinson's disease tremor', *Parkinsonism Relat Disord*, 18 Suppl 1: S90-2.

Beitz, J. M. 2014. 'Parkinson's disease: a review', *Front Biosci (Schol Ed)*, 6: 65-74.

Bender, A., K. J. Krishnan, C. M. Morris, G. A. Taylor, A. K. Reeve, R. H. Perry, E. Jaros, J. S. Hersheson, J. Betts, T. Klopstock, R. W. Taylor, and D. M. Turnbull. 2006. 'High levels of mitochondrial DNA deletions in substantia nigra neurons in aging and Parkinson disease', *Nat Genet*, 38: 515-7.

'Biomarkers and surrogate endpoints: preferred definitions and conceptual framework'. 2001. *Clin Pharmacol Ther*, 69: 89-95.

Böing, A. N., E. van der Pol, A. E. Grootemaat, F. A. W. Coumans, A. Sturk, and R. Nieuwland. 2014. 'Single-step isolation of extracellular vesicles by size-exclusion chromatography', *J Extracell Vesicles*, 3.

Bonello, F., S. M. Hassoun, F. Mouton-Liger, Y. S. Shin, A. Muscat, C. Tesson, S. Lesage, P. M. Beart, A. Brice, J. Krupp, J. C. Corvol, and O. Corti. 2019. 'LRRK2 impairs PINK1/Parkin-dependent mitophagy via its kinase activity: pathologic insights into Parkinson's disease', *Hum Mol Genet*, 28: 1645-60.

Bonifacino, J. S., D. C. Gershlick, and E. C. Dell'Angelica. 2016. 'Immunoprecipitation', *Curr Protoc Cell Biol*, 71.

Bonifati, V., P. Rizzu, M. J. van Baren, O. Schaap, G. J. Breedveld, E. Krieger, M. C. Dekker, F. Squitieri, P. Ibanez, M. Joosse, J. W. van Dongen, N. Vanacore, J. C. van Swieten, A. Brice, G. Meco, C. M. van Duijn, B. A. Oostra, and P. Heutink. 2003. 'Mutations in the DJ-1 gene associated with autosomal recessive early-onset parkinsonism', *Science*, 299: 256-9.

Borges, F. T., L. A. Reis, and N. Schor. 2013. 'Extracellular vesicles: structure, function, and potential clinical uses in renal diseases', *Braz J Med Biol Res*, 46: 824-30.

Borsche, M., S. L. Pereira, C. Klein, and A. Grünewald. 2021. 'Mitochondria and Parkinson's Disease: Clinical, Molecular, and Translational Aspects', *J Parkinsons Dis*, 11: 45-60.

Braak, H., U. Rüb, W. P. Gai, and K. Del Tredici. 2003. 'Idiopathic Parkinson's disease: possible routes by which vulnerable neuronal types may be subject to neuroinvasion by an unknown pathogen', *J Neural Transm (Vienna)*, 110: 517-36.

Brück, D., G. K. Wenning, N. Stefanova, and L. Fellner. 2016. 'Glia and alpha-synuclein in neurodegeneration: A complex interaction', *Neurobiol Dis*, 85: 262-74.

Bury, A. G., A. Pyle, J. L. Elson, L. Greaves, C. M. Morris, G. Hudson, and I. S. Pienaar. 2017. 'Mitochondrial DNA changes in pedunculopontine cholinergic neurons in Parkinson disease', *Ann Neurol*, 82: 1016-21.

Cao, Z., Y. Wu, G. Liu, Y. Jiang, X. Wang, Z. Wang, and T. Feng. 2019. 'α-Synuclein in salivary extracellular vesicles as a potential biomarker of Parkinson's disease', *Neurosci Lett*, 696: 114-20.

Chan, S. S., and W. C. Copeland. 2009. 'DNA polymerase gamma and mitochondrial disease: understanding the consequence of POLG mutations', *Biochim Biophys Acta*, 1787: 312-9.

Chen, Q., L. Sun, and Z. J. Chen. 2016. 'Regulation and function of the cGAS-STING pathway of cytosolic DNA sensing', *Nat Immunol*, 17: 1142-9.

Cheng, Y., and J. S. Schorey. 2013. 'Exosomes carrying mycobacterial antigens can protect mice against Mycobacterium tuberculosis infection', *Eur J Immunol*, 43: 3279-90.

Chinta, S. J., J. K. Mallajosyula, A. Rane, and J. K. Andersen. 2010. 'Mitochondrial α-synuclein accumulation impairs complex I function in dopaminergic neurons and results in increased mitophagy in vivo', *Neurosci Lett*, 486: 235-9.

Chivet, M., C. Javalet, F. Hemming, K. Pernet-Gallay, K. Laulagnier, S. Fraboulet, and R. Sadoul. 2013. 'Exosomes as a novel way of interneuronal communication', *Biochem Soc Trans*, 41: 241-4.

Chou, K. L. 2021. 'Diagnosis and differential diagnosis of Parkinson disease.' in UpToDate Eichler AF (ed.), *UpToDate, Waltham, MA*.

Chou, K. L. , and D. Tarsy. 2022. 'Device-assisted and lesioning procedures for Parkinson disease.' in UpToDate Eichler AF (ed.), *UpToDate, Waltham, MA*.

Cocucci, E., and J. Meldolesi. 2015. 'Ectosomes and exosomes: shedding the confusion between extracellular vesicles', *Trends Cell Biol*, 25: 364-72.

Cocucci, E., G. Racchetti, and J. Meldolesi. 2009. 'Shedding microvesicles: artefacts no more', *Trends Cell Biol*, 19: 43-51.

Colombo, M., G. Raposo, and C. Thery. 2014. 'Biogenesis, secretion, and intercellular interactions of exosomes and other extracellular vesicles', *Annu Rev Cell Dev Biol*, 30: 255-89.

Corti, O., S. Lesage, and A. Brice. 2011. 'What genetics tells us about the causes and mechanisms of Parkinson's disease', *Physiol Rev*, 91: 1161-218.

Cotzias, G. C., M. H. Van Woert, and L. M. Schiffer. 1967. 'Aromatic amino acids and modification of parkinsonism', *N Engl J Med*, 276: 374-9.

Coxhead, J., M. Kurzawa-Akanbi, R. Hussain, A. Pyle, P. Chinnery, and G. Hudson. 2016. 'Somatic mtDNA variation is an important component of Parkinson's disease', *Neurobiol Aging*, 38: 217.e1-17.e6.

Crenshaw, B. J., L. Gu, B. Sims, and Q. L. Matthews. 2018. 'Exosome Biogenesis and Biological Function in Response to Viral Infections', *Open Virol J*, 12: 134-48.

Danzer, Karin M., Lisa R. Kranich, Wolfgang P. Ruf, Ozge Cagsal-Getkin, Ashley R. Winslow, Liya Zhu, Charles R. Vanderburg, and Pamela J. McLean. 2012. 'Exosomal cell-to-cell transmission of alpha synuclein oligomers', *Mol Neurodegener*, 7: 42.

Davidzon, G., P. Greene, M. Mancuso, K. J. Klos, J. E. Ahlskog, M. Hirano, and S. DiMauro. 2006. 'Early-onset familial parkinsonism due to POLG mutations', *Ann Neurol*, 59: 859-62.

De Virgilio, A., A. Greco, G. Fabbrini, M. Inghilleri, M. I. Rizzo, A. Gallo, M. Conte, C. Rosato, M. Ciniglio Appiani, and M. de Vincentiis. 2016. 'Parkinson's disease: Autoimmunity and neuroinflammation', *Autoimmun Rev*, 15: 1005-11.

Del Tredici, K., and H. Braak. 2012. 'Lewy pathology and neurodegeneration in premotor Parkinson's disease', *Mov Disord*, 27: 597-607.

DeMaagd, G., and A. Philip. 2015. 'Parkinson’s Disease and Its Management: Part 1: Disease Entity, Risk Factors, Pathophysiology, Clinical Presentation, and Diagnosis', *P t*, 40: 504-32.

Di Vizio, D., M. Morello, A. C. Dudley, P. W. Schow, R. M. Adam, S. Morley, D. Mulholland, M. Rotinen, M. H. Hager, L. Insabato, M. A. Moses, F. Demichelis, M. P. Lisanti, H. Wu, M. Klagsbrun, N. A. Bhowmick, M. A. Rubin, C. D'Souza-Schorey, and M. R. Freeman. 2012. 'Large oncosomes in human prostate cancer tissues and in the circulation of mice with metastatic disease', *Am J Pathol*, 181: 1573-84.

Dolle, C., I. Flones, G. S. Nido, H. Miletic, N. Osuagwu, S. Kristoffersen, P. K. Lilleng, J. P. Larsen, O. B. Tysnes, K. Haugarvoll, L. A. Bindoff, and C. Tzoulis. 2016. 'Defective mitochondrial DNA homeostasis in the substantia nigra in Parkinson disease', *Nat Commun*, 7: 13548.

Edgar, J. R., E. R. Eden, and C. E. Futter. 2014. 'Hrs- and CD63-dependent competing mechanisms make different sized endosomal intraluminal vesicles', *Traffic*, 15: 197-211.

Erickson, P. A., G. P. Lewis, and S. K. Fisher. 1993. 'Postembedding immunocytochemical techniques for light and electron microscopy', *Methods Cell Biol*, 37: 283-310.

Fauré, J., G. Lachenal, M. Court, J. Hirrlinger, C. Chatellard-Causse, B. Blot, J. Grange, G. Schoehn, Y. Goldberg, V. Boyer, F. Kirchhoff, G. Raposo, J. Garin, and R. Sadoul. 2006. 'Exosomes are released by cultured cortical neurones', *Mol Cell Neurosci*, 31: 642-8.

Fénelon, G., F. Mahieux, R. Huon, and M. Ziégler. 2000. 'Hallucinations in Parkinson's disease: prevalence, phenomenology and risk factors', *Brain*, 123 ( Pt 4): 733-45.

Fernando, M. Rohan, Chao Jiang, Gary D. Krzyzanowski, and Wayne L. Ryan. 2017. 'New evidence that a large proportion of human blood plasma cell-free DNA is localized in exosomes', *PLoS One*, 12: e0183915-e15.

Fiandaca, M. S., D. Kapogiannis, M. Mapstone, A. Boxer, E. Eitan, J. B. Schwartz, E. L. Abner, R. C. Petersen, H. J. Federoff, B. L. Miller, and E. J. Goetzl. 2015. 'Identification of preclinical Alzheimer's disease by a profile of pathogenic proteins in neurally derived blood exosomes: A case-control study', *Alzheimers Dement*, 11: 600-7.e1.

Fischer, M., I. Gemende, W. C. Marsch, and P. A. Fischer. 2001. 'Skin function and skin disorders in Parkinson's disease', *J Neural Transm (Vienna)*, 108: 205-13.

Fraser, K. B., M. S. Moehle, J. P. Daher, P. J. Webber, J. Y. Williams, C. A. Stewart, T. A. Yacoubian, R. M. Cowell, T. Dokland, T. Ye, D. Chen, G. P. Siegal, R. A. Galemmo, E. Tsika, D. J. Moore, D. G. Standaert, K. Kojima, J. A. Mobley, and A. B. West. 2013. 'LRRK2 secretion in exosomes is regulated by 14-3-3', *Hum Mol Genet*, 22: 4988-5000.

Fraser, K. B., A. B. Rawlins, R. G. Clark, R. N. Alcalay, D. G. Standaert, N. Liu, and A. B. West. 2016. 'Ser(P)-1292 LRRK2 in urinary exosomes is elevated in idiopathic Parkinson's disease', *Mov Disord*, 31: 1543-50.

Freed, C. R., P. E. Greene, R. E. Breeze, W. Y. Tsai, W. DuMouchel, R. Kao, S. Dillon, H. Winfield, S. Culver, J. Q. Trojanowski, D. Eidelberg, and S. Fahn. 2001. 'Transplantation of embryonic dopamine neurons for severe Parkinson's disease', *N Engl J Med*, 344: 710-9.

Furi, I., F. Momen-Heravi, and G. Szabo. 2017. 'Extracellular vesicle isolation: present and future', *Ann Transl Med*, 5.

Galvan, A., and T. Wichmann. 2008. 'Pathophysiology of Parkinsonism', *Clin Neurophysiol*, 119: 1459-74.

Gao, X., H. Chen, M. A. Schwarzschild, D. B. Glasser, G. Logroscino, E. B. Rimm, and A. Ascherio. 2007. 'Erectile function and risk of Parkinson's disease', *Am J Epidemiol*, 166: 1446-50.

Ghidoni, R., L. Benussi, and G. Binetti. 2008. 'Exosomes: the Trojan horses of neurodegeneration', *Med Hypotheses*, 70: 1226-7.

Giannoccaro, M. P., C. La Morgia, G. Rizzo, and V. Carelli. 2017. 'Mitochondrial DNA and primary mitochondrial dysfunction in Parkinson's disease', *Mov Disord*, 32: 346-63.

Goetzl, E. J., M. Mustapic, D. Kapogiannis, E. Eitan, I. V. Lobach, L. Goetzl, J. B. Schwartz, and B. L. Miller. 2016. 'Cargo proteins of plasma astrocyte-derived exosomes in Alzheimer's disease', *Faseb j*, 30: 3853-59.

Greenamyre, J. T., D. S. Higgins, and R. V. Eller. 1992. 'Quantitative autoradiography of dihydrorotenone binding to complex I of the electron transport chain', *J Neurochem*, 59: 746-9.

Grünewald, A., K. A. Rygiel, P. D. Hepplewhite, C. M. Morris, M. Picard, and D. M. Turnbull. 2016. 'Mitochondrial DNA Depletion in Respiratory Chain-Deficient Parkinson Disease Neurons', *Ann Neurol*, 79: 366-78.

Guescini, M., S. Genedani, V. Stocchi, and L. F. Agnati. 2010. 'Astrocytes and Glioblastoma cells release exosomes carrying mtDNA', *J Neural Transm (Vienna)*, 117: 1-4.

Gui, Y., H. Liu, L. Zhang, W. Lv, and X. Hu. 2015. 'Altered microRNA profiles in cerebrospinal fluid exosome in Parkinson disease and Alzheimer disease', *Oncotarget*, 6: 37043-53.

Guo, M., J. Wang, Y. Zhao, Y. Feng, S. Han, Q. Dong, M. Cui, and K. Tieu. 2020. 'Microglial exosomes facilitate α-synuclein transmission in Parkinson's disease', *Brain*, 143: 1476-97.

Gurung, S., D. Perocheau, L. Touramanidou, and J. Baruteau. 2021. 'The exosome journey: from biogenesis to uptake and intracellular signalling', *Cell Commun Signal*, 19: 47.

Gyorgy, B., T. G. Szabo, M. Pasztoi, Z. Pal, P. Misjak, B. Aradi, V. Laszlo, E. Pallinger, E. Pap, A. Kittel, G. Nagy, A. Falus, and E. I. Buzas. 2011. 'Membrane vesicles, current state-of-the-art: emerging role of extracellular vesicles', *Cell Mol Life Sci*, 68: 2667-88.

Harding, C., and P. Stahl. 1983. 'Transferrin recycling in reticulocytes: pH and iron are important determinants of ligand binding and processing', *Biochem Biophys Res Commun*, 113: 650-8.

Hedrich, K., C. Eskelson, B. Wilmot, K. Marder, J. Harris, J. Garrels, H. Meija-Santana, P. Vieregge, H. Jacobs, S. B. Bressman, A. E. Lang, M. Kann, G. Abbruzzese, P. Martinelli, E. Schwinger, L. J. Ozelius, P. P. Pramstaller, C. Klein, and P. Kramer. 2004. 'Distribution, type, and origin of Parkin mutations: review and case studies', *Mov Disord*, 19: 1146-57.

Helwa, I., J. Cai, M. D. Drewry, A. Zimmerman, M. B. Dinkins, M. L. Khaled, M. Seremwe, W. M. Dismuke, E. Bieberich, W. D. Stamer, M. W. Hamrick, and Y. Liu. 2017. 'A Comparative Study of Serum Exosome Isolation Using Differential Ultracentrifugation and Three Commercial Reagents', *PLoS One*, 12: e0170628.

Hely, M. A., W. G. Reid, M. A. Adena, G. M. Halliday, and J. G. Morris. 2008. 'The Sydney multicenter study of Parkinson's disease: the inevitability of dementia at 20 years', *Mov Disord*, 23: 837-44.

Hessvik, N. P., and A. Llorente. 2018. 'Current knowledge on exosome biogenesis and release', *Cell Mol Life Sci*, 75: 193-208.

Ho, D. H., S. Yi, H. Seo, I. Son, and W. Seol. 2014. 'Increased DJ-1 in urine exosome of Korean males with Parkinson's disease', *Biomed Res Int*, 2014: 704678.

Holt, I. J., A. E. Harding, and J. A. Morgan-Hughes. 1988. 'Deletions of muscle mitochondrial DNA in patients with mitochondrial myopathies', *Nature*, 331: 717-9.

Hong, Z., M. Shi, K. A. Chung, J. F. Quinn, E. R. Peskind, D. Galasko, J. Jankovic, C. P. Zabetian, J. B. Leverenz, G. Baird, T. J. Montine, A. M. Hancock, H. Hwang, C. Pan, J. Bradner, U. J. Kang, P. H. Jensen, and J. Zhang. 2010. 'DJ-1 and alpha-synuclein in human cerebrospinal fluid as biomarkers of Parkinson's disease', *Brain*, 133: 713-26.

Hughes, A. J., S. E. Daniel, L. Kilford, and A. J. Lees. 1992. 'Accuracy of clinical diagnosis of idiopathic Parkinson's disease: a clinico-pathological study of 100 cases', *J Neurol Neurosurg Psychiatry*, 55: 181-4.

Ikebe, S., M. Tanaka, K. Ohno, W. Sato, K. Hattori, T. Kondo, Y. Mizuno, and T. Ozawa. 1990. 'Increase of deleted mitochondrial DNA in the striatum in Parkinson's disease and senescence', *Biochem Biophys Res Commun*, 170: 1044-8.

Indyk, Harvey E., Jacob W. Williams, and Hasmukh A. Patel. 2008. 'Analysis of denaturation of bovine IgG by heat and high pressure using an optical biosensor', *International Dairy Journal*, 18: 359-66.

Jahn, R., and R. H. Scheller. 2006. 'SNAREs--engines for membrane fusion', *Nat Rev Mol Cell Biol*, 7: 631-43.

Jaiswal, J. K., N. W. Andrews, and S. M. Simon. 2002. 'Membrane proximal lysosomes are the major vesicles responsible for calcium-dependent exocytosis in nonsecretory cells', *J Cell Biol*, 159: 625-35.

James Parkinson, Member of the Royal College of Surgeons. 2002. 'An Essay on the Shaking Palsy', *The Journal of Neuropsychiatry and Clinical Neurosciences*, 14: 223-36.

Jankovic, J. 2008. 'Parkinson's disease: clinical features and diagnosis', *J Neurol Neurosurg Psychiatry*, 79: 368-76.

Jankovic, J. 2021. 'Etiology and pathogenesis of Parkinson disease.' in UpToDate Eichler AF (ed.), *UpToDate, Waltham, MA*.

Jeppesen, D. K., A. M. Fenix, J. L. Franklin, J. N. Higginbotham, Q. Zhang, L. J. Zimmerman, D. C. Liebler, J. Ping, Q. Liu, R. Evans, W. H. Fissell, J. G. Patton, L. H. Rome, D. T. Burnette, and R. J. Coffey. 2019. 'Reassessment of Exosome Composition', *Cell*, 177: 428-45.e18.

Jiang, Z., T. Bahr, C. Zhou, T. Jin, H. Chen, S. Song, Y. Ikeno, H. Tian, and Y. Bai. 2020. 'Diagnostic value of circulating cell-free mtDNA in patients with suspected thyroid cancer: ND4/ND1 ratio as a new potential plasma marker', *Mitochondrion*, 55: 145-53.

Jin, Yang, Keyan Chen, Zongying Wang, Yan Wang, Jianzhi Liu, Li Lin, Yong Shao, Lihua Gao, Huihui Yin, Cong Cui, Zhaoli Tan, Liejun Liu, Chuanhua Zhao, Gairong Zhang, Ru Jia, Lijuan Du, Yuling Chen, Rongrui Liu, Jianming Xu, Xianwen Hu, and Youliang %J BMC Cancer Wang. 2016. 'DNA in serum extracellular vesicles is stable under different storage conditions', 16: 753.

Johnstone, R. M., M. Adam, J. R. Hammond, L. Orr, and C. Turbide. 1987. 'Vesicle formation during reticulocyte maturation. Association of plasma membrane activities with released vesicles (exosomes)', *J Biol Chem*, 262: 9412-20.

Kaboord, Barbara, and Maria Perr. 2008. 'Isolation of Proteins and Protein Complexes by Immunoprecipitation.' in Anton Posch (ed.), *2D PAGE: Sample Preparation and Fractionation* (Humana Press: Totowa, NJ).

Kakiuchi, C., M. Ishiwata, M. Kametani, C. Nelson, K. Iwamoto, and T. Kato. 2005. 'Quantitative analysis of mitochondrial DNA deletions in the brains of patients with bipolar disorder and schizophrenia', *Int J Neuropsychopharmacol*, 8: 515-22.

Kalia, S. K., T. Sankar, and A. M. Lozano. 2013. 'Deep brain stimulation for Parkinson's disease and other movement disorders', *Curr Opin Neurol*, 26: 374-80.

Kalluri, R., and V. S. LeBleu. 2016. 'Discovery of Double-Stranded Genomic DNA in Circulating Exosomes', *Cold Spring Harb Symp Quant Biol*, 81: 275-80.

Kalluri, R., and V. S. LeBleu. 2020. 'The biology, function, and biomedical applications of exosomes', *Science*, 367.

Kalra, H., C. G. Adda, M. Liem, C. S. Ang, A. Mechler, R. J. Simpson, M. D. Hulett, and S. Mathivanan. 2013. 'Comparative proteomics evaluation of plasma exosome isolation techniques and assessment of the stability of exosomes in normal human blood plasma', *Proteomics*, 13: 3354-64.

Kanagal-Shamanna, R. 2016. 'Digital PCR: Principles and Applications', *Methods Mol Biol*, 1392: 43-50.

Kang, Hyejin, Jiyoon Kim, and Jaesung Park. 2017. 'Methods to isolate extracellular vesicles for diagnosis', *Micro and Nano Systems Letters*, 5: 15.

Kaufmann, H., K. Nahm, D. Purohit, and D. Wolfe. 2004. 'Autonomic failure as the initial presentation of Parkinson disease and dementia with Lewy bodies', *Neurology*, 63: 1093-5.

Keerthikumar, S., D. Chisanga, D. Ariyaratne, H. Al Saffar, S. Anand, K. Zhao, M. Samuel, M. Pathan, M. Jois, N. Chilamkurti, L. Gangoda, and S. Mathivanan. 2016. 'ExoCarta: A Web-Based Compendium of Exosomal Cargo', *J Mol Biol*, 428: 688-92.

Kenwrick, S., A. Watkins, and E. De Angelis. 2000. 'Neural cell recognition molecule L1: relating biological complexity to human disease mutations', *Hum Mol Genet*, 9: 879-86.

Keogh, M. J., and P. F. Chinnery. 2015. 'Mitochondrial DNA mutations in neurodegeneration', *Biochim Biophys Acta*, 1847: 1401-11.

Kim, C. Y., and R. N. Alcalay. 2017. 'Genetic Forms of Parkinson's Disease', *Semin Neurol*, 37: 135-46.

Kim, Hye-Suk, Sang-Myung Cheon, Jung-Wook Seo, Hyun-Ju Ryu, Kyung-Won Park, and Jae Woo Kim. 2013. 'Nonmotor symptoms more closely related to Parkinson's disease: Comparison with normal elderly', *Journal of the Neurological Sciences*, 324: 70-73.

Kitamura, Y., M. Kojima, T. Kurosawa, R. Sasaki, S. Ichihara, Y. Hiraku, H. Tomimoto, M. Murata, and S. Oikawa. 2018. 'Proteomic Profiling of Exosomal Proteins for Blood-based Biomarkers in Parkinson's Disease', *Neuroscience*, 392: 121-28.

Kong, S. M., B. K. Chan, J. S. Park, K. J. Hill, J. B. Aitken, L. Cottle, H. Farghaian, A. R. Cole, P. A. Lay, C. M. Sue, and A. A. Cooper. 2014. 'Parkinson's disease-linked human PARK9/ATP13A2 maintains zinc homeostasis and promotes α-Synuclein externalization via exosomes', *Hum Mol Genet*, 23: 2816-33.

Kösel, S., R. Egensperger, N. M. Schnopp, and M. B. Graeber. 1997. 'The 'common deletion' is not increased in parkinsonian substantia nigra as shown by competitive polymerase chain reaction', *Mov Disord*, 12: 639-45.

Krämer-Albers, E. M., N. Bretz, S. Tenzer, C. Winterstein, W. Möbius, H. Berger, K. A. Nave, H. Schild, and J. Trotter. 2007. 'Oligodendrocytes secrete exosomes containing major

myelin and stress-protective proteins: Trophic support for axons?', *Proteomics Clin Appl*, 1: 1446-61.

Krishnan, S., G. Sarma, S. Sarma, and A. Kishore. 2011. 'Do nonmotor symptoms in Parkinson's disease differ from normal aging?', *Mov Disord*, 26: 2110-3.

Kubista, M., J. M. Andrade, M. Bengtsson, A. Forootan, J. Jonák, K. Lind, R. Sindelka, R. Sjöback, B. Sjögreen, L. Strömbom, A. Ståhlberg, and N. Zoric. 2006. 'The real-time polymerase chain reaction', *Mol Aspects Med*, 27: 95-125.

Kuroda, Y., T. Mitsui, M. Kunishige, M. Shono, M. Akaike, H. Azuma, and T. Matsumoto. 2006. 'Parkin enhances mitochondrial biogenesis in proliferating cells', *Hum Mol Genet*, 15: 883-95.

Lachenal, G., K. Pernet-Gallay, M. Chivet, F. J. Hemming, A. Belly, G. Bodon, B. Blot, G. Haase, Y. Goldberg, and R. Sadoul. 2011. 'Release of exosomes from differentiated neurons and its regulation by synaptic glutamatergic activity', *Mol Cell Neurosci*, 46: 409-18.

Langston, J. William, Philip Ballard, James W. Tetrud, and Ian Irwin. 1983. 'Chronic Parkinsonism in Humans Due to a Product of Meperidine-Analog Synthesis', *Science*, 219: 979-80.

Larsson, N. G., and D. A. Clayton. 1995. 'Molecular genetic aspects of human mitochondrial disorders', *Annu Rev Genet*, 29: 151-78.

Lau, A., and M. Tymianski. 2010. 'Glutamate receptors, neurotoxicity and neurodegeneration', *Pflugers Arch*, 460: 525-42.

LaVoie, M. J., and T. G. Hastings. 1999. 'Dopamine quinone formation and protein modification associated with the striatal neurotoxicity of methamphetamine: evidence against a role for extracellular dopamine', *J Neurosci*, 19: 1484-91.

Lazo, S., N. Noren Hooten, J. Green, E. Eitan, N. A. Mode, Q. R. Liu, A. B. Zonderman, N. Ezike, M. P. Mattson, P. Ghosh, and M. K. Evans. 2021. 'Mitochondrial DNA in extracellular vesicles declines with age', *Aging Cell*, 20: e13283.

LeWitt, P. A. 2015. 'Levodopa therapy for Parkinson's disease: Pharmacokinetics and pharmacodynamics', *Mov Disord*, 30: 64-72.

Li, P., M. Kaslan, S. H. Lee, J. Yao, and Z. Gao. 2017. 'Progress in Exosome Isolation Techniques', *Theranostics*, 7: 789-804.

Lim, S. Y., and A. E. Lang. 2010. 'The nonmotor symptoms of Parkinson's disease--an overview', *Mov Disord*, 25 Suppl 1: S123-30.

Lin, M. T., I. Cantuti-Castelvetri, K. Zheng, K. E. Jackson, Y. B. Tan, T. Arzberger, A. J. Lees, R. A. Betensky, M. F. Beal, and D. K. Simon. 2012. 'Somatic mitochondrial DNA mutations in early Parkinson and incidental Lewy body disease', *Ann Neurol*, 71: 850-4.

Lizarraga-Valderrama, L. R., and G. K. Sheridan. 2021. 'Extracellular vesicles and intercellular communication in the central nervous system', *FEBS Lett*, 595: 1391-410.

Lood, C., L. P. Blanco, M. M. Purmalek, C. Carmona-Rivera, S. S. De Ravin, C. K. Smith, H. L. Malech, J. A. Ledbetter, K. B. Elkon, and M. J. Kaplan. 2016. 'Neutrophil extracellular traps enriched in oxidized mitochondrial DNA are interferogenic and contribute to lupus-like disease', *Nat Med*, 22: 146-53.

Luong, John H. T., and Sandeep K. Vashist. 2019. 'Chemistry of Biotin-Streptavidin and the Growing Concern of an Emerging Biotin Interference in Clinical Immunoassays', *ACS omega*, 5: 10-18.

Mainer, G., E. Domínguez, M. Randrup, L. Sánchez, and M. Calvo. 1999. 'Effect of heat treatment on anti-rotavirus activity of bovine colostrum', *J Dairy Res*, 66: 131-7.

Mann, V. M., J. M. Cooper, and A. H. Schapira. 1992. 'Quantitation of a mitochondrial DNA deletion in Parkinson's disease', *FEBS Lett*, 299: 218-22.

Mao, S., G. Xiong, B. N. Johnson, N. A. Cohen, and A. S. Cohen. 2021. 'Blocking Cross-Species Secondary Binding When Performing Double Immunostaining With Mouse and Rat Primary Antibodies', *Front Neurosci*, 15: 579859.

McLelland, G. L., V. Soubannier, C. X. Chen, H. M. McBride, and E. A. Fon. 2014. 'Parkin and PINK1 function in a vesicular trafficking pathway regulating mitochondrial quality control', *Embo j*, 33: 282-95.

Mishra, P., and D. C. Chan. 2014. 'Mitochondrial dynamics and inheritance during cell division, development and disease', *Nat Rev Mol Cell Biol*, 15: 634-46.

Mollenhauer, B., J. J. Locascio, W. Schulz-Schaeffer, F. Sixel-Döring, C. Trenkwalder, and M. G. Schlossmacher. 2011. 'α-Synuclein and tau concentrations in cerebrospinal fluid of patients presenting with parkinsonism: a cohort study', *Lancet Neurol*, 10: 230-40.

Morais, V. A., D. Haddad, K. Craessaerts, P. J. De Bock, J. Swerts, S. Vilain, L. Aerts, L. Overbergh, A. Grünewald, P. Seibler, C. Klein, K. Gevaert, P. Verstreken, and B. De Strooper. 2014. 'PINK1 loss-of-function mutations affect mitochondrial complex I activity via NdufA10 ubiquinone uncoupling', *Science*, 344: 203-7.

Müller-Nedebock, A. C., R. R. Brennan, M. Venter, I. S. Pienaar, F. H. van der Westhuizen, J. L. Elson, O. A. Ross, and S. Bardien. 2019. 'The unresolved role of mitochondrial DNA in Parkinson's disease: An overview of published studies, their limitations, and future prospects', *Neurochem Int*, 129: 104495.

Mustapic, M., E. Eitan, J. K. Werner, Jr., S. T. Berkowitz, M. P. Lazaropoulos, J. Tran, E. J. Goetzl, and D. Kapogiannis. 2017. 'Plasma Extracellular Vesicles Enriched for Neuronal Origin: A Potential Window into Brain Pathologic Processes', *Front Neurosci*, 11: 278.

Nakano, M., J. Komatsu, S. Matsuura, K. Takashima, S. Katsura, and A. Mizuno. 2003. 'Single-molecule PCR using water-in-oil emulsion', *J Biotechnol*, 102: 117-24.

Neuhaus, J. F., O. R. Baris, S. Hess, N. Moser, H. Schröder, S. J. Chinta, J. K. Andersen, P. Kloppenburg, and R. J. Wiesner. 2014. 'Catecholamine metabolism drives generation of mitochondrial DNA deletions in dopaminergic neurons', *Brain*, 137: 354-65.

Noerholm, M., L. Balaj, T. Limperg, A. Salehi, L. D. Zhu, F. H. Hochberg, X. O. Breakefield, B. S. Carter, and J. Skog. 2012. 'RNA expression patterns in serum microvesicles from patients with glioblastoma multiforme and controls', *BMC Cancer*, 12: 22.

Norman, M., D. Ter-Ovanesyan, W. Trieu, R. Lazarovits, E. J. K. Kowal, J. H. Lee, A. S. Chen-Plotkin, A. Regev, G. M. Church, and D. R. Walt. 2021. 'L1CAM is not associated with extracellular vesicles in human cerebrospinal fluid or plasma', *Nat Methods*, 18: 631-34.

Olanow, C. W. 2007. 'The pathogenesis of cell death in Parkinson's disease--2007', *Mov Disord*, 22 Suppl 17: S335-42.

Olanow, C. W., C. G. Goetz, J. H. Kordower, A. J. Stoessl, V. Sossi, M. F. Brin, K. M. Shannon, G. M. Nauert, D. P. Perl, J. Godbold, and T. B. Freeman. 2003. 'A double-blind controlled trial of bilateral fetal nigral transplantation in Parkinson's disease', *Ann Neurol*, 54: 403-14.

Olson, Eric J., Bradley F. Boeve, and Michael H. Silber. 2000. 'Rapid eye movement sleep behaviour disorder: demographic, clinical and laboratory findings in 93 cases', *Brain*, 123: 331-39.

Ouzren, N., S. Delcambre, J. Ghelfi, P. Seibler, M. J. Farrer, I. R. König, J. O. Aasly, J. Trinh, C. Klein, and A. Grünewald. 2019. 'Mitochondrial DNA Deletions Discriminate Affected from Unaffected LRRK2 Mutation Carriers', *Ann Neurol*, 86: 324-26.

Ozawa, T., M. Tanaka, S. Ikebe, K. Ohno, T. Kondo, and Y. Mizuno. 1990. 'Quantitative determination of deleted mitochondrial DNA relative to normal DNA in parkinsonian striatum by a kinetic PCR analysis', *Biochem Biophys Res Commun*, 172: 483-9.

Pan, B. T., K. Teng, C. Wu, M. Adam, and R. M. Johnstone. 1985. 'Electron microscopic evidence for externalization of the transferrin receptor in vesicular form in sheep reticulocytes', *J Cell Biol*, 101: 942-8.

Pickrell, A. M., C. H. Huang, S. R. Kennedy, A. Ordureau, D. P. Sideris, J. G. Hoekstra, J. W. Harper, and R. J. Youle. 2015. 'Endogenous Parkin Preserves Dopaminergic Substantia Nigral Neurons following Mitochondrial DNA Mutagenic Stress', *Neuron*, 87: 371-81.

Pickrell, A. M., and R. J. Youle. 2015. 'The roles of PINK1, parkin, and mitochondrial fidelity in Parkinson's disease', *Neuron*, 85: 257-73.

Podlesniy, P., J. Figueiro-Silva, A. Llado, A. Antonell, R. Sanchez-Valle, D. Alcolea, A. Lleo, J. L. Molinuevo, N. Serra, and R. Trullas. 2013. 'Low cerebrospinal fluid concentration of mitochondrial DNA in preclinical Alzheimer disease', *Ann Neurol*, 74: 655-68.

Polymeropoulos, M. H., C. Lavedan, E. Leroy, S. E. Ide, A. Dehejia, A. Dutra, B. Pike, H. Root, J. Rubenstein, R. Boyer, E. S. Stenroos, S. Chandrasekharappa, A. Athanassiadou, T. Papapetropoulos, W. G. Johnson, A. M. Lazzarini, R. C. Duvoisin, G. Di Iorio, L. I. Golbe, and R. L. Nussbaum. 1997. 'Mutation in the alpha-synuclein gene identified in families with Parkinson's disease', *Science*, 276: 2045-7.

Ponsen, M. M., D. Stoffers, J. Booij, B. L. van Eck-Smit, ECh Wolters, and H. W. Berendse. 2004. 'Idiopathic hyposmia as a preclinical sign of Parkinson's disease', *Ann Neurol*, 56: 173-81.

Potolicchio, I., G. J. Carven, X. Xu, C. Stipp, R. J. Riese, L. J. Stern, and L. Santambrogio. 2005. 'Proteomic analysis of microglia-derived exosomes: metabolic role of the aminopeptidase CD13 in neuropeptide catabolism', *J Immunol*, 175: 2237-43.

Poulet, G., J. Massias, and V. Taly. 2019. 'Liquid Biopsy: General Concepts', *Acta Cytol*, 63: 449-55.

Pyle, A., H. Anugrha, M. Kurzawa-Akanbi, A. Yarnall, D. Burn, and G. Hudson. 2016. 'Reduced mitochondrial DNA copy number is a biomarker of Parkinson's disease', *Neurobiol Aging*, 38: 216.e7-16.e10.

Pyle, A., R. Brennan, M. Kurzawa-Akanbi, A. Yarnall, A. Thouin, B. Mollenhauer, D. Burn, P. F. Chinnery, and G. Hudson. 2015. 'Reduced cerebrospinal fluid mitochondrial DNA is a biomarker for early-stage Parkinson's disease', *Ann Neurol*, 78: 1000-4.

Radhakrishnan, D. M., and V. Goyal. 2018. 'Parkinson's disease: A review', *Neurol India*, 66: S26-s35.

Ramirez, A., A. Heimbach, J. Gründemann, B. Stiller, D. Hampshire, L. P. Cid, I. Goebel, A. F. Mubaidin, A. L. Wriekat, J. Roeper, A. Al-Din, A. M. Hillmer, M. Karsak, B. Liss, C. G. Woods, M. I. Behrens, and C. Kubisch. 2006. 'Hereditary parkinsonism with dementia is caused by mutations in ATP13A2, encoding a lysosomal type 5 P-type ATPase', *Nat Genet*, 38: 1184-91.

Ramonet, D., A. Podhajska, K. Stafa, S. Sonnay, A. Trancikova, E. Tsika, O. Pletnikova, J. C. Troncoso, L. Glauser, and D. J. Moore. 2012. 'PARK9-associated ATP13A2 localizes to intracellular acidic vesicles and regulates cation homeostasis and neuronal integrity', *Hum Mol Genet*, 21: 1725-43.

Raposo, G, H W Nijman, W Stoorvogel, R Liejendekker, C V Harding, C J Melief, and H J Geuze. 1996. 'B lymphocytes secrete antigen-presenting vesicles', *The Journal of Experimental Medicine*, 183: 1161-72.

Raposo, G., and W. Stoorvogel. 2013. 'Extracellular vesicles: exosomes, microvesicles, and friends', *J Cell Biol*, 200: 373-83.

Rashed, M., E. Bayraktar, K. Helal G, M. F. Abd-Ellah, P. Amero, A. Chavez-Reyes, and C. Rodriguez-Aguayo. 2017. 'Exosomes: From Garbage Bins to Promising Therapeutic Targets', *Int J Mol Sci*, 18.

Riboldi, G. M., and A. B. Di Fonzo. 2019. 'GBA, Gaucher Disease, and Parkinson's Disease: From Genetic to Clinic to New Therapeutic Approaches', *Cells*, 8.

Rijk, M.C. de, M.M.B. Breteler, G.A. Graveland, A. Ott, D.E. Grobbee, F.G.A. van der Meche, and A. Hofman. 1995. 'Prevalence of Parkinson's disease in the elderly', *The Rotterdam Study*, 45: 2143-46.

Salinas, Sara, Christos Proukakis, Andrew Crosby, and Thomas T. Warner. 2008. 'Hereditary spastic paraplegia: clinical features and pathogenetic mechanisms', *The Lancet Neurology*, 7: 1127-38.

Samii, A., J. G. Nutt, and B. R. Ransom. 2004. 'Parkinson's disease', *Lancet*, 363: 1783-93.

Savina, A., M. Furlán, M. Vidal, and M. I. Colombo. 2003. 'Exosome release is regulated by a calcium-dependent mechanism in K562 cells', *J Biol Chem*, 278: 20083-90.

Savina, A., M. Vidal, and M. I. Colombo. 2002. 'The exosome pathway in K562 cells is regulated by Rab11', *J Cell Sci*, 115: 2505-15.

Schapira, A. H., J. M. Cooper, D. Dexter, P. Jenner, J. B. Clark, and C. D. Marsden. 1989. 'Mitochondrial complex I deficiency in Parkinson's disease', *Lancet*, 1: 1269.

Schmidt, O., and D. Teis. 2012. 'The ESCRT machinery', *Curr Biol*, 22: R116-20.

Schroeder, H. W., Jr., and L. Cavacini. 2010. 'Structure and function of immunoglobulins', *J Allergy Clin Immunol*, 125: S41-52.

Schuurman, A. G., M. van den Akker, K. T. Ensinck, J. F. Metsemakers, J. A. Knottnerus, A. F. Leentjens, and F. Buntinx. 2002. 'Increased risk of Parkinson's disease after depression: a retrospective cohort study', *Neurology*, 58: 1501-4.

Shahmoradian, S. H., A. J. Lewis, C. Genoud, J. Hench, T. E. Moors, P. P. Navarro, D. Castaño-Díez, G. Schweighauser, A. Graff-Meyer, K. N. Goldie, R. Sütterlin, E. Huisman, A. Ingrassia, Y. Gier, A. J. M. Rozemuller, J. Wang, A. Paepe, J. Erny, A. Staempfli, J. Hoernschemeyer, F. Großerüschkamp, D. Niedieker, S. F. El-Mashtoly, M. Quadri, IJcken W. F. J. Van, V. Bonifati, K. Gerwert, B. Bohrmann, S. Frank, M. Britschgi, H. Stahlberg, W. D. J. Van de Berg, and M. E. Lauer. 2019. 'Lewy pathology in Parkinson's disease consists of crowded organelles and lipid membranes', *Nat Neurosci*, 22: 1099-109.

Sharma, P., P. Mesci, C. Carromeu, D. R. McClatchy, L. Schiapparelli, J. R. Yates, 3rd, A. R. Muotri, and H. T. Cline. 2019. 'Exosomes regulate neurogenesis and circuit assembly', *Proc Natl Acad Sci U S A*, 116: 16086-94.

Shi, M. 2014. 'Plasma exosomal α-synuclein is likely CNS-derived and increased in Parkinson's disease', 128: 639-50.

Shi, M., A. Kovac, A. Korff, T. J. Cook, C. Ginghina, K. M. Bullock, L. Yang, T. Stewart, D. Zheng, P. Aro, A. Atik, K. F. Kerr, C. P. Zabetian, E. R. Peskind, S. C. Hu, J. F. Quinn, D. R. Galasko, T. J. Montine, W. A. Banks, and J. Zhang. 2016. 'CNS tau efflux via exosomes is likely increased in Parkinson's disease but not in Alzheimer's disease', *Alzheimers Dement*, 12: 1125-31.

Shi, M., C. Liu, T. J. Cook, K. M. Bullock, Y. Zhao, C. Ginghina, Y. Li, P. Aro, R. Dator, C. He, M. J. Hipp, C. P. Zabetian, E. R. Peskind, S. C. Hu, J. F. Quinn, D. R. Galasko, W. A. Banks, and J. Zhang. 2014. 'Plasma exosomal α-synuclein is likely CNS-derived and increased in Parkinson's disease', *Acta Neuropathol*, 128: 639-50.

Shi, M., C. P. Zabetian, A. M. Hancock, C. Ginghina, Z. Hong, D. Yearout, K. A. Chung, J. F. Quinn, E. R. Peskind, D. Galasko, J. Jankovic, J. B. Leverenz, and J. Zhang. 2010. 'Significance and confounders of peripheral DJ-1 and alpha-synuclein in Parkinson's disease', *Neurosci Lett*, 480: 78-82.

Shokolenko, I., N. Venediktova, A. Bochkareva, G. L. Wilson, and M. F. Alexeyev. 2009. 'Oxidative stress induces degradation of mitochondrial DNA', *Nucleic Acids Res*, 37: 2539-48.

Skog, J., T. Würdinger, S. van Rijn, D. H. Meijer, L. Gainche, M. Sena-Esteves, W. T. Curry, Jr., B. S. Carter, A. M. Krichevsky, and X. O. Breakefield. 2008. 'Glioblastoma microvesicles transport RNA and proteins that promote tumour growth and provide diagnostic biomarkers', *Nat Cell Biol*, 10: 1470-6.

Soubannier, V., G. L. McLelland, R. Zunino, E. Braschi, P. Rippstein, E. A. Fon, and H. M. McBride. 2012. 'A vesicular transport pathway shuttles cargo from mitochondria to lysosomes', *Curr Biol*, 22: 135-41.

Spindler, M. A., and D. Tarsy. 2021. 'Initial pharmacologic treatment of Parkinson disease.' in UpToDate Eichler AF (ed.), *UpToDate, Waltham, MA*.

Stenmark, H. 2009. 'Rab GTPases as coordinators of vesicle traffic', *Nat Rev Mol Cell Biol*, 10: 513-25.

Stoessl, A. J., S. Lehericy, and A. P. Strafella. 2014. 'Imaging insights into basal ganglia function, Parkinson's disease, and dystonia', *Lancet*, 384: 532-44.

Stoorvogel, W., G. J. Strous, H. J. Geuze, V. Oorschot, and A. L. Schwartz. 1991. 'Late endosomes derive from early endosomes by maturation', *Cell*, 65: 417-27.

Storch, A., A. C. Ludolph, and J. Schwarz. 2004. 'Dopamine transporter: involvement in selective dopaminergic neurotoxicity and degeneration', *J Neural Transm (Vienna)*, 111: 1267-86.

Strauss, Katrin, Cornelia Goebel, Heiko Runz, Wiebke Möbius, Sievert Weiss, Ivo Feussner, Mikael Simons, and Anja Schneider. 2010. 'Exosome secretion ameliorates lysosomal storage of cholesterol in Niemann-Pick type C disease', *J Biol Chem*, 285: 26279-88.

Stuendl, Anne, Marcel Kunadt, Niels Kruse, Claudia Bartels, Wiebke Moebius, Karin M. Danzer, Brit Mollenhauer, and Anja Schneider. 2016. 'Induction of α-synuclein aggregate formation by CSF exosomes from patients with Parkinson's disease and dementia with Lewy bodies', *Brain : a journal of neurology*, 139: 481-94.

Stuffers, S., C. Sem Wegner, H. Stenmark, and A. Brech. 2009. 'Multivesicular endosome biogenesis in the absence of ESCRTs', *Traffic*, 10: 925-37.

Sullivan, R., F. Saez, J. Girouard, and G. Frenette. 2005. 'Role of exosomes in sperm maturation during the transit along the male reproductive tract', *Blood Cells Mol Dis*, 35: 1-10.

Sung, J. Y., J. Kim, S. R. Paik, J. H. Park, Y. S. Ahn, and K. C. Chung. 2001. 'Induction of neuronal cell death by Rab5A-dependent endocytosis of alpha-synuclein', *J Biol Chem*, 276: 27441-8.

Svec, David, Ales Tichopad, Vendula Novosadova, Michael W. Pfaffl, and Mikael Kubista. 2015. 'How good is a PCR efficiency estimate: Recommendations for precise and robust qPCR efficiency assessments', *Biomol Detect Quantif*, 3: 9-16.

Szilágyi, M., O. Pös, É Márton, G. Buglyó, B. Soltész, J. Keserű, A. Penyige, T. Szemes, and B. Nagy. 2020. 'Circulating Cell-Free Nucleic Acids: Main Characteristics and Clinical Application', *Int J Mol Sci*, 21.

Tang, Y. T., Y. Y. Huang, L. Zheng, S. H. Qin, X. P. Xu, T. X. An, Y. Xu, Y. S. Wu, X. M. Hu, B. H. Ping, and Q. Wang. 2017. 'Comparison of isolation methods of exosomes and exosomal RNA from cell culture medium and serum', *Int J Mol Med*, 40: 834-44.

Tanner, C. M., and S. M. Goldman. 1996. 'Epidemiology of Parkinson's disease', *Neurol Clin*, 14: 317-35.

Tauro, B. J., D. W. Greening, R. A. Mathias, H. Ji, S. Mathivanan, A. M. Scott, and R. J. Simpson. 2012. 'Comparison of ultracentrifugation, density gradient separation, and immunoaffinity capture methods for isolating human colon cancer cell line LIM1863-derived exosomes', *Methods*, 56: 293-304.

Teune, L. K., A. L. Bartels, B. M. de Jong, A. T. Willemsen, S. A. Eshuis, J. J. de Vries, J. C. van Oostrom, and K. L. Leenders. 2010. 'Typical cerebral metabolic patterns in neurodegenerative brain diseases', *Mov Disord*, 25: 2395-404.

Thakur, Basant Kumar, Haiying Zhang, Annette Becker, Irina Matei, Yujie Huang, Bruno Costa-Silva, Yan Zheng, Ayuko Hoshino, Helene Brazier, Jenny Xiang, Caitlin Williams, Ruth Rodriguez-Barrueco, Jose M. Silva, Weijia Zhang, Stephen Hearn, Olivier Elemento, Navid Paknejad, Katia Manova-Todorova, Karl Welte, Jacqueline Bromberg, Héctor Peinado, and David Lyden. 2014. 'Double-stranded DNA in exosomes: a novel biomarker in cancer detection', *Cell Research*, 24: 766.

Thenganatt, M. A., and J. Jankovic. 2014. 'Parkinson disease subtypes', *JAMA Neurol*, 71: 499-504.

Thery, C., S. Amigorena, G. Raposo, and A. Clayton. 2006. 'Isolation and characterization of exosomes from cell culture supernatants and biological fluids', *Curr Protoc Cell Biol*, Chapter 3: Unit 3.22.

Théry, C., M. Boussac, P. Véron, P. Ricciardi-Castagnoli, G. Raposo, J. Garin, and S. Amigorena. 2001. 'Proteomic analysis of dendritic cell-derived exosomes: a secreted subcellular compartment distinct from apoptotic vesicles', *J Immunol*, 166: 7309-18.

Thery, C., L. Zitvogel, and S. Amigorena. 2002. 'Exosomes: composition, biogenesis and function', *Nat Rev Immunol*, 2: 569-79.

Théry, Clotilde, Kenneth W. Witwer, Elena Aikawa, Maria Jose Alcaraz, Johnathon D. Anderson, Ramaroson Andriantsitohaina, Anna Antoniou, Tanina Arab, Fabienne Archer, Georgia K. Atkin-Smith, D. Craig Ayre, Jean-Marie Bach, Daniel Bachurski, Hossein Baharvand, Leonora Balaj, Shawn Baldacchino, Natalie N. Bauer, Amy A. Baxter, Mary Bebawy, Carla Beckham, Apolonija Bedina Zavec, Abderrahim Benmoussa, Anna C. Berardi, Paolo Bergese, Ewa Bielska, Cherie Blenkiron, Sylwia Bobis-Wozowicz, Eric Boilard, Wilfrid Boireau, Antonella Bongiovanni, Francesc E. Borràs, Steffi Bosch, Chantal M. Boulanger, Xandra Breakefield, Andrew M. Breglio, Meadhbh Á Brennan, David R. Brigstock, Alain Brisson, Marike L. D. Broekman, Jacqueline F. Bromberg, Paulina Bryl-Górecka, Shilpa Buch, Amy H. Buck, Dylan Burger, Sara Busatto, Dominik Buschmann, Benedetta Bussolati, Edit I. Buzás, James Bryan Byrd, Giovanni Camussi, David R. F. Carter, Sarah Caruso, Lawrence W. Chamley, Yu-Ting Chang, Chihchen Chen, Shuai Chen, Lesley Cheng, Andrew R. Chin, Aled Clayton, Stefano P. Clerici, Alex Cocks, Emanuele Cocucci, Robert J. Coffey, Anabela Cordeiro-da-Silva, Yvonne Couch, Frank A. W. Coumans, Beth Coyle, Rossella Crescitelli, Miria Ferreira Criado, Crislyn D'Souza-Schorey, Saumya Das, Amrita Datta Chaudhuri, Paola de Candia, Eliezer F. De Santana, Olivier De Wever, Hernando A. del Portillo, Tanguy Demaret, Sarah Deville, Andrew Devitt, Bert Dhondt, Dolores Di Vizio, Lothar C. Dieterich, Vincenza Dolo, Ana Paula Dominguez Rubio, Massimo Dominici, Mauricio R. Dourado, Tom A. P. Driedonks, Filipe V. Duarte, Heather M. Duncan, Ramon M. Eichenberger, Karin Ekström, Samir El Andaloussi, Celine Elie-Caille, Uta Erdbrügger, Juan M. Falcón-Pérez, Farah Fatima, Jason E. Fish, Miguel Flores-Bellver, András Försönits, Annie Frelet-Barrand, Fabia Fricke, Gregor Fuhrmann, Susanne Gabrielsson, Ana Gámez-Valero, Chris Gardiner, Kathrin Gärtner, Raphael Gaudin, Yong Song Gho, Bernd Giebel, Caroline Gilbert, Mario Gimona, Ilaria Giusti, Deborah C. I. Goberdhan, André Görgens, Sharon M. Gorski, David W. Greening, Julia Christina Gross, Alice Gualerzi, Gopal N. Gupta, Dakota Gustafson, Aase Handberg, Reka A. Haraszti, Paul Harrison, Hargita Hegyesi, An Hendrix, Andrew F. Hill, Fred H. Hochberg, Karl F. Hoffmann, Beth Holder, Harry Holthofer, Baharak Hosseinkhani, Guoku Hu, Yiyao Huang, Veronica Huber, Stuart Hunt, Ahmed Gamal-Eldin Ibrahim, Tsuneya Ikezu, Jameel M. Inal, Mustafa Isin, Alena Ivanova, Hannah K. Jackson, Soren Jacobsen, Steven M. Jay, Muthuvel Jayachandran, Guido Jenster, Lanzhou Jiang, Suzanne M. Johnson, Jennifer C. Jones, Ambrose Jong, Tijana Jovanovic-Talisman, Stephanie Jung, Raghu Kalluri, Shin-ichi Kano, Sukhbir Kaur, Yumi Kawamura, Evan T. Keller, Delaram Khamari, Elena Khomyakova, Anastasia

Khvorova, Peter Kierulf, Kwang Pyo Kim, Thomas Kislinger, Mikael Klingeborn, David J. Klinke, Miroslaw Kornek, Maja M. Kosanović, Árpád Ferenc Kovács, Eva-Maria Krämer-Albers, Susanne Krasemann, Mirja Krause, Igor V. Kurochkin, Gina D. Kusuma, Sören Kuypers, Saara Laitinen, Scott M. Langevin, Lucia R. Languino, Joanne Lannigan, Cecilia Lässer, Louise C. Laurent, Gregory Lavieu, Elisa Lázaro-Ibáñez, Soazig Le Lay, Myung-Shin Lee, Yi Xin Fiona Lee, Debora S. Lemos, Metka Lenassi, Aleksandra Leszczynska, Isaac T. S. Li, Ke Liao, Sten F. Libregts, Erzsebet Ligeti, Rebecca Lim, Sai Kiang Lim, Aija Linē, Karen Linnemannstöns, Alicia Llorente, Catherine A. Lombard, Magdalena J. Lorenowicz, Ákos M. Lörincz, Jan Lötvall, Jason Lovett, Michelle C. Lowry, Xavier Loyer, Quan Lu, Barbara Lukomska, Taral R. Lunavat, Sybren L. N. Maas, Harmeet Malhi, Antonio Marcilla, Jacopo Mariani, Javier Mariscal, Elena S. Martens-Uzunova, Lorena Martin-Jaular, M. Carmen Martinez, Vilma Regina Martins, Mathilde Mathieu, Suresh Mathivanan, Marco Maugeri, Lynda K. McGinnis, Mark J. McVey, David G. Meckes, Katie L. Meehan, Inge Mertens, Valentina R. Minciacchi, Andreas Möller, Malene Møller Jørgensen, Aizea Morales-Kastresana, Jess Morhayim, François Mullier, Maurizio Muraca, Luca Musante, Veronika Mussack, Dillon C. Muth, Kathryn H. Myburgh, Tanbir Najrana, Muhammad Nawaz, Irina Nazarenko, Peter Nejsum, Christian Neri, Tommaso Neri, Rienk Nieuwland, Leonardo Nimrichter, John P. Nolan, Esther N. M. Nolte-'t Hoen, Nicole Noren Hooten, Lorraine O'Driscoll, Tina O'Grady, Ana O'Loghlen, Takahiro Ochiya, Martin Olivier, Alberto Ortiz, Luis A. Ortiz, Xabier Osteikoetxea, Ole Østergaard, Matias Ostrowski, Jaesung Park, D. Michiel Pegtel, Hector Peinado, Francesca Perut, Michael W. Pfaffl, Donald G. Phinney, Bartijn C. H. Pieters, Ryan C. Pink, David S. Pisetsky, Elke Pogge von Strandmann, Iva Polakovicova, Ivan K. H. Poon, Bonita H. Powell, Ilaria Prada, Lynn Pulliam, Peter Quesenberry, Annalisa Radeghieri, Robert L. Raffai, Stefania Raimondo, Janusz Rak, Marcel I. Ramirez, Graça Raposo, Morsi S. Rayyan, Neta Regev-Rudzki, Franz L. Ricklefs, Paul D. Robbins, David D. Roberts, Silvia C. Rodrigues, Eva Rohde, Sophie Rome, Kasper M. A. Rouschop, Aurelia Rughetti, Ashley E. Russell, Paula Saá, Susmita Sahoo, Edison Salas-Huenuleo, Catherine Sánchez, Julie A. Saugstad, Meike J. Saul, Raymond M. Schiffelers, Raphael Schneider, Tine Hiorth Schøyen, Aaron Scott, Eriomina Shahaj, Shivani Sharma, Olga Shatnyeva, Faezeh Shekari, Ganesh Vilas Shelke, Ashok K. Shetty, Kiyotaka Shiba, Pia R. M. Siljander, Andreia M. Silva, Agata Skowronek, Orman L. Snyder, Rodrigo Pedro Soares, Barbara W. Sódar, Carolina Soekmadji, Javier Sotillo, Philip D. Stahl, Willem Stoorvogel, Shannon L. Stott, Erwin F. Strasser, Simon Swift, Hidetoshi Tahara, Muneesh Tewari, Kate Timms, Swasti Tiwari, Rochelle Tixeira, Mercedes Tkach, Wei Seong Toh, Richard Tomasini, Ana Claudia Torrecilhas, Juan Pablo Tosar, Vasilis Toxavidis, Lorena Urbanelli, Pieter Vader, Bas W. M. van Balkom, Susanne G. van der Grein, Jan Van Deun, Martijn J. C. van Herwijnen, Kendall Van Keuren-Jensen, Guillaume van Niel, Martin E. van Royen, Andre J. van Wijnen, M. Helena Vasconcelos, Ivan J. Vechetti, Tiago D. Veit, Laura J. Vella, Émilie Velot, Frederik J. Verweij, Beate Vestad, Jose L. Viñas, Tamás Visnovitz, Krisztina V. Vukman, Jessica Wahlgren, Dionysios C. Watson, Marca H. M. Wauben, Alissa Weaver, Jason P. Webber, Viktoria Weber, Ann M. Wehman, Daniel J. Weiss, Joshua A. Welsh, Sebastian Wendt, Asa M. Wheelock, Zoltán Wiener, Leonie Witte, Joy Wolfram, Angeliki Xagorari, Patricia Xander, Jing Xu, Xiaomei Yan, María Yáñez-Mó, Hang Yin, Yuana Yuana, Valentina Zappulli, Jana Zarubova, Vytautas Žėkas, Jian-ye Zhang, Zezhou Zhao, Lei Zheng, Alexander R. Zheutlin, Antje M. Zickler, Pascale Zimmermann, Angela M. Zivkovic, Davide Zocco, and Ewa K. Zuba-Surma. 2018. 'Minimal information for studies of extracellular vesicles 2018 (MISEV2018): a position statement of the International

Society for Extracellular Vesicles and update of the MISEV2014 guidelines', *J Extracell Vesicles*, 7: 1535750.

Tkach, M., J. Kowal, A. E. Zucchetti, L. Enserink, M. Jouve, D. Lankar, M. Saitakis, L. Martin-Jaular, and C. Théry. 2017. 'Qualitative differences in T-cell activation by dendritic cell-derived extracellular vesicle subtypes', *Embo j*, 36: 3012-28.

Tomlinson, P. R., Y. Zheng, R. Fischer, R. Heidasch, C. Gardiner, S. Evetts, M. Hu, R. Wade-Martins, M. R. Turner, J. Morris, K. Talbot, B. M. Kessler, and G. K. Tofaris. 2015. 'Identification of distinct circulating exosomes in Parkinson's disease', *Ann Clin Transl Neurol*, 2: 353-61.

Trajkovic, K., C. Hsu, S. Chiantia, L. Rajendran, D. Wenzel, F. Wieland, P. Schwille, B. Brügger, and M. Simons. 2008. 'Ceramide triggers budding of exosome vesicles into multivesicular endosomes', *Science*, 319: 1244-7.

Trams, E. G., C. J. Lauter, N. Salem, Jr., and U. Heine. 1981. 'Exfoliation of membrane ecto-enzymes in the form of micro-vesicles', *Biochim Biophys Acta*, 645: 63-70.

Tsunemi, T., K. Hamada, and D. Krainc. 2014. 'ATP13A2/PARK9 regulates secretion of exosomes and α-synuclein', *J Neurosci*, 34: 15281-7.

Tysnes, O. B., and A. Storstein. 2017. 'Epidemiology of Parkinson's disease', *J Neural Transm (Vienna)*, 124: 901-05.

Valadi, H., K. Ekström, A. Bossios, M. Sjöstrand, J. J. Lee, and J. O. Lötvall. 2007. 'Exosome-mediated transfer of mRNAs and microRNAs is a novel mechanism of genetic exchange between cells', *Nat Cell Biol*, 9: 654-9.

Vella, L. J., R. A. Sharples, V. A. Lawson, C. L. Masters, R. Cappai, and A. F. Hill. 2007. 'Packaging of prions into exosomes is associated with a novel pathway of PrP processing', *J Pathol*, 211: 582-90.

Vincent-Schneider, H., P. Stumptner-Cuvelette, D. Lankar, S. Pain, G. Raposo, P. Benaroch, and C. Bonnerot. 2002. 'Exosomes bearing HLA-DR1 molecules need dendritic cells to efficiently stimulate specific T cells', *Int Immunol*, 14: 713-22.

Wang, H., T. Li, S. Chen, Y. Gu, and S. Ye. 2015. 'Neutrophil Extracellular Trap Mitochondrial DNA and Its Autoantibody in Systemic Lupus Erythematosus and a Proof-of-Concept Trial of Metformin', *Arthritis Rheumatol*, 67: 3190-200.

Wang, S., F. Cesca, G. Loers, M. Schweizer, F. Buck, F. Benfenati, M. Schachner, and R. Kleene. 2011. 'Synapsin I is an oligomannose-carrying glycoprotein, acts as an oligomannose-binding lectin, and promotes neurite outgrowth and neuronal survival when released via glia-derived exosomes', *J Neurosci*, 31: 7275-90.

West, A. P., W. Khoury-Hanold, M. Staron, M. C. Tal, C. M. Pineda, S. M. Lang, M. Bestwick, B. A. Duguay, N. Raimundo, D. A. MacDuff, S. M. Kaech, J. R. Smiley, R. E. Means, A. Iwasaki, and G. S. Shadel. 2015. 'Mitochondrial DNA stress primes the antiviral innate immune response', *Nature*, 520: 553-7.

West, A. P., and G. S. Shadel. 2017. 'Mitochondrial DNA in innate immune responses and inflammatory pathology', *Nat Rev Immunol*, 17: 363-75.

White, M. J., K. McArthur, D. Metcalf, R. M. Lane, J. C. Cambier, M. J. Herold, M. F. van Delft, S. Bedoui, G. Lessene, M. E. Ritchie, D. C. Huang, and B. T. Kile. 2014. 'Apoptotic caspases suppress mtDNA-induced STING-mediated type I IFN production', *Cell*, 159: 1549-62.

Williams, R. L., and S. Urbe. 2007. 'The emerging shape of the ESCRT machinery', *Nat Rev Mol Cell Biol*, 8: 355-68.

Willms, E., C. Cabañas, I. Mäger, M. J. A. Wood, and P. Vader. 2018. 'Extracellular Vesicle Heterogeneity: Subpopulations, Isolation Techniques, and Diverse Functions in Cancer Progression', *Front Immunol*, 9: 738.

Wu, L., and X. Qu. 2015. 'Cancer biomarker detection: recent achievements and challenges', *Chem Soc Rev*, 44: 2963-97.

Wu, W., H. Xu, Z. Wang, Y. Mao, L. Yuan, W. Luo, Z. Cui, T. Cui, X. L. Wang, and Y. H. Shen. 2015. 'PINK1-Parkin-Mediated Mitophagy Protects Mitochondrial Integrity and Prevents Metabolic Stress-Induced Endothelial Injury', *PLoS One*, 10: e0132499.

Wu, Z., S. Oeck, A. P. West, K. C. Mangalhara, A. G. Sainz, L. E. Newman, X. O. Zhang, L. Wu, Q. Yan, M. Bosenberg, Y. Liu, P. L. Sulkowski, V. Tripple, S. M. Kaech, P. M. Glazer, and G. S. Shadel. 2019. 'Mitochondrial DNA Stress Signalling Protects the Nuclear Genome', *Nat Metab*, 1: 1209-18.

Yang, X., Y. Ma, H. Xie, S. Dong, G. Rao, Z. Yang, J. Zhang, and Q. Wu. 2021. 'Extracellular Vesicles in the Treatment of Parkinson's Disease: A Review', *Curr Med Chem*, 28: 6375-94.

Yasuda, Toru, and Hideki Mochizuki. 2010. 'The regulatory role of α-synuclein and parkin in neuronal cell apoptosis; possible implications for the pathogenesis of Parkinson's disease', *Apoptosis*, 15: 1312-21.

Zhang, J., T. J. Montine, M. A. Smith, S. L. Siedlak, G. Gu, D. Robertson, and G. Perry. 2002. 'The mitochondrial common deletion in Parkinson's disease and related movement disorders', *Parkinsonism Relat Disord*, 8: 165-70.

Zhou, Q., M. Li, X. Wang, Q. Li, T. Wang, Q. Zhu, X. Zhou, X. Wang, X. Gao, and X. Li. 2012. 'Immune-related microRNAs are abundant in breast milk exosomes', *Int J Biol Sci*, 8: 118-23.

Zierath, J.R., and U. Lendahl. 2013. 'Machinery regulating vesicle traffic, a major transport system in our cells.', The 2013 Nobel Prize in Physiology or Medicine.

Zitvogel, Laurence, Armelle Regnault, Anne Lozier, Joseph Wolfers, Caroline Flament, Danielle Tenza, Paola Ricciardi-Castagnoli, Graça Raposo, and Sebastian Amigorena. 1998. 'Eradication of established murine tumors using a novel cell-free vaccine: dendritic cell derived exosomes', *Nature Medicine*, 4: 594.

# 8. Affidavit

I declare that I have written my doctoral thesis entitled “Mitochondrial DNA in Extracellular Vesicles: A Diagnostic Biomarker for Parkinson’s Disease?” independently, that I have not used other than the declared sources/resources, and that I have explicitly marked all material which has been quoted either literally or by content from the used sources.

Dr. Katharina Hipp performed the TEM experiments at the Max Planck Institute for Biology Tübingen. Prof. Dr. Anja Schneider and her team did the NTA measurements at the German Center for Neurodegenerative Diseases (DZNE) in Bonn. Dr. Milan Zimmermann from the Clinic of Neurology of the University Hospital Tübingen assisted me at the rtPCR experiments.

Heidelberg, 26.10.2023 Hans Siegrist

# 9. Acknowledgements

This work could not have been possible without the help and support of many people whom I would like to thank at this point.

… The IZKF Promotionskolleg for its financial and professional support.

… The Hertie foundation for granting the Sigmund-Kiener scholarship to me. The financial support helped to focus on the laboratory work.

… My lab members for their open ears for any questions, for their teaching, and for the enjoyable time in the lab.

… Dr. Katharina Hipp from the Max Planck Institute for Developmental Biology Tübingen for performing electron microscopy.

… Prof. Dr. Anja Schneider and her team from the DZNE Bonn for performing the NTA experiments.

… Milan Zimmermann for sharing his PCR protocol with me, for choosing the biobank samples, and for supporting me in carrying out the PCR experiments.

… Julia Fitzgerald for her tireless support in all questions of my thesis, including the teaching of new techniques, the discussion of results, the development of new ideas and the help in financial issues. For proofreading and correcting this work, and for her encouragement of my scientific work. I really learned a lot. Thank you for a really good time.

… My supervisor Prof. Dr. Thomas Gasser for introducing me to the topic, his professional support, and for allowing me to work independently and follow my own ideas.

… Meinen Eltern für das Willkommensein zu Hause egal wann und für wie lange, für die Freiheiten, die sie mir gewährt haben und für die Unterstützung in allen Lebenslagen.

# 10. Appendix

## 10.1. Cohort characteristics

### 10.1.1. PD patients

***Table 16:*** *Demographics of analysed CSF and serum samples from the cohort (patients).*

| Pat ID | date of examination | age at sample picking | diagnosis | sex | birth date | age of disease onset | samples | |
|---|---|---|---|---|---|---|---|---|
| | | | | | | | serum | CSF |
| **ID12962** | 04.05.2010 | 66 | IPD | male | 01.11.1943 | 55 | X | X |
| **ID13776** | 13.04.2011 | 69 | IPD (equivalent type) | female | 01.12.1941 | 60 | X | X |
| **ID14511** | 06.09.2012 | 59 | IPD (equivalent type) | male | 01.06.1953 | 50 | X | X |
| **ID15038** | 31.05.2010 | 66 | IPD (akinetic-rigid type) | male | 01.09.1943 | 64 | X | X |
| **ID16459** | 06.11.2013 | 62 | IPD | male | 01.02.1951 | 58 | X | X |
| **ID16991** | 24.01.2017 | 64 | IPD (tremor-dominant type) | male | 01.12.1952 | 55 | X | X |
| **ID17086** | 03.05.2012 | 71 | IPD (akinetic-rigid type) | female | 01.01.1941 | 67 | X | X |
| **ID17399** | 18.04.2018 | 65 | IPD (equivalent type) | female | 01.06.1952 | 54 | X | X |
| **ID17846** | 23.03.2010 | 68 | IPD (tremor-dominant type) | male | 01.04.1941 | 68 | X | X |
| **ID17949** | 07.04.2010 | 69 | IPD (equivalent type) | male | 01.03.1941 | 61 | X | X |
| **ID18031** | 29.10.2010 | 55 | IPD | male | 17.10.1955 | 51 | X | X |
| **ID18341** | 17.09.2014 | 77 | IPD | female | 01.11.1936 | 71 | X | X |
| **ID20456** | 16.03.2015 | 79 | IPD (equivalent type) | female | 01.07.1935 | 73 | X | X |
| **ID20492** | 02.07.2012 | 55 | IPS | female | 01.04.1957 | 54 | X | X |
| **ID20924** | 24.03.2017 | 58 | IPD (akinetic-rigid type) | female | 01.09.1958 | 50 | X | X |
| **ID21317** | 29.05.2015 | 66 | IPD | male | 01.03.1949 | 57 | X | X |
| **ID21595** | 26.07.2017 | 78 | IPD (equivalent type) | male | 09.07.1939 | 72 | X | X |
| **ID22039** | 18.03.2015 | 69 | IPD (tremor-dominant type) | male | 01.04.1945 | 66 | X | X |
| **ID23347** | 07.04.2014 | 65 | IPD | male | 01.02.1949 | 53 | X | X |
| **ID23558** | 10.11.2017 | 67 | IPD (tremor-dominant type) | male | 01.05.1950 | 59 | X | X |
| **ID25010** | 16.05.2018 | 64 | IPD | male | 01.02.1954 | 60 | X | X |
| **ID00761** | 16.11.2009 | 61 | genetic PD (PINKK1) | female | 20.03.1948 | 41 | X | X |
| **ID14486** | 08.11.2018 | 66 | IPD (equivalent type) | female | 05.02.1952 | 52 | X | X |
| **ID17553** | 17.11.2010 | 48 | IPD (akinetic-rigid type) | female | 25.03.1962 | 42 | X | |
| **ID17589** | 06.07.2017 | 53 | IPD (equivalent type) | male | 01.02.1964 | 29 | X | X |
| **ID31779** | 07.11.2018 | 69 | IPD | female | 23.02.1949 | ? | X | |
| **ID22424** | 27.06.2016 | 69 | mitochondriopathy | male | 21.10.1946 | ? | X | |
| **ID20405** | 01.03.2018 | 56 | IPD (equivalent type) | male | 23.09.1961 | 48 | X | X |
| **ID13314** | 14.10.2009 | 66 | IPD | male | 12.10.1943 | 59 | X | |

| | | | | | | | | |
|---|---|---|---|---|---|---|---|---|
| **ID14333** | 04.07.2012 | 68 | IPD (equivalent type) | male | 21.05.1944 | 58 | X | X |
| **ID20349** | 06.11.2014 | 53 | IPD (equivalent type) | female | 09.08.1961 | 37 | X | X |
| **ID19995** | 26.07.2011 | 67 | PSP-P | female | 29.04.1944 | 64 | X | X |
| **ID22305** | 29.04.2013 | 52 | PSP-P | female | 18.01.1961 | 50 | X | X |
| **ID23490** | 15.05.2014 | 66 | PSP-P | male | 15.10.1947 | 60 | X | X |
| **ID13327** | 21.11.2014 | 66 | mitochondriopathy | male | 10.11.1948 | 51 | X | X |

## 10.1.2. Controls

***Table 17:*** *Demographics of analysed serum samples from the cohort (controls).*

| Pat ID | date of examination | age | diagnosis | sex | sample |
|---|---|---|---|---|---|
| **ID11514** | 01.06.2015 | 70 | Control person | female | serum |
| **ID11515** | 01.06.2015 | 65 | Control person | male | serum |
| **ID11570** | 14.04.2009 | 55 | Control person | male | serum |
| **ID11650** | 04.08.2009 | 67 | Control person | male | serum |
| **ID11713** | 20.09.2010 | 64 | Control person | male | serum |
| **ID11785** | 22.11.2010 | 65 | Control person | female | serum |
| **ID11853** | 11.08.2009 | 71 | Control person | female | serum |
| **ID11867** | 14.05.2009 | 62 | Control person | male | serum |
| **ID11872** | 31.01.2011 | 66 | Control person | male | serum |
| **ID12045** | 05.10.2010 | 59 | Control person | male | serum |
| **ID12373** | 29.09.2010 | 66 | Control person | male | serum |
| **ID12780** | 08.06.2016 | 77 | Control person | female | serum |
| **ID12815** | 07.10.2010 | 69 | Control person | female | serum |
| **ID12823** | 20.09.2010 | 69 | Control person | male | serum |
| **ID13084** | 30.09.2010 | 66 | Control person | male | serum |
| **ID14828** | 10.06.2010 | 61 | Control person | female | serum |
| **ID15955** | 21.04.2010 | 64 | Control person | male | serum |
| **ID16026** | 12.08.2010 | 77 | Control person | female | serum |
| **ID16053** | 21.09.2010 | 55 | Control person | male | serum |
| **ID16071** | 04.05.2011 | 66 | Control person | male | serum |
| **ID16082** | 24.08.2010 | 68 | Control person | male | serum |
| **ID16123** | 03.07.2017 | 66 | Control person | female | serum |
| **ID16124** | 26.03.2010 | 58 | Control person | female | serum |
| **ID16161** | 06.04.2010 | 69 | Control person | female | serum |
| **ID17739** | 19.06.2017 | 70 | Control person | male | serum |
| **ID17845** | 19.04.2011 | 52 | Control person | female | serum |
| **ID18085** | 30.04.2013 | 78 | Control person | male | serum |
| **ID18093** | 04.06.2012 | 66 | Control person | male | serum |
| **ID18156** | 11.06.2010 | 55 | Control person | female | serum |
| **ID18184** | 21.05.2010 | 53 | Control person | male | serum |
| **ID18220** | 26.11.2012 | 69 | Control person | male | serum |
| **ID27133** | 30.03.2016 | 66 | Control person | male | serum |
| **ID27361** | 25.05.2016 | 69 | Control person | male | serum |

| | | | | | |
|---|---|---|---|---|---|
| **ID28862** | 29.03.2017 | 48 | Control person | female | serum |
| **ID31916** | 05.12.2018 | 50 | Control person | female | serum |

## 10.2. Standard operating procedure (SOP) for cohort samples

### 10.2.1. Serum samples

- Thaw serum on ice
- Centrifuge 500 µl serum at 3,000 x g for 15 min at 4°C
- Transfer supernatant to a fresh tube and add 125 µl of ExoQuick™ exosome solution and gently mix by inversion
- Incubate suspension for 60 min at 4°C to precipitate total EVs
- Centrifuge at 1,500 × g for 30 min at 4°C
- Discard the supernatant
- Centrifuge at 1,500 x g for 5 min at 4°C
- Resuspend the pellet containing EVs in 100 µl PBS + 1 PIC
- Set up the DNase digestion reaction as follows:
    - Add 10 µl of 10x reaction buffer to the sample
    - Add 10 µl of RNase-free DNase to the sample
- Incubate at 37°C for 30 minutes
- Add 10 µl of RQ1 DNase Stop Solution to terminate the reaction.
- Incubate at 65°C for 10 minutes to inactivate the DNase.
- Continue with DNA isolation with the QIAamp DNA Micro Kit
- Add 100 µl Buffer AL, close the lid, and mix by pulse-vortexing for 15 s
- Add 1 µl of carrier RNA (which has been dissolved in 310 µl AE buffer)
- Incubate for 10 min at room temperature
- Add 10 µl proteinase K
- Incubate at 56°C for 10 min.
- Briefly centrifuge the 1.5 ml tube to remove drops from inside the lid.
- Add 100 µl ethanol (100%), close the lid, and mix thoroughly by pulse-vortexing for 15 s
- Incubate for 3 min at room temperature.

- Briefly centrifuge the 1.5 ml tube to remove drops from inside the lid.
- Carefully transfer the entire lysate to the QIAamp MinElute column (in a 2 ml collection tube) without wetting the rim. NOTE: The columns are stored in the fridge
- Close the lid, and centrifuge at 6000 x g (8000 rpm) for 1 min.
- Place the QIAamp MinElute column in a clean 2 ml collection tube and discard the collection tube containing the flow-through.
- Add 500 µl Buffer AW1
- Centrifuge at 6000 x g (8000 rpm) for 1 min.
- Place the QIAamp MinElute column in a clean 2 ml collection tube and discard the collection tube containing the flow-through.
- Add 500 µl Buffer AW2
- Centrifuge at 6000 x g (8000 rpm) for 1 min.
- Place the QIAamp MinElute column in a clean 2 ml collection tube and discard the collection tube.
- Centrifuge at full speed (20,000 x g; 14,000 rpm) for 3 min to dry the membrane completely.
- Place the QIAamp MinElute column in a clean 1.5 ml microcentrifuge tube and discard the collection tube containing the flow-through.
- Apply 30 µl Buffer AE to the centre of the membrane.
- Incubate at room temperature for 5 min
- Centrifuge at 20,000 x g for 1 min
- Add the flow-through again to the centre of the membrane and centrifuge at 20,000 x g for 1 min
- Transfer the flow-through to a 500 µl PCR-tube

### 10.2.2. CSF samples

- Thaw CSF on ice
- Add 1 x PIC (diluted in PCR grade water) to the samples
- Centrifuge 400 µl CSF (= 1 tube) at 3,000 x g for 15 min at 4°C

- Transfer supernatant to a fresh tube and add 100 µl of ExoQuick-TC™ exosome solution and gently mix by inversion
- Incubate suspension overnight at 4°C to precipitate total EVs
- Centrifuge at 1,500 × g for 30 min at 4°C
- Discard the supernatant
- Centrifuge at 1,500 x g for 5 min at 4°C
- Resuspend the pellet containing EVs in 100 µl PCR grade water
- Continue with the digestion of extra-vesicular DNA and the DNA isolation with the QIAamp DNA Micro Kit as described for serum samples

## 10.3. Detailed IP protocol

*(Modified from: Plasma Extracellular Vesicles Enriched for Neuronal Origin: A Potential Window into Brain Pathologic Processes (Mustapic et al, 2017))*

- Thaw frozen serum on ice.
- If the protease inhibitor cocktail has not been added to the sample yet, add 50x PIC to a final concentration of 1 x PIC
- Centrifuge serum at 3,000 x g for 15 min at 4°C
- Transfer 500 µl of the supernatant to fresh tubes and add 125 µl of ExoQuick™ exosome solution and gently mix by inversion
- Incubate suspension with ExoQuick™ for 60 min at 4°C to precipitate total EVs
- Centrifuge at 1,500 × g for 30 min at 4°C
- Discard the supernatant
- Centrifuge at 1,500 x g for 5 min at 4°C
- Resuspend the pellet containing EVs after centrifugation in 0.5 ml of Ultra-pure distilled water or PBS (containing two times the suggested concentrations of protease and phosphatase inhibitors)
- Incubate suspension 1 h at 4°C with 4 µg of mouse anti-human CD171 (L1CAM) in total volume of 50 µl of 3% per tube with mixing on a rotation mixer
- Prepare Streptavidin Magnetic Beads

  - Gently vortex and thoroughly suspend magnetic beads (vortex > 30 seconds or mix by end-over-end inversion for > 5 minutes)
  - Transfer 200 µl of magnetic beads to microcentrifuge tube. Apply magnet to pull beads to the side of the tube and remove supernatant
  - Wash beads in total 3 times through resuspending in 1 ml binding buffer (20 mM Tris-HCl, pH 7.5; 0.5 M NaCl; 1 mM EDTA) and removing the supernatant
- Add the exosome sample (with antibodies) to the washed streptavidin magnetic beads and incubate for 30 min at 4°C with continuous mixing on a rotation mixer
- Wash the beads three times with 1 ml 0.1% BSA in PBS, pH = 7.5 (mix the sample by inverting the tube about 20 times)
- Resuspend the beads in 200 µl of 0.1 M glycine, pH = 2
- Transfer the complete solution (glycine + beads) to a new microcentrifuge tube (0.5 ml PCR-tube)
- Vortex strongly for at least 30 s and centrifuge at 4,500 × g for 10 min at 4°C to detach L1CAM+EVs from the bead-antibody complex
- Transfer supernatants to clean tubes containing 25 µl of 10% BSA and 15 µl of 1 M TRIS-HCl and mix to neutralize the sample

<u>Modifications of the elution:</u>

- glycine
  - Resuspend the beads (after washing) in 110 µl of 0.1 M glycine (pH = 2) and incubate for 1 hour at room temperature with gentle shaking on a vortex
  - Centrifuge at 4,500 × g for 10 min at 4°C and collect the supernatant
  - Transfer supernatants to clean tubes and add 10 µl of 1 M Tris-HCl and mix
- SDS loading buffer and other buffers containing detergents
  - Resuspend the beads (after washing) in 110 µl of 1:4 diluted 4 x NuPAGE LDS sample buffer

- Place the tube in a thermomixer and boil the solution for 10 min at 95°C (70°C) with gentle shaking
- Centrifuge at 10,000 x g for 3 minutes at 4°C and collect the supernatant

## 10.4. Setting of the LightCycler® machine (ROCHE)

***Table 18:*** *Machine settings for the rtPCR (LightCycler® from ROCHE).*

| **Detection Format** | | | **SYBR Green I** |
|---|---|---|---|
| **Reaction Volume** | | | 13 µl |
| **Preincubation** | | ramp | 4.4°C/s |
| | | duration | 600 s |
| | | target | 95°C |
| **3-Step-Amplification** | 1 | ramp | 4.4°C/s |
| | | duration | 10 s |
| | | target | 95°C |
| | | acquisition mode | none |
| | 2 | ramp | 2.2°C/s |
| | | duration | 20 s |
| | | target | 60°C |
| | | acquisition mode | single |
| | 3 | ramp | 4.4°C/s |
| | | duration | 30 s |
| | | target | 72°C |
| | | acquisition mode | none |
| **High Resolution Melting** | 1 | ramp | 4.4°C/s |
| | | duration | 60 s |
| | | target | 95°C |
| | | acquisition mode | none |
| | 2 | ramp | 2.2°C/s |
| | | duration | 60 s |
| | | target | 40°C |
| | | acquisition mode | none |
| | 3 | ramp | 4.4°C/s |
| | | duration | 1 s |
| | | target | 50°C |
| | | acquisition mode | none |
| | 4 | ramp | - |
| | | duration | - |
| | | target | 95°C |
| | | acquisition mode | continuous - 25 readings/°C |

| | | |
|---|---|---|
| **Cooling** | ramp | 2.2°C/s |
| | duration | 30 s |
| | target | 40°C |
| | acquisition mode | none |

## 10.5. Data for L1CAM/TSG101 ratio

This table shows the relative intensity of TSG101 and L1CAM bands in different Western Blots with different serum and CSF samples. Data were obtained using ImageJ.

***Table 19:*** *Overview of the data for the calculation of the L1CAM/TSG101 ratio.*

| **date of Western Blot** | **sample** | | **intensity L1CAM band** | **intensity TSG101 band** | **L1CAM/TSG101** |
|---|---|---|---|---|---|
| | **serum** | **CSF** | | | |
| **07. + 08.03.2019** | X | | 21,433% | 17,395% | 1,23 |
| | | X | 11,428% | 11,312% | 1,01 |
| | X | | 15,709% | 19,381% | 0,81 |
| | | X | 14,132% | 12,086% | 1,05 |
| | X | | 18,421% | 24,503% | 0,75 |
| | | X | 18,876% | 15,342% | 1,23 |
| **18. + 19.03.2019** | X | | 16,13% | 19,371% | 0,83 |
| | | X | 4,222% | 1,395% | 3,03 |
| | X | | 21,152% | 23,569% | 0,90 |
| | | X | 5,115% | 1,529% | 3,35 |
| | X | | 23,416% | 25,217% | 0,93 |
| | | X | 4,687% | 1,537% | 3,05 |
| | X | | 20,341% | 25,624% | 0,79 |
| | | X | 4,938% | 1,758% | 2,81 |
| **31.01. + 01.02.2019** | X | | 32,441% | 43,228% | 0,75 |
| | | X | 25,309% | 17,711% | 1,43 |
| | X | | 23,737% | 30,418% | 0,78 |
| | | X | 18,514% | 8,643% | 2,14 |
| **21. + 22.03.2019** | X | | 16,822% | 18,048% | 0,93 |
| | | X | 3,735% | 0,925% | 4,04 |
| | X | | 17,502% | 19,018% | 0,92 |
| | | X | 3,681% | 0,891% | 4,13 |
| | X | | 16,671% | 20,827% | 0,80 |
| | | X | 3,625% | 0,893% | 4,06 |
| | X | | 15,295% | 19,739% | 0,77 |
| | | X | 4,3% | 1,035% | 4,15 |
| | X | | 14,264% | 17,948% | 0,79 |
| | | X | 4,105% | 0,676% | 6,07 |

## 10.6. Results of the cohort in detail

***Table 20:*** *Complete data from the serum and CSF samples of the cohort (PD = Parkinson's disease patient, C = control person, conc. = concentration).*

| PD | C | sample | ID | protein conc. [mg/ml] | DNA conc. [ng/µl] | Ct (ND1) | Ct (ND4) | ND4/ ND1 | ND1/ DNA conc. | ND4/ DNA conc. |
|---|---|---|---|---|---|---|---|---|---|---|
| X | | Serum | ID15038 | 38.13 | 0.285 | 19.93 | 20.22 | 1.015 | 69.930 | 70.947 |
| X | | Serum | ID17846 | 50.27 | 0.0424 | 35.14 | 34.95 | 0.995 | 828.774 | 824.292 |
| X | | Serum | ID17949 | 41.91 | 0.048 | 35.53 | 35.73 | 1.006 | 740.208 | 744.375 |
| X | | Serum | ID18031 | 35.69 | 0.264 | 21.76 | 22.28 | 1.024 | 82.424 | 84.394 |
| X | | Serum | ID20492 | 39.94 | 0.333 | 19.41 | 20.02 | 1.031 | 58.288 | 60.120 |
| | X | Serum | ID11570 | 40.52 | 0.800 | 20.61 | 21.38 | 1.037 | 25.763 | 26.725 |
| | X | Serum | ID11650 | 37.60 | 0.484 | 21.36 | 22.11 | 1.035 | 44.132 | 45.682 |
| | X | Serum | ID16124 | 49.55 | 0.237 | 21.68 | 22.54 | 1.040 | 91.477 | 95.105 |
| | X | Serum | ID18093 | 38.81 | 0.209 | 19.2 | 19.79 | 1.031 | 91.866 | 94.689 |
| | X | Serum | ID18220 | 40.44 | 0.234 | 19.07 | 19.77 | 1.037 | 81.496 | 84.487 |
| X | | Serum | ID12962 | 57.73 | 0.174 | 19.99 | 20.62 | 1.032 | 114.885 | 118.506 |
| X | | Serum | ID13776 | 69.31 | 0.219 | 19.69 | 20.51 | 1.042 | 89.909 | 93.653 |
| X | | Serum | ID14511 | 53.37 | 0.526 | 19.72 | 20.3 | 1.029 | 37.490 | 38.593 |
| X | | Serum | ID17086 | 61.59 | 0.200 | 19.78 | 20.52 | 1.037 | 98.900 | 102.600 |
| X | | Serum | ID00761 | 65.70 | 0.207 | 17.48 | 18.09 | 1.035 | 84.444 | 87.391 |
| | X | Serum | ID14828 | 61.14 | 0.202 | 19.12 | 20.18 | 1.055 | 94.653 | 99.901 |
| | X | Serum | ID15955 | 50.52 | 0.201 | 19.4 | 20.6 | 1.062 | 96.517 | 102.488 |
| | X | Serum | ID16161 | 63.31 | 0.199 | 20.64 | 21.51 | 1.042 | 103.719 | 108.090 |
| | X | Serum | ID18156 | 53.13 | 0.508 | 18.48 | 19.34 | 1.047 | 36.378 | 38.071 |
| | X | Serum | ID18184 | 67.10 | 0.158 | 19.08 | 20.2 | 1.059 | 120.759 | 127.848 |
| X | | Serum | ID16991 | 70.95 | 0.106 | 18.96 | 19.95 | 1.052 | 178.868 | 188.208 |
| X | | Serum | ID20924 | 65.46 | 0.124 | 18.4 | 19.21 | 1.044 | 148.387 | 154.919 |
| X | | Serum | ID21595 | 58.44 | 0.160 | 19.34 | 20.33 | 1.051 | 120.875 | 127.063 |
| X | | Serum | ID23558 | 65.28 | 0.113 | 18.49 | 19.39 | 1.049 | 163.628 | 171.593 |
| X | | Serum | ID20405 | 69.59 | 0.190 | 19.49 | 20.65 | 1.060 | 102.579 | 108.684 |
| | X | Serum | ID12045 | 65.39 | 0.171 | 18.25 | 19.18 | 1.051 | 106.725 | 112.164 |
| | X | Serum | ID12815 | 59.28 | 0.728 | 19.47 | 20.32 | 1.044 | 26.745 | 27.912 |
| | X | Serum | ID16026 | 52.34 | 0.135 | 18.65 | 19.77 | 1.060 | 138.148 | 146.444 |
| | X | Serum | ID16053 | 66.31 | 0.164 | 18.92 | 20.18 | 1.067 | 115.366 | 123.049 |
| | X | Serum | ID16082 | 56.79 | 1.07 | 18.99 | 20.03 | 1.055 | 17.748 | 18.720 |
| X | | Serum | ID16459 | 61.70 | 0.404 | 19.29 | 20.98 | 1.088 | 47.748 | 51.931 |
| X | | Serum | ID17399 | 66.22 | 0.488 | 21.5 | 23.6 | 1.098 | 44.057 | 48.361 |
| X | | Serum | ID25010 | 65.28 | 0.728 | 20.34 | 21.99 | 1.081 | 27.940 | 30.206 |
| X | | Serum | ID31779 | 52.86 | 0.448 | 19.64 | 21.32 | 1.086 | 43.839 | 47.589 |
| X | | Serum | ID22305 | 67.80 | 0.379 | 20.9 | 22.46 | 1.075 | 55.145 | 59.261 |

| | | | | | | | | | | |
|---|---|---|---|---|---|---|---|---|---|---|
| | X | Serum | ID11713 | 59.35 | 1.14 | 19.69 | 21.32 | 1.083 | 17.272 | 18.702 |
| | X | Serum | ID11785 | 72.22 | 0.596 | 18.03 | 19.47 | 1.080 | 30.252 | 32.668 |
| | X | Serum | ID16071 | 58.16 | 0.948 | 20.24 | 21.71 | 1.073 | 21.350 | 22.901 |
| | X | Serum | ID17845 | 47.92 | 0.864 | 18.95 | 20.42 | 1.078 | 21.933 | 23.634 |
| | X | Serum | ID31916 | 61.61 | 0.358 | 18.78 | 20.31 | 1.081 | 52.458 | 56.732 |
| X | | Serum | ID18341 | 56.74 | 0.396 | 18.99 | 20.54 | 1.082 | 47.955 | 51.869 |
| X | | Serum | ID23347 | 49.09 | 0.744 | 19.05 | 20.61 | 1.082 | 25.605 | 27.702 |
| X | | Serum | ID14333 | 56.66 | 1.38 | 17.26 | 18.52 | 1.073 | 12.507 | 13.420 |
| X | | Serum | ID19995 | 63.39 | 1.56 | 18.78 | 20.35 | 1.084 | 12.038 | 13.045 |
| X | | Serum | ID23490 | 64.49 | 0.460 | 18.34 | 19.77 | 1.078 | 39.870 | 42.978 |
| | X | Serum | ID12373 | 52.33 | 0.268 | 20.98 | 21.71 | 1.035 | 78.284 | 81.007 |
| | X | Serum | ID12780 | 76.14 | 0.384 | 19.98 | 20.46 | 1.024 | 52.031 | 53.281 |
| | X | Serum | ID12823 | 78.77 | 0.260 | 20.51 | 21.51 | 1.049 | 78.885 | 82.731 |
| | X | Serum | ID13084 | 137.58 | 0.616 | 20.47 | 21.32 | 1.042 | 33.231 | 34.610 |
| | X | Serum | ID27361 | 91.81 | 0.676 | 20.98 | 21.83 | 1.041 | 31.036 | 32.293 |
| X | | Serum | ID20456 | - | 0.395 | 18.61 | 19.07 | 1.025 | 47.114 | 48.278 |
| X | | Serum | ID21317 | - | 1.02 | 20.32 | 21.08 | 1.037 | 19.922 | 20.667 |
| X | | Serum | ID22039 | - | 1.02 | 19.7 | 20.43 | 1.037 | 19.314 | 20.029 |
| X | | Serum | ID20349 | - | 0.444 | 18.84 | 19.55 | 1.038 | 42.432 | 44.032 |
| X | | Serum | ID13327 | - | 0.390 | 20.65 | 21.27 | 1.030 | 52.949 | 54.538 |
| | X | Serum | ID11853 | - | 0.424 | 20.69 | 21.45 | 1.037 | 48.797 | 50.590 |
| | X | Serum | ID11867 | - | 0.736 | 19.33 | 20.06 | 1.038 | 26.264 | 27.255 |
| | X | Serum | ID16123 | - | 0.448 | 19.91 | 20.65 | 1.037 | 44.442 | 46.094 |
| | X | Serum | ID17739 | - | 0.341 | 19.28 | 19.86 | 1.030 | 56.540 | 58.240 |
| | X | Serum | ID18085 | - | 0.628 | 18.91 | 19.71 | 1.042 | 30.111 | 31.385 |
| X | | Serum | ID14486 | 56.90 | 0.836 | 20.22 | 20.96 | 1.037 | 24.187 | 25.072 |
| X | | Serum | ID17553 | 64.94 | 0.828 | 19.47 | 20.11 | 1.033 | 23.514 | 24.287 |
| X | | Serum | ID17589 | 61.87 | 1.18 | 20.52 | 21.22 | 1.034 | 17.390 | 17.983 |
| X | | Serum | ID22424 | 67.42 | 1.16 | 19.18 | 20.01 | 1.043 | 16.534 | 17.250 |
| X | | Serum | ID13314 | 55.70 | 0.864 | 19.69 | 20.38 | 1.035 | 22.789 | 23.588 |
| | X | Serum | ID11514 | 56.83 | 1.05 | 19.06 | 19.66 | 1.031 | 18.152 | 18.724 |
| | X | Serum | ID11515 | 58.59 | 0.712 | 18.19 | 18.91 | 1.040 | 25.548 | 26.559 |
| | X | Serum | ID27133 | 56.44 | 0.780 | 20.3 | 20.81 | 1.025 | 26.026 | 26.679 |
| | X | Serum | ID11872 | 53.06 | 2.07 | 17.23 | 17.82 | 1.034 | 8.324 | 8.609 |
| | X | Serum | ID28862 | 50.70 | 0.528 | 18.06 | 18.38 | 1.018 | 34.205 | 34.811 |
| X | | CSF | ID13776 | 0.23 | 1.20 | 30.76 | 31.75 | 1.032 | 25.633 | 26.458 |
| X | | CSF | ID17086 | 0.30 | 1.17 | 25.56 | 26.6 | 1.041 | 21.846 | 22.735 |
| X | | CSF | ID14511 | 0.24 | 1.44 | 29.39 | 30.29 | 1.031 | 20.410 | 21.035 |
| X | | CSF | ID15038 | 0.29 | 0.383 | 31.67 | 33.2 | 1.048 | 82.689 | 86.684 |
| X | | CSF | ID17846 | 0.42 | 1.12 | 33.16 | 33.16 | 1.000 | 29.607 | 29.607 |
| X | | CSF | ID20492 | 0.10 | 0.472 | 32.67 | 38.03 | 1.164 | 69.216 | 80.572 |

| | | | | | | | | | |
|---|---|---|---|---|---|---|---|---|---|
| X | CSF | ID18031 | 0.11 | 0.444 | 32.53 | 35.99 | 1.106 | 73.266 | 81.059 |
| X | CSF | ID12962 | 0.22 | 0.440 | 32.23 | 35.41 | 1.099 | 73.250 | 80.477 |
| X | CSF | ID17949 | 0.20 | 0.608 | 31.27 | 35.07 | 1.122 | 51.431 | 57.681 |
| X | CSF | ID00761 | 0.14 | 0.828 | 32.61 | 35.99 | 1.104 | 39.384 | 43.466 |
| X | CSF | ID22305 | 0.09 | 0.484 | 30.22 | 33.72 | 1.116 | 62.438 | 69.669 |
| X | CSF | ID16459 | 0.16 | 0.736 | 29.16 | 32.88 | 1.128 | 39.620 | 44.674 |
| X | CSF | ID23347 | 0.11 | 0.640 | 29.97 | 34.17 | 1.140 | 46.828 | 53.391 |
| X | CSF | ID14333 | 0.14 | - | - | - | - | - | - |
| X | CSF | ID23490 | 0.28 | 0.548 | 30.8 | 34.42 | 1.118 | 56.204 | 62.810 |
| X | CSF | ID13327 | 0.11 | 1.38 | 27.12 | 30.91 | 1.140 | 19.652 | 22.399 |
| X | CSF | ID20456 | 1.60 | 0.292 | 28.17 | 31.99 | 1.136 | 96.473 | 109.555 |
| X | CSF | ID22039 | 0.27 | 0.424 | 31.33 | 36.01 | 1.149 | 73.892 | 84.929 |
| X | CSF | ID21317 | 0.26 | 0.580 | 30.54 | 34.44 | 1.128 | 52.655 | 59.379 |
| X | CSF | ID20405 | 0.33 | 0.600 | 32.15 | 32.94 | 1.025 | 53.583 | 54.900 |
| X | CSF | ID17399 | 0.20 | 0.265 | 28.87 | 30.22 | 1.047 | 108.943 | 114.038 |
| X | CSF | ID25010 | 0.36 | 0.900 | 29.66 | 30.96 | 1.044 | 32.956 | 34.400 |
| X | CSF | ID14486 | 0.26 | 0.386 | 30.87 | 32.41 | 1.050 | 79.974 | 83.964 |
| X | CSF | ID16991 | 0.26 | 0.295 | 32.46 | 34.12 | 1.051 | 110.034 | 115.661 |
| X | CSF | ID20924 | 0.28 | 0.358 | 28.52 | 29.7 | 1.041 | 79.665 | 82.961 |
| X | CSF | ID17589 | 0.31 | 0.656 | 29.36 | 30.85 | 1.051 | 44.756 | 47.027 |
| X | CSF | ID21595 | 0.26 | 0.444 | 30.93 | 32.12 | 1.038 | 69.662 | 72.342 |
| X | CSF | ID23558 | 0.43 | 1.13 | 30.77 | 32.36 | 1.052 | 27.230 | 28.637 |
| X | CSF | ID18341 | 0.26 | 0.225 | 31.13 | 32.54 | 1.045 | 138.356 | 144.622 |
| X | CSF | ID19995 | 0.61 | 0.620 | 30.7 | 32.83 | 1.069 | 49.516 | 52.952 |
| X | CSF | ID20349 | 0.66 | 0.370 | 29.87 | 31.31 | 1.048 | 80.730 | 84.622 |